A Systematic Re-evaluation of Methods for Quantification of Bulk Particle-phase Organic Nitrates Using Real-time Aerosol Mass Spectrometry

Douglas A. Day,[1,2] Pedro Campuzano-Jost,[1,2] Benjamin A. Nault,[1,2,a] Brett B. Palm,[1,2,b] Weiwei Hu,[1,2,c] Hongyu Guo,[1,2] Paul J. Wooldridge,[3] Ronald C. Cohen,[3,4] Kenneth. S. Docherty,[5] J. Alex Huffman,[6] Suzane S. de Sá,[7] Scot T. Martin,[7,8] Jose L. Jimenez[1,2]

[1]Cooperative Institute for Research in Environmental Sciences, University of Colorado, Boulder, CO, USA
[2]Dept. of Chemistry, University of Colorado, Boulder, CO, USA
[3]Department of Chemistry, University of California Berkeley, Berkeley, CA, USA
[4]Department of Earth and Planetary Science, University of California Berkeley, Berkeley, CA, USA
[5]Jacobs Technology, Inc., Research Triangle Park, NC, USA
[6]Department of Chemistry and Biochemistry, University of Denver, Denver, CO USA
[7]School of Engineering and Applied Sciences, Harvard University, Cambridge, Massachusetts, USA
[8]Department of Earth and Planetary Sciences, Harvard University, Cambridge, Massachusetts, USA

[a]now at: Center for Aerosol and Cloud Chemistry, Aerodyne Research Inc., Billerica, MA, USA
[b]now at: Atmospheric Chemistry Observations and Modeling Laboratory, National Center for Atmospheric Research, Boulder, CO, USA
[c]now at: State Key Laboratory at Organic Geochemistry, Guangzhou Institute of Geochemistry, Chinese Academy of Sciences, Guangzhou, China

Abstract

Organic nitrate ($RONO_2$) formation in the atmosphere represents a sink of NO_x (NO_x = NO + NO_2) and termination of the NO_x/HO_x (HO_x = HO_2 + OH) ozone formation and radical propagation cycles, can act as a NO_x reservoir transporting reactive nitrogen, and contributes to secondary organic aerosol formation. While some fraction of $RONO_2$ is thought to reside in the particle phase, particle-phase organic nitrates ($pRONO_2$) are infrequently measured and thus poorly understood. There is an increasing prevalence of aerosol mass spectrometer (AMS) instruments, which have shown promise for determining quantitative total organic nitrate functional group contribution to aerosols. A simple approach that relies on the relative intensities of NO^+ and NO_2^+ ions in the AMS spectrum, the calibrated NO_x^+ ratio for NH_4NO_3, and the inferred ratio for $pRONO_2$ has been proposed as a way to apportion the total nitrate signal to NH_4NO_3 and $pRONO_2$. This method is increasingly being applied to field and laboratory data. However, the methods applied have been largely inconsistent and poorly characterized, and therefore, a detailed evaluation is timely. Here, we compile an extensive survey of NO_x^+ ratios measured for various $pRONO_2$ compounds and mixtures from multiple AMS instruments, groups, and laboratory and field measurements. All data and analysis presented here is for using the standard AMS vaporizer. We show that, in the absence of $pRONO_2$ standards, the $pRONO_2$ NO_x^+ ratio can be estimated using a ratio referenced to the calibrated NH_4NO_3 ratio, a so-called "Ratio-of-Ratios" method (*RoR*=2.75±0.41). We systematically explore the basis for quantifying $pRONO_2$ (and NH_4NO_3) with the *RoR* method using ground and aircraft field measurements conducted over a large range of conditions. The method is compared to another AMS method (positive matrix factorization, PMF) and other $pRONO_2$ and related (e.g., total gas + particle $RONO_2$) measurements, generally showing good agreement / correlation. A broad survey of ground and aircraft AMS measurements shows a pervasive trend of higher fractional contribution of $pRONO_2$ to total nitrate with lower total nitrate concentrations, which generally corresponds to shifts from urban-influenced to rural/remote regions. Compared to ground campaigns, observations from all aircraft campaigns showed substantially lower $pRONO_2$ contributions at mid ranges of total nitrate (0.01-0.1 up to 2-5 μg m^{-3}), suggesting that the balance of effects controlling NH_4NO_3 and $pRONO_2$ formation and lifetimes — such as higher humidity, lower temperatures, greater dilution, different sources, higher particle acidity, and $pRONO_2$ hydrolysis (possibly accelerated by particle acidity) — favors lower $pRONO_2$ contributions for those environments and altitudes sampled.

1 Introduction

Organic nitrate ($RONO_2$) formation in the atmosnumphere, through oxidation of VOCs (volatile organic compounds) in the presence of NO_x (NO_x = NO + NO_2), represents a sink of NO_x and termination of the catalytic NO_x/HO_x (HO_x = OH + HO_2) ozone formation and radical propagation cycles, can act as a NO_x reservoir transporting (or removing) reactive nitrogen, and contribute to secondary organic aerosol formation (Zare et al., 2018 and references therein). Particle-phase organic nitrates ($pRONO_2$) have been shown to contribute substantial mass to organic aerosol (OA) (Ng et al., 2017 and references therein), can provide insight into the chemistry controlling SOA formation (e.g., Pye et al., 2015; Xu et al., 2015b; Lee et al., 2016; Ng et al., 2017), may constitute a semivolatile component of OA and dynamically partition between the gas- and particle-phases (e.g., Fry et al., 2013; Rollins et al., 2013; Pye et al., 2015), and represent a loss mechanism for $RONO_2$ or reactive nitrogen oxides (e.g., via hydrolysis or deposition) (Fisher et al., 2016; Lee et al., 2016; Zare et al., 2018). However, $pRONO_2$ have infrequently been measured in ambient air until recently and thus are still poorly understood (Ng et al., 2017).

The recent emergence of a variety of online and offline methods of both speciated and bulk $pRONO_2$ and their applications to ambient aerosol measurements are summarized in Ng et al. (2017). Instrumentation and methods include: (online bulk) aerosol mass spectrometry (AMS; (Jayne et al., 2000)) and its monitoring versions (known as Aerosol Chemical Speciation Monitors, ACSM; (Ng et al., 2011; Fröhlich et al., 2013)); thermal dissociation - laser induced fluorescence (TD-LIF; (Day et al., 2002)); (online speciated) filter inlet for gases and aerosols (FIGAERO) - chemical ionization mass spectrometry (CIMS) (Lopez-Hilfiker et al., 2014); (offline speciated) high-pressure liquid chromatography - mass spectrometry (HPLC/MS) often with electrospray ionization (ESI) (Surratt et al., 2006); (offline bulk) Fourier Transform InfraRed (FTIR) spectroscopy (Maria et al., 2002). While speciated methods can provide more detailed source or mechanistic information, they are slow and, to date, none (online nor offline) has demonstrated quantitative measurement of the bulk of $pRONO_2$ for ambient measurements. Therefore, bulk measurements provide useful constraints on the budgets, formation and loss rates of gas- and aerosol-phase $RONO_2$ in the atmosphere; and fast online methods are essential when ambient concentrations are rapidly changing, especially for aircraft sampling.

For most field applications of the AMS, typically aerosol nitrate concentrations have been reported as a single total (organic plus inorganic) concentration, due to the fact that nearly all of the signal of the nitrate functional group for any nitrate type (or nitrite) is measured at a couple of common ion peaks (NO^+ and NO_2^+ in high-resolution (HR) instruments or *m/z* 30 and *m/z* 46 in unit mass resolution (UMR) instruments) (Farmer et al., 2010). Early on in the application of the AMS, an implicit assumption was often made that ammonium nitrate (NH_4NO_3) typically dominated aerosol nitrate, based on early urban studies that showed semivolatile behavior consistent with NH_4NO_3 (e.g., Jimenez et al., 2003; Hogrefe et al., 2004; Zhang et al., 2004). However, a few early reports on field measurements using UMR AMS (Allan et al., 2004b, 2006) showed that the *m/z* 46 - to - *m/z* 30 ratio (hereinafter "46/30 ratio") was too low to be associated with only NH_4NO_3, suggesting substantial contributions from mineral nitrates ($NaNO_3$, $Ca(NO_3)_2$), $pRONO_2$, or possibly other reduced organo-nitrogen, or organic ion interferences. In a study focusing on cluster analysis of ambient (UMR) AMS spectra, Marcolli et al. (2006) also reported 46/30 ratios substantially smaller than NH_4NO_3 and found several spectra cluster categories with dominant *m/z* 30 peaks (but not *m/z* 46) and suggested that these signals may be associated with organic nitrates. Similarly, Alfarra et al. (2006) reported 46/30 ratios from chamber-generated SOA (photooxidation of trimethyl benzene and α-pinene) ~2–4 times lower than NH_4NO_3, which they

attributed to $pRONO_2$ or nitro-compounds. A few years later, reports from chamber studies where $pRONO_2$-rich SOA was generated (β-pinene or isoprene +NO_3 radicals), using an HR-AMS, showed NO_2^+/NO^+ ratios (hereafter "NO_x^+ ratio") ~2–4 times lower than pure NH_4NO_3 (Fry et al., 2009; Rollins et al., 2009).

Subsequently, broader surveys of the fragmentation patterns of aerosol nitrates (and nitrites) in the AMS were reported, including consistently low NO_x^+ ratios for $pRONO_2$ (Bruns et al., 2010; Farmer et al., 2010). Farmer et al. (2010) evaluated the fragmentation patterns of single-component $pRONO_2$ isolated from SOA, and showed that ~95% the nitrogen-containing signal was observed as NO_x^+ ions with the balance as HNO_3^+ and very little signal at $C_xH_yO_zN^+$ ions. Farmer et al. evaluated several methods for constraining $pRONO_2$ contribution to AMS nitrate signal including using: 1) NO_x^+ ratios, 2) HNO_3^+ ions, 3) $C_xH_yO_zN^+$ ions, 4) "ammonium balance", and 5) AMS total nitrate comparison to inorganic nitrate-only measured with another instrument (typically ion chromatography-based). For the urban dataset evaluated in that study, all methods appeared to be associated with relatively large uncertainties. Bruns et al. (2010) reported NO_x^+ ratios for SOA formed from several monoterpenes and isoprene (with NO_3 radicals) as well as $NaNO_3$ and $NaNO_2$ (with the sodium salts showing greatly reduced NO_x^+ ratios). Other studies have used the ammonium balance (hereafter NH_{4_Bal}) of AMS data, or comparisons to other instruments to estimate $pRONO_2$ content (Aiken et al., 2009; Zaveri et al., 2010; Docherty et al., 2011; Häkkinen et al., 2012; Xu et al., 2015a); however, in most cases, uncertainties were large or not assessed. Since the Farmer et al. study, several other laboratory studies reported NO_x^+ ratios for $pRONO_2$-containing SOA, which are summarized in Sect. 3. Additionally, a number of analyses of field studies have used the NO_x^+ ratios (or its 46/30 UMR equivalent) to support qualitative or semi-quantitative statements about the presence (or low contribution) of $pRONO_2$ (Setyan et al., 2012; Brown et al., 2013; Xu et al., 2016; Schneider et al., 2017; Bottenus et al., 2018) or to quantify $pRONO_2$ (Fry et al., 2013, 2018; Ayres et al., 2015; Kostenidou et al., 2015; Xu et al., 2015a, 2021; Fisher et al., 2016; Kiendler-Scharr et al., 2016; Lee et al., 2016, 2019; Nault et al., 2016; Zhou et al., 2016; Zhu et al., 2016, 2021; Florou et al., 2017; Palm et al., 2017; Brito et al., 2018; de Sá et al., 2018, 2019; Reyes-Villegas et al., 2018; Schulz et al., 2018; Avery et al., 2019; Dai et al., 2019; Huang et al., 2019a, 2019b; Yu et al., 2019; Chen et al., 2020, 2021; Lin et al., 2021). Yu et al. (2019) also used the particle size dependence of the 46/30 ratio to investigate particle size and temporal (diurnal and seasonal) trends in $pRONO_2$. Other studies have used positive matrix factorization (PMF) of AMS spectra including both the OA and NO_x^+ signals to quantify $pRONO_2$ (Sun et al., 2012; Hao et al., 2014; Xu et al., 2015a; Zhang et al., 2016; Kortelainen et al., 2017; Yu et al., 2019; Lin et al., 2021; Zhu et al., 2021). Recently, Xu et al., (2021) demonstrated another method, using AMS thermal denuder measurements.Thus there is promising use of AMS measurements for quantifying bulk $pRONO_2$ functional group contribution to ambient aerosols (and in addition, providing higher quality NH_4NO_3 concentrations). However, the methods have not been standardized and uncertainties of the different methods have not been well-characterized, and were reported to be large by at least some studies. Together with the increasing prevalence of AMS (and ACSM) field measurements, a detailed evaluation of $pRONO_2$ quantification methods is timely.

Here we explore the application of the AMS NO_x^+ ratio method to separate and quantify inorganic and organic nitrate and discuss the methods in detail, as well as comparison to other methods, and some scientific applications. In addition to drawing from available literature whenever possible, new analyses for several field and laboratory datasets are used extensively throughout this manuscript to explore and support findings. Descriptions of those datasets and data processing methods can be found in Supp. Info. Sect. S1 (including Fig. S1). All data, analysis, and recommendations presented here is for use with the

Commented [1]: Lin et al. 2021 added

Commented [2]: Lin et al. 2021 added

standard AMS vaporizer; while in practice, similar methods could be applied to explore the possibility of using data from an AMS equipped with the capture vaporizer to apportion nitrate, although it would likely have higher detection limits (Hu et al., 2017a).

2 Previous use and methods for $pRONO_2$ quantification using AMS NO_x^+ ratios

An equation for quantitative apportionment of the AMS nitrate signal into $pRONO_2$ and NH_4NO_3 using the NO_x^+ ratio was first presented by Farmer et al. (2010) (equation 1 from Farmer et al., and derived in their supporting information, here substituting different notation for some terms for consistency with this manuscript):

$$f_{pRONO_2} = \frac{(R_{ambient} - R_{NH_4NO_3})(1 + R_{pRONO_2})}{(R_{pRONO_2} - R_{NH_4NO_3})(1 + R_{ambient})} \quad (1)$$

where f_{pRONO2} is the fraction of total AMS nitrate (hereafter pNO_3) that is $pRONO_2$, and R_{NH4NO3}, R_{pRONO2}, and $R_{ambient}$ are the NO_x^+ ratios (NO_2^+/NO^+) for pure NH_4NO_3, pure $pRONO_2$, and the ambient aerosol nitrate mixture measured, respectively. Note that here we use the NO_2^+/NO^+ ratio for all terms, while Farmer et al. and some others have used NO^+/NO_2^+. This formulation is preferred since NO_2^+ tends to be lower than NO^+ for all nitrates, and thus using NO_2^+/NO^+ avoids ratios trending toward infinity as detection limits are approached. This usage has been applied in several publications, such as Fry et al. (2013) and Kiendler-Scharr et al. (2016), as presented in equations 11 and 1 in those papers, respectively. The equation is identical regardless of the inversion of the NO_x^+ ratio. That can be shown by simply swapping all the instances of NO and NO_2 in the definitions and derivation shown in Farmer et al. or by substituting $1/R_x$ for each ratio term in Eq. 1 above, multiplying all parenthetical terms by $R_{ambient}R_{NH4NO3}R_{pRONO2}$, factoring out the same term in the numerator and denominator then canceling, and finally multiplying the first parenthetical terms in the numerator and denominator by -1. While typically R_{NH4NO3} is measured frequently as pure NH_4NO_3 is periodically sampled by the AMS as a primary calibrant for sensitivity (Canagaratna et al., 2007), regular calibration using $pRONO_2$ is generally not practical. Moreover, it is not immediately clear that all $pRONO_2$ produce the same R_{pRONO2} in the AMS. Values reported in the literature for R_{NH4NO3} and R_{pRONO2} both appear to have a substantial range (factor of ~3) and generally R_{pRONO2} is 2–4 times lower than R_{NH4NO3} (see Sects. 1 and 3).

Several studies have applied Eq. 1 to quantify $pRONO_2$ and NH_4NO_3, using different assumptions regarding R_{pRONO2}. Farmer et al. (2010) applied their measurements of R_{pRONO2} from their lab study to estimate an upper limit of 50% for the $pRONO_2$ contribution to pNO_3 for the urban SOAR campaign, substantially higher than with other methods they applied. They considered that method to be a high upper limit, due to the possible influence of non-refractory nitrates. However, we note that the R_{pRONO2} used in that early study was nearly a factor of two different than we suggest in this study, in the direction favorable to higher $pRONO_2$ fractions. For calculation of $pRONO_2$ for the BEACHON-RoMBAS campaign, Fry et al. (2013) assert that R_{NH4NO3} and R_{pRONO2} likely co-vary for an instrument and therefore define the term "ratio-of-ratios" (hereafter $RoR = R_{NH4NO3}/R_{pRONO2}$) in order to estimate R_{pRONO2} from in-field R_{NH4NO3} measurements and literature reports of R_{pRONO2} and R_{NH4NO3}. The RoR value applied by Fry et al. (2013) was 2.25, based on the Farmer et al. (2010) average. On the other hand, in an analysis of $pRONO_2$ contribution to OA throughout Europe, Kiendler-Scharr et al. (2016) applied a fixed R_{pRONO2} of 0.1 based on literature reports of R_{pRONO2}, and the argument that it was the minimum ratio observed in the ambient datasets examined (noting that "such low ratios of NO_2^+/NO^+ were also detected in some data sets where R_{NH4NO3} was reported high"). Those authors state that their approach represents a lower limit of $pRONO_2$. Similarly, Brito et al. (2018), Schulz et al. (2018), Huang et al. (2019a, 2019b), and Avery et al.

(2019), applied a fixed R_{pRONO2} of 0.1 (citing Kiendler-Sharr et al. (2016)) for aircraft measurements in West Africa, aircraft measurements in the Amazon, rural forest and urban sites in Germany, and seasonal variations of indoor/outdoor air, respectively. The same method has been applied to laboratory studies of biomass burning aging (Tiitta et al., 2016), composition from photooxidation of terpenes (Zhao et al., 2018; Pullinen et al., 2020), and the composition, optical properties, and aging of particles from a wide variety of biomass burning fuel sources (Cappa et al., 2020; McClure et al., 2020). However, in the latter study, the organic component is classified as "organonitrogen", assuming it includes contributions from both organic nitrate and nitro-organic (i.e. nitroaromatics) functional groups (and assumed to have the same NO_x^+ ratio).

In a regional and seasonal survey of $pRONO_2$ in the SE US, Xu et al. (2015a) used the *RoR* concept. They estimated lower (2.2) and upper (4.4) limits for *RoR* (or R_{pRONO2} = 0.1-0.2 for their corresponding R_{NH4NO3}) from literature reports of SOA formed from isoprene+NO_3 radicals (Bruns et al., 2010) and β-pinene+NO_3 radicals (Fry et al., 2009; Bruns et al., 2010; Boyd et al., 2015), respectively. The rationale for their approach is that, for their region of study, those two BVOC may represent major contributions to the mixture of $pRONO_2$, and that the literature suggests there may be some source/composition dependence of R_{pRONO2}. For the same region, Chen et al. (2020) used bounds of R_{pRONO2} (0.1-0.2), based on similar logic, however not derived from a *RoR* calculation (however equivalent to a *RoR* of 1.7-3.3). In a study of $pRONO_2$ and SOA formation from Alberta oil sands extraction emissions from ground and aircraft measurements, Lee et al. (2019) used the same bounds of R_{pRONO2} (0.1-0.2), also not derived from a *RoR* calculation and citing Xu et al (2015a) and Farmer et al. (2010) (equivalent to a *RoR* of 1.4-2.9 and 1.5-3.0 for the two datasets). The same methods as Xu et al. (2015a) were used (applying the same range of *RoR*), for measurements conducted in Houston, TX (Dai et al., 2019) and the North China Plain (Xu et al., 2021). However Xu et al. (2021) adjusted the R_{NH4NO3} to match the highest NO_2^+/NO^+ ratios observed, since it was substantially higher than the calibration R_{NH4NO3} (assuming for those periods, nitrate was purely NH_4NO_3). Thus, those five studies report their concentrations and inorganic/organic nitrate split accordingly, and report lower and upper bounds; however, Lee et al., (2019) largely focused on results for the upper limit $pRONO_2$ concentrations for the scientific analysis (with equivalent *RoRs*: 1.4/1.5). Zhou et al. (2016), Zhu et al. (2016), and Yu et al. (2019) applied the *RoR* concept, citing a range of 2–4 from the literature, and thus reported estimated lower/upper limit averages for contribution of $pRONO_2$ to pNO_3 in New York City (summer, 67%/95%), a background site in China (spring, 15/22%), and an urban site in China (during spring, 13%/21%; summer, 41%/64%; autumn, 16%/25%), respectively. Similarly Zhu et al., (2021) applied the *RoR* concept, citing a range of 1.4–4.0 from the literature reporting upper(12%)/lower(7.8%) bounds for contribution of $pRONO_2$ to pNO_3 at a rural site in the North China Plains during summer. Kostenidou et al. (2015), on the other hand, estimated the R_{pRONO2} as the minimum $R_{ambient}$ observed in ambient data during the campaigns, resulting in effective *RoR*s of 5.6 and 12 for the two campaigns investigated. The same method is used by Reyes-Villegas et al. (2018) (using 46/30, and resulting in an effective *RoR* of 5) and Florou et al. (2017) (resulting in high effective *RoR*s of 14 and 15 for the two campaigns investigated). Other field studies have followed the methods of Fry et al. (2013) (but using a few different fixed values for the *RoR*) using HR data (Ayres et al., 2015; Fisher et al., 2016; Lee et al., 2016; Palm et al., 2017; de Sá et al., 2018, 2019; Nault et al., 2018; Chen et al., 2021) or UMR data (Fry et al., 2018; Schulz et al., 2018).

3 Survey of NO_x^+ ratios for particle-phase nitrates

Given the numerous applications of NO_x^+ ratios to separate $pRONO_2$ and NH_4NO_3 in AMS measurements, yet many variations in methods and the numerical values used within each method, we have conducted a systematic survey of literature values and trends of NO_x^+ ratios for different nitrates. Such data compilation is aimed at evaluating the evidence that supports using a fixed *RoR* to estimate R_{pRONO2} from the calibration R_{NH4NO3} and to investigate the variability in R_{pRONO2} produced from different sources. Figure 1 shows a compilation of *RoR* values for $pRONO_2$ derived for chamber-generated SOA, isolated compounds (from chamber SOA or standards), and ambient measurements (using instrument comparisons or PMF separation). Figure 1 also shows the *RoR* for the same data as a histogram and average, as well as the correlations of the $pRONO_2$ vs NH_4NO_3 (inverse) NO_x^+ ratios. Details of the values used to compute the ratios and uncertainties, data sources, and any additional calculations for the information included in Fig. 1, are provided in Table S1.

The correlation between the R_{pRONO2} and R_{NH4NO3} is fairly strong (R^2=0.54), considering the variety of data sources and substantial measurement uncertainties. It provides strong evidence that, to first order, the *RoR* method is consistent and supported by various methods, species/mixtures, instruments and operating conditions. The slopes of the linear regression constrained to a zero intercept using an ODR fit (2.66±0.11; assuming both variables contribute comparable uncertainty) is equivalent to an overall *RoR* and is similar to the average of the individual *RoR* datapoints (mean±standard error: 2.75±0.11). Highlighted in the scatterplot in Fig. 1 are a couple of pairs of datapoints that are averages from several experiments conducted in our laboratory with two different AMS during two different years, with substantially different measured calibration R_{NH4NO3} while sampling the same chamber SOA (see S1.2). The trends in those points are similar to the overall trend and provide an example of the validity of the *RoR* method when only differences in instrument / operating conditions are present. Fig. S2 shows a complementary histogram to that in Fig. 1 for the R_{pRONO2}, without normalizing to R_{NH4NO3}. Compared to the normalized values shown in Fig. 1 (i.e., *RoR*s), a factor of two larger relative variability is apparent, with a relative standard deviation of 49% compared to 25%. Also of note is that the average value is 0.21±0.10, twice as high as used in several literature studies. Finally, Fig. S3 shows a complementary plot to the scatter plot in Fig. 1, with the inverse NO_x^+ ratios and axes swapped, which emphasizes different data and outliers, and yields similar but slightly higher (<10%), *RoR* slopes and the same degree of correlation. While the representation in Fig. S3 uses the inverse NO_x^+ ratio of that used throughout this manuscript, it places the R_{NH4NO3} on the x-axis, and thus a non-ODR fit may be appropriate under the assumption that most uncertainty is contributed by the $pRONO_2$ ratios. The ODR and non-ODR fits (2.83±0.12, 2.66±0.12, respectively) bracket the simple average value (2.75).

The compilation shown in Fig. 1 allows for consideration of dependencies of the *RoR* on species/mixtures or methods. Generally, the *RoR*s cluster around 1.5–4 for most studies. The variability within duplicated VOC-oxidant pairs (e.g., β-pinene+NO_3 SOA), similar compound classes (e.g., monoterpenes, isoprene, aromatics, long-chain alkanes or alkenes), or measurement methods (SOA mixtures, isolated compounds, ambient measurements) is similar to the variability between such groupings. Therefore, given the data currently available, there does not appear to be any strong evidence to support any general chemical-dependence of the $pRONO_2$ *RoR*. While such a dependence may in fact exist, evaluation likely would require comparison of several organic nitrate molecules and/or mixtures systematically with the same instrumentation, operation conditions, and analysis methods, together with duplication by different instruments.

Therefore, for applications and further evaluation described in this manuscript, we use the average and variability of the *RoR* determined from data highlighted in Fig. 1: 2.75 (mean) and standard deviation (±0.70, 25%) or standard error (±0.11, 4.0%). The $25^{th}/50^{th}/75^{th}$ percentiles are 2.12, 2.73, 3.12 (interquartile range / median +14%/-22%). Given the approximate symmetry for the limited statistics available, we treat the variability and uncertainty of the *RoR* as approximately a normal distribution. The standard deviation should be considered an upper limit of the uncertainty of the applicable *RoR* and corresponds to the assumption that the variability in reported values is primarily attributable to true differences in ratios for different types of $pRONO_2$. The lack of clear differences among different sources suggests that some of the variability may instead be instrument/operator related, and that the std. error may be a more relevant characterization of the uncertainty. Complex mixtures of $pRONO_2$ in the atmosphere would likely represent an ensemble of those ratios, and thus result in values closer to the average. In fact, for the limited (7) examples of ambient-derived *RoR*s, the average is similar and the variability somewhat smaller (2.99±0.51, ±17%) compared to the overall survey data. The standard error of the overall survey can be considered a measure of the uncertainty under the assumption that the *RoR* is invariable with source/type and the R_{NH4NO3} for an instrument is a perfect predictor of R_{pRONO2}. A separate manuscript will include further discussions on the *RoR* uncertainty and applications to estimation of the overall nitrate apportionment and concentrations uncertainties.

We recommend the use of the average *RoR* value computed here for future separations of $pRONO_2$ and NH_4NO_3 in ambient aerosol with AMS until there is additional information available to support a different or more complex formulation. On the other hand, where additional constraints on the expected $pRONO_2$ ratio response may be available, a more specific value may be applied. For example, Takeuchi and Ng (2019) measured *RoR*s during dry chamber experiments for different SOA types where only $pRONO_2$ nitrate was generated, and then used those system-specific *RoR*s to separate $pRONO_2$ and NH_4NO_3 during wet experiments where substantial NH_4NO_3 was also formed. We note that in a recent study, Xu et al., (2021) inferred a substantial variability in R_{pRONO2} for ambient measurements on diurnal timescales and with varying pollution levels; however, that relied on comparison of the NO_x^+ ratio method to a newly-proposed method using thermal denuder profiles, which they acknowledge has several potentially large uncertainties or biases that were not quantified.

It is important to emphasize that under strong influence of particle-phase *nitrites* or semi/non-refractory nitrates (e.g., $NaNO_3$, $Ca(NO_3)_2$), quantitative separation of nitrate types may be hindered or simply not feasible (Schroder et al., 2018). As a few studies have reported, nitrites and mineral nitrates produce substantially lower NO_2^+/NO^+ ratios (thus higher *RoR*) in the AMS. For example, *RoR*s of ~10–60 for $NaNO_3$ (Alfarra, 2004; Bruns et al., 2010; Hu et al., 2017b), 17 for $Ca(NO_3)_2$ (Alfarra, 2004), 3.9 for $Mg(NO_3)_2$ (Alfarra, 2004), 9.7 for KNO_3 (Drewnick et al., 2015), and ~300 for $NaNO_2$ (Alfarra, 2004) have been previously reported. We report additional measurements from our laboratory for $NaNO_3$, KNO_3, and KNO_2 showing similarly high values. Table S2 provides additional details and Fig. S4 shows a graphical representation and comparison to $pRONO_2$ for literature reports and our new data. Consequently, even if the expected ratios of other compounds were~~as~~ accurately known, apportioning the different nitrates or nitrites using a formulation like Eq. 1 would be under-constrained, as there would be more unknowns than equations. Therefore, care must be taken to screen for measurements that may be substantially influenced by such interferences (e.g., seasalt, dust). Additionally, during a recent aircraft campaign focused on biomass burning, we conducted regular calibrations with 4-nitrocatechol, a nitroaromatic (Pagonis et al., 2021). The *RoR* was relatively similar to $pRONO_2$ at 3.35 ± 0.81 (1σ, standard deviation) (Table S2, Figs. S4, S5).

4 Evaluation of calibration R_{NH4NO3} and *RoR* using ambient data

A survey of NO_x^+ ratios for multiple field studies is explored here in order to assess the framework of using measured calibration R_{NH4NO3} and a *RoR* to apportion NH_4NO_3 and $pRONO_2$ concentrations. See Sect. S1.1 and Table S3 for details and a summary of all field campaigns for which data is used within this manuscript. Figure 2 shows frequency distributions of $R_{ambient}$ for ambient aerosol from two aircraft-based remote continental (SEAC[4]RS, DC3) and two ground-based forest campaigns (SOAS, BEACHON-RoMBAS). The data is shown as the calibration R_{NH4NO3} divided by $R_{ambient}$, so that all data is comparable. For all campaigns, the large majority of the data fall between the R_{NH4NO3} (1 on Fig. 2, indicating all NH_4NO_3) and the *RoR*-determined R_{pRONO2} (2.75 on Fig. 2, indicating all $pRONO_2$). The small fraction of data outside that range may be due to a combination of instrument noise, drifts in the instrument NO_x^+ ratio response not captured by periodic calibrations, and/or the inability of the fixed *RoR* to perfectly capture the R_{pRONO2} response. However, these results show that under a large range of chemical conditions and instrument R_{NH4NO3} (spanning a factor of 2.4 for these campaign averages), the data are generally consistent with the *RoR* apportionment model. Figure S6 shows the same distributions as Fig. 2, except as simple frequency distributions, rather than weighted by mass concentration as in Fig. 2. The broadening and shift to the right for simple frequency distributions (compared to those weighted by mass concentration), reflect the typical trend that $pRONO_2$ tends to constitute higher fractions of pNO_3 when pNO_3 is lower. Distributions are similar for other campaigns (not shown in Figs. 2, S6), as can be inferred from Figs. 5 and S9, which are discussed below.

The effects of estimating R_{pRONO2} using time-variant vs constant R_{NH4NO3} is explored in Fig. S7. For the SEAC[4]RS campaign, the flight-to-flight calibration R_{NH4NO3} were highly variable due to some instrument instability (range: 0.40–1.49, mean±stdev: 0.80±0.31; Figs. S8, S9e), compared to the very stable ratios measured during the other campaigns (see Fig. 2 caption). Therefore, two histograms are shown overlaid in Fig. S7, one normalized to flight-dependent calibration R_{NH4NO3} and the other normalized to the campaign-averaged R_{NH4NO3}. For the standard frequency distributions (Fig. S7a), there is substantial narrowing when using the flight-dependent ratios, indicating that application of the time-variant ratios provides better constraints on the instrument response to the NH_4NO_3 — $pRONO_2$ mixture. Conversely, normalizing to arbitrary R_{NH4NO3} would be expected to broaden the distribution. The most prominent differences for the mass concentration-weighted distributions (Fig. S7b) are largely due to data with high NH_4NO_3 concentrations where the measured $R_{ambient}$ were beyond the campaign-averaged R_{NH4NO3} (resulting in a substantial fraction of the distribution <1). There is also subtle broadening toward the $pRONO_2$ portion of the distribution. These comparisons support that using the variable calibration R_{NH4NO3} better represents ambient NH_4NO_3 ratios (left side of plots) and tying R_{pRONO2} to R_{NH4NO3} (i.e. using the *RoR* method, rather than fixed R_{pRONO2}) better represents $pRONO_2$ ratios (right side of plot).

Additional support for the practice of using the measured calibration R_{NH4NO3} and anchoring the R_{pRONO2} to those calibrations with a fixed *RoR* can be drawn from the $R_{ambient}$ vs pNO_3 plots shown in Fig. S9a/b. Five studies shown in those figures had relatively constant (within each campaign), but differing (among campaigns; factor of 3.2 range), calibration R_{NH4NO3} (SOAR, MILAGRO, SOAS, BEACHON-RoMBAS, KORUS-AQ; 0.47, 0.84, 0.44, 0.30, 0.97, respectively). However, as pNO_3 increases for the urban-influenced studies (SOAR, MILAGRO, SOAS, KORUS-AQ) or for the oxidation flow reactor (OFR) measurements during SOAS (Fig. S9~~8~~c), $R_{ambient}$ tends to approximately converge at the calibration R_{NH4NO3}. This suggests that NH_4NO_3 in mixed ambient aerosol is well-represented by offline-calibrations for a range of conditions and instruments. Additionally, the corresponding average ratios at the lowest

pNO_3 concentration (same 5 studies in Fig. S9a/b) converge at a similar range of ratios (0.26, 0.52, 0.15, 0.10, 0.40, respectively; range of 4.0). If assuming that the low-pNO_3 observed $R_{ambient}$ approximate pure $pRONO_2$ ratios, a relatively narrower range is computed for an inferred *RoR* (1.6–3.0, factor of 1.9; 2.36±0.63), which is also similar to expected *RoR*s (albeit low possibly due to urban ground studies never sampling pure $pRONO_2$).

Further evidence supporting the use of calibration R_{NH4NO3} and the *RoR* using ambient data is presented in Sect. S2 using campaign datasets where the calibration R_{NH4NO3} showed large variability (DAURE, SEAC^{4}RS campaigns). Exploration of the NO_x^+ ratios vs pNO_3 relationships showed similar relationships to those discussed above for campaigns where R_{NH4NO3} was constant or changed little, but with the curves shifting with the measured R_{NH4NO3}. Similar values of *RoR* to those presented in the literature survey in Sect. 3 were also inferred from the SEAC^{4}RS dataset. Finally, both datasets were used to evaluate biases when using a fixed value of R_{pRONO2} vs estimation of a dynamic value using the *RoR* method. Additional evidence from ambient measurements supporting use of calibration R_{NH4NO3} and the *RoR* is presented in Sect. 5.2 where applications of PMF separation are discussed.

5 Demonstrations of *RoR* apportionment and comparisons to other measurements/methods

5.1 $pRONO_2$ - NH_4NO_3 separation compared to total (gas+particle) $RONO_2$ (Tot-$RONO_2$)

Figure 3 shows time series of AMS $pRONO_2$ and NH_4NO_3 concentrations for a SEAC^{4}RS flight (RF16) in the Southeast US. The nitrate components were apportioned according to Eqs. 2/3 and a *RoR* of 2.75. "Total $RONO_2$" (gas+particle; hereafter Tot-$RONO_2$) concentrations, as measured by thermal dissociation - laser induced fluorescence (TD-LIF) (Day et al., 2002; Perring et al., 2009), are shown for comparison. A wide range of sources were sampled including (and indicated by) biogenic (monoterpenes and/or isoprene and photochemical products such as IEPOX, MVK), anthropogenic (e.g., NO_x, NO_y, aromatics), biomass burning (e.g., acetonitrile and f_{60}, an AMS tracer (Cubison et al., 2011)), likely agricultural, as well as mixtures of these sources or relatively clean free tropospheric air. Flight tracks are shown in Fig. S10 and approximate periods and corresponding source influences are listed in the caption. A large and variable range of pNO_3 was observed (<10 ng m^{-3} or <4 ppt up to ~5 µg m^{-3} or ~1800 ppt) and ranging from $pRONO_2$-dominated to NH_4NO_3-dominated. The $pRONO_2$ and Tot-$RONO_2$ tracked remarkably closely. NH_4NO_3 concentrations exhibited more plume-like behavior, rapidly increasing and decreasing, often while both $pRONO_2$ and Tot-$RONO_2$ remained relatively constant or in some cases showed moderate and similar increases. Overall, $pRONO_2$ was correlated with Tot-$RONO_2$ (R^2=0.49 for all data, R^2=0.69 for data with f_{pRONO2} >0.3) with a regression slope of 0.029 (0.033), indicating that on average ~3% of $RONO_2$ was in the particle phase (Fig. 3, bottom left). NH_4NO_3 showed little overall relationship to Tot-$RONO_2$ beyond the trend that at higher altitudes, well above the boundary layer and outside of plumes, both concentrations tended to be low (Fig. 3, top and bottom right). Note that the reference R_{NH4NO3} in the particle nitrate apportionment here (in Eqs. 2/3) was 0.70 which was based on the measured calibration R_{NH4NO3} and PMF results (see Sect. 5.2 just below). Measured R_{NH4NO3} during calibrations in days bracketing this flight were 0.96 (2 days before) and 0.71 (1 day after). PMF results support a value of 0.70 (see Sect. 5.2.2), which was used here since it was similar to the nearest calibrations and provides an additional constraint on the otherwise variable calibration R_{NH4NO3} characteristic of this campaign (see Sect. 4). Using a higher R_{NH4NO3} increases the $pRONO_2$ vs Tot-$RONO_2$ slope in Fig 4 (bottom left) and can improve the correlation a bit (mainly by moving the low values at low f_{pRONO2} toward the regression line).

Taken together, these observations indicate that the AMS nitrate apportionment method effectively separated $pRONO_3$ and NH_4NO_3 over a large range of concentrations, relative contributions, and source influences. However, it is clear that there are limitations when the f_{pRONO2} is very low (see Sect. 5.2). It would not be surprising if the $pRONO_2$ and Tot-$RONO_2$ showed large variability in relative ratios for different sources and locations, since: 1) $pRONO_2$ is only a small subset of Tot-$RONO_2$ and 2) changes in chemical composition and ambient conditions (e.g., OA concentration, temperature) could have large impacts on gas-particle partitioning. However, in this case those effects do not appear to be large factors (or fortuitously cancel out), which in part may be due to relatively similar temperatures and OA concentrations combined with regionally consistent biogenic chemical sources of $RONO_2$ compounds. Regardless of the exact reasons for the relatively invariant partitioning, it provides an excellent test case, since it would be very unlikely that the strong temporal/spatial correlation would be observed if there were major artifacts in either or both the AMS and TD-LIF methods.

There were no measurements of inorganic nitrate onboard the aircraft with fast enough time resolution to compare with the rapidly changing NH_4NO_3 concentrations calculated from the AMS. Therefore, as a rough indicator of possible changes in the NH_4 related to NH_4NO_3, "Excess NH_4" was calculated as the AMS-measured NH_4 - 1.2 x SO_4 (as molar concentrations). A molar ratio of 1.2 was roughly consistent with the observed ratio when no indications of NH_4NO_3 were present (NH_4=1.2 x SO_4) and substantial concentrations of SO_4 were present, as shown in Fig. S11. That ratio represents a mixture of $(NH_4)_2SO_4$ and ammonium bisulfate or an ammonium balance (NH_{4_Bal}) of ~0.7 (NH_{4_Bal} = molar ratio of $NH_4/(NO_3+2SO_4)$). During periods of elevated NH_4NO_3 concentrations, the measured NH_4NO_3 tracked the estimated "Excess NH_4" very closely with roughly half the concentration (Fig. S11). As suggested by some negative "Excess NH_4" values and the factor of two between NH_4NO_3 and "Excess NH_4", the assumption of constant NH_4/SO_4 ratios based on composition in the absence of NH_4NO_3 is not always valid (and not surprising) and clearly a more sophisticated thermodynamic model would be required to accurately predict NH_4NO_3 concentrations. Nonetheless, the similar features suggest the assignment of NH_4NO_3 is consistent with variations in the other AMS-measured inorganic compounds. The factor of two suggests that ~half of the "Excess NH_4" was associated with sulfate and half with nitrate. During this flight, with the exception of the large biomass burning plume, the elevated NH_4NO_3 concentrations were observed when the aircraft flew at altitudes of ~2000–4000 m and never during the low-altitude (~300–400 m) legs (S20 bottom left/middle). This effect may have been due to the substantially cooler temperatures (0–15°C vs 25–30°C) at those altitudes, favoring partitioning to the particle-phase, since there did not appear to be any clear relationship between NH_4NO_3 and gas-phase HNO_3 (Fig. S11, bottom right). Increases in available NH_3 gas (not measured) could also be a factor (and consistent with both more sulfate- and nitrate-associated ammonium).

Another example for a different flight (RF18) during the SEAC^{4}RS aircraft campaign is shown in Fig. S12, and was also selected due to large relative and absolute variability in calculated $pRONO_2$ and NH_4NO_3 concentrations and diverse source types sampled (see Fig. S13 for flight track and description). Similarly, the $pRONO_2$ and Tot-$RONO_2$ track remarkably well during periods when NH_4NO_3 concentrations are low or elevated and variable, and there is little correlation between NH_4NO_3 and Tot-$RONO_2$. Overall, $pRONO_2$ was correlated with Tot-$RONO_2$ (R^2=0.51 for all data, R^2=0.71 for data with f_{pRONO2}>0.3) with a regression slope of 0.050 (0.068), indicating that on average ~5–7% of $RONO_2$ was in the particle phase (Fig. S12a, bottom left). The measured NH_4NO_3 tracked the estimated "Excess NH_4" reasonably well and showing similar sharp features (and roughly half the concentration; Fig. S12b, top).

In contrast to RF16 discussed above, for RF18 most of the elevated NH_4NO_3 was observed in the warm boundary layer and often coincident with elevated $pRONO_2$ (Fig. S12a,b).

5.2 Positive Matrix Factorization separation of AMS nitrate

5.2.1 Prior studies using PMF for $pRONO_2$ separation

For the vast majority of analyses of AMS data using PMF, only traditional OA ions have been included in the input data matrices. Ions typically associated with nitrate, sulfate, ammonium, and chloride have generally been excluded, with the mindset that they are already separated as unambiguous inorganic species using the standard AMS analyses. However, since organic molecules (e.g., organic nitrates, organosulfates, reduced organic nitrogen) can in fact produce some of the same ions as those inorganic species, inclusion with the OA ions in PMF analysis may allow for separation of inorganic and organic components, as well help identify associations with more well-established source factors.

A few studies have reported results for using PMF of ambient AMS spectra including both the OA and NO_x^+ signals to quantify $pRONO_2$ (and sometimes NH_4NO_3), with mixed results (Sun et al., 2012; Hao et al., 2014; Xu et al., 2015a, 2021; Zhang et al., 2016; Kortelainen et al., 2017; Yu et al., 2019; Zhu et al., 2021). Additionally, a couple other studies have reported results where NO_x^+ ions or calculated $pRONO_2$ (using the NO_x^+ ratio method) are included in PMF analysis, while not explicitly apportioning the inorganic-organic nitrate directly with the PMF results in the laboratory (Tiitta et al., 2016) and field (Kim et al., 2018; Reyes-Villegas et al., 2018). Lin et al. (2021) conducted PMF using only the NO_x^+ ions and nitro-polycyclic aromatic hydrocarbon (NPAH) ions. Details and discussions of those studies are presented in Sect. S3 and key results are summarized in Table S4, as related to the PMF analyses.

5.2.2 New results for PMF separation of $pRONO_2$ and comparison to *RoR* method

We conducted PMF on the combined OA and NO_x^+ ion time series for the same two flights from the SEAC[4]RS campaign (as discussed above in Sect. 5.1; RF16, RF18) to test PMF separation of nitrates and the information it can provide, explore strategies, and compare to the *RoR* method. Details and an extended discussion of that analysis is documented in Sect. S4 and key results are summarized in Table S4 alongside previous published analyses. A brief summary is provided here.

As discussed in Sect. 5.1, those two flights included sampling of a wide range of source types and concentrations. PMF was conducted initially on 1-s data; however, although robust overall factors were separated, results suggested that the S/N was not adequate to apportion the NO_x^+ ions to secondary factors at ratios that reflected $pRONO_2$ ratios. Therefore, all analyses discussed here are from 1-min measurements (which were more effective). Several strategies were used to explore the separation of OA, nitrate, and the NO_x^+ ratios (in separate and combined factors), including: number of factors, rotations (varying FPEAK), upweighting and downweighting NO_x^+ ions, bootstrapping, seeding, constraining NO_x^+ ratios, and removing large biomass burning plumes. For both flights, five factors were robustly separated: NH_4NO_3, BBOA (biomass burning OA), IEPOX-SOA (IEPOX-derived SOA), LO-OOA (less-oxidized oxygenated OA), and MO-OOA (more-oxidized OOA) (Figs. S14–S28). See the Glossary and Sects. S3/S4 for more details on factor types. Generally, the best separations with the most information were for FPEAK at or near 0, using standard NO_x^+ ion S/N (no downweighting/upweighting), not constraining NO_x^+ ratios, not removing any plume data, and using bootstrapping to extract averages and assess uncertainty/robustness.

The NH_4NO_3 factors and the BBOA factors had very similar NO_x^+ ratios that were consistent with calibration R_{NH4NO3}, with little variability across the 100 bootstrapping runs (Figs. S17, S25). While the apportionment of nitrate between the NH_4NO_3 and BBOA factors was very consistent across bootstrapping runs, changes in FPEAK had large effects on that relative apportionment as well as the amount of OA ions in the NH_4NO_3 factor spectrum. For the OOA/SOA factors (IEPOX-SOA, LO-OOA, and MO-OOA) the NO_x^+ ratios for LO-OOA and the combination of all three factors were consistent with expected $pRONO_2$ NO_x^+ ratios using the *RoR* (Figs. S17, S25). Across bootstrapping runs, there was modest variability for those ratios (Figs. S17, S25), including some solutions where the LO-OOA had only NO^+ (but not for the combined OAA/SOA factor). The averages and standard deviations of the NO_x^+ ratios for the combined OOA/SOA factor are included in the survey of $pRONO_2$ *RoR*s (Fig. 1, Table S1). For calculation of NH_4NO_3 and $pRONO_2$ concentrations, the nitrate contributions from the NH_4NO_3 and BBOA factors were summed as were the three OOA/SOA factors, respectively. The majority of the $pRONO_2$ was contributed by the LO-OOA factor, followed by MO-OOA and then IEPOX-SOA (Figs. S18, S27). The variability in the factor spectra NO_x^+ ratios and nitrate concentration apportionment across bootstrapping tended to follow the same trend (higher variability for factors with lower $pRONO_2$ contribution; e.g., Figs. S17, S18a, S25, S27). Additionally, substantial trends were observed between factor spectra NO_x^+ ratios and the amount of nitrate apportioned to that factor for some OOA/SOA factors. Bootstrapping and exploration of FPEAK was useful to investigate those dependencies.

Comparisons of NH_4NO_3 and $pRONO_2$ concentrations using the *RoR* and PMF methods are shown for each flight in Figs. 4 and S12a as time series and scatter plots. For both flights there is very good agreement (near unity slope, 0.99–1.04, and R^2>0.99) between methods for NH_4NO_3, certainly in part due to the dominance of NH_4NO_3 during higher concentrations periods. There is reasonable agreement for $pRONO_2$ (slopes of 0.86–1.50, R^2 of 0.51–0.65 depending of the flight and fitting method; and improved to slopes of 1.04–1.42, R^2 of 0.68–0.84 for f_{pRONO2}>0.3) but with notable differences. $pRONO_2$ concentrations tended to be noisier for the *RoR* method compared to the PMF method when nitrate was dominated by NH_4NO_3 or when pNO_3 was very low. This may be due to the additional S/N and constraints that the inclusion of the other OA ions provide, as well as the sensitivity (for both precision and accuracy) of apportionment for the *RoR* method when ratios approach the R_{NH4NO3} limit. On the other hand, the PMF method may dampen some real variability due to the fact that the factor spectra are fixed and cannot chemically evolve in the PMF model. In order to assess the true accuracy of either method, an independent and reliable determination of $pRONO_2$ would be required. Finally, the comparison between the PMF-determined $pRONO_2$ and the TD-LIF Tot-$RONO_2$ showed substantially-improved correlation (compared to using the *RoR* method) for one of the two flights (Fig. 4 vs 3).

5.2.3 Summary of PMF method for nitrate separation

The results from our investigation of PMF and analyses described in the literature summarized above highlight some general aspects, as well as some potential advantages and disadvantages of using PMF to apportion nitrate between organic and inorganic. One major potential advantage is that with PMF, the nitrates can be immediately associated with different source factors. On the other hand, the NO_x^+ ratio method can be used first and then correlations of nitrates with OA-only factors can be explored and even apportioned. PMF may provide additional resolving power and S/N by inclusion of associated OA ions, potentially more precisely separating nitrate concentrations, especially when either $pRONO_2$ or NH_4NO_3 dominate the nitrate. Also, prior knowledge of the NO_x^+ ratio for NH_4NO_3 (or $pRONO_2$) may not be necessary if the ratios are robustly resolved with PMF. Additionally, the NO_x^+ ratios resolved for PMF

factors is a product for exploring ratios for ambient aerosol response, and validating application of offline calibration R_{NH4NO3} and *RoR*s derived largely from laboratory studies. PMF may also be useful in separating other species that produce NO_x^+ ions (e.g. nitrites, nitro-organics, mineral nitrates), from just NH_4NO_3 and $pRONO_2$, when they are present and have a unique NO_x^+ ratio.

Some potential drawbacks or cautionary aspects are as follows. Since the PMF model requires fixed profile spectra, this means that nitrate-to-OA ratios are fixed for each factor. Therefore, if this ratio is in fact substantially variable over the period/space of analysis, for example driven by processes such as $pRONO_2$ hydrolysis or gas-particle partitioning, substantial biases or uncertainties in nitrate apportionment can be introduced. While consideration of additional factors could help mitigate such effects, PMF is not designed to concisely separate profiles that are a continuum. Sometimes factors with clear NH_4NO_3 or $pRONO_2$ NO_x^+ ratio signatures are not resolved. We suspect that datasets where neither type of nitrate is dominant for some periods may be more susceptible to that issue; however, those issues may sometimes be resolvable with more extensive investigation with available PMF exploration tools (e.g., seeding, bootstrapping, FPEAK, constraining a NH_4NO_3 factor from offline calibrations). Otherwise, apportioning nitrate using results with profile spectra that do not have clear nitrate signatures may introduce large uncertainties which are difficult to estimate. Variable NO_x^+ ratios due to instrument drifts or changes (e.g., vaporizer bias voltage drifts or tuning) may lead to uncertainty in nitrate apportionment since PMF computes fixed factor spectra. In practice, for using the NO_x^+ ratio method this is not problematic, as long as regular offline NH_4NO_3 calibrations were performed. For PMF, separating the dataset into periods where the NO_x^+ ratio was stable/constant and performing PMF separately for each period is one option to mitigate instrument drift issues; however, this can be very laborious if the dataset requires separate analysis of multiple periods. Another option may be to apply the "rolling method" recently made available with ME-2/SoFi, where a sub-window is moved across the PMF input along the time coordinate, allowing factor profiles to vary with each sub-window shift (Canonaco et al., 2021). Theoretically, offline calibration ratios of NH_4NO_3 may not be necessary for such application, although they would be preferable to have for validation.

A few other notable trends and observations are as follows (with details provided in Sect. S3, S4). PMF-resolved $pRONO_2$ often tends to have the largest contribution from (and association with) LO-OOA/SV-OOA, followed by MO-OOA/LV-OOA, especially for biogenically-influenced locations (Sun et al., 2012; Hao et al., 2014; Xu et al., 2015a; Zhang et al., 2016; Kortelainen et al., 2017; Yu et al., 2019; Sect. S3, Table S4). That is consistent with $pRONO_2$ forming in fresh SOA (i.e. LO-OOA/SV-OOA) and being partly lost as the OA ages and/or MO-OOA/LV-OOA consisting of a mix of aged OA, some of which was not associated with $pRONO_2$. Nitrate associated with aged ambient BBOA can~~ends to~~ be domina~~tedly~~ted by NH_4NO_3 (shown with aircraft data with PMF in this study, and discussed more broadly in Nault et al. (2021)); however, primary and secondary $pRONO_2$ (or other oxidized organic nitrogen) associated with BBOA emission has been reported in the laboratory and field, sometimes as large contributions (Tiitta et al., 2016; Reyes-Villegas et al., 2018; McClure et al., 2020; Lin et al., 2021). When NH_4NO_3 factors are resolved, they tend to contain substantial contributions (~~20~~15–80%) of OA (non-NO_x^+) ions (Sun et al., 2012; Hao et al., 2014; Xu et al., 2015a; Zhang et al., 2016; Kortelainen et al., 2017). Generally, those non-NO_x^+ contributions seem to be higher for strongly biogenically-influenced measurements and less so during cooler wintertime periods when NH_4NO_3 comprises a larger fraction of nitrates (Xu et al., 2015a; this study). Our experience through exploration of various approaches (e.g., upweighting the NO_x^+ ions, increasingly positive FPEAK, increasing number of factors) suggests that efforts at "cleaning" the NH_4NO_3 factor tends to be ineffective and/or lead to degradation of

Commented [3]: references added

Commented [4]: references added

Commented [5]: references added

Commented [6]: references added

the overall PMF solutions. Since the OA contained in the NH_4NO_3 tends to not be a large overall fraction of the OA, this does not appear to be a major issue. Finally, evidence suggests that inclusion of NO_x^+ ions in PMF does not tend to have much influence on overall OA-dominated factors (factor spectra nor concentration time series), which is not surprising given that their overall contribution to the S/N among the many OA ions is fairly small. Consequently, there does not appear to be any drawbacks or complications associated with also including NO_x^+ ions when running PMF on AMS data.

Overall, PMF appears to be a useful tool for apportioning nitrates and investigating their associations with sources. The case for quantitative apportionment of nitrate with PMF is strongly bolstered when the NO_x^+ ratios resolved for both the NH_4NO_3 factor and separate or combined $pRONO_2$-associated factors are similar to NH_4NO_3 calibration and expected $pRONO_2$ NO_x^+ ratios. When those criteria are not met, using the NO_x^+ ratio method may be better, as it is likely less prone to such biases or ambiguities, and uncertainties can be better defined.

5.3 Comparison of $pRONO_2$ quantification with AMS and other instruments in the lab and field

Several studies have reported quantitative comparisons of $pRONO_2$ concentrations, as measured by AMS vs other instrumental methods (alternate AMS-based methods, FTIR, TD-(LIF/CRDS/CAPS), and FIGAERO-CIMS). Section S5 provides details and discussions and Table S5 presents a summary of key aspects of those comparisons. Overall, those comparisons show good agreement in most cases (1:1 within known uncertainties) and substantial differences in a few cases (factors up to 2–4). In some of the cases where substantial differences were observed, possible explanations were discussed and sometimes explored. There do not appear to be any consistent reasons for the differences. In some of the field comparisons and all of the laboratory experiments, the nitrate sampled was dominated by (or exclusively) $pRONO_2$, and thus largely serve as a test of $pRONO_2$ quantification (general calibration/quantification factors, RIE, collection efficiency, etc.). Consequently, taken together the evidence available does not support use of an RIE for $pRONO_2$ quantification with AMS that is significantly different from that measured for (and regularly calibrated with) NH_4NO_3. In order to narrow the uncertainties in $pRONO_2$ quantification (in the field and laboratory), controlled laboratory-based intercomparisons of total and speciated organic nitrates using AMS and other methods are needed.

6 Physical basis for NO_x^+ ratios observed for nitrate types and variability among instruments

As Farmer et al. (2010) points out, it is probable that a large fraction of $RONO_2$ molecules thermally decompose to RO and NO_2 at the AMS vaporizer after which NO_2 gas is ionized. For example, the TD-LIF technique (and CRDS/CAPS equivalent methods) rely on quantitative thermal dissociation of $RONO_2$ to NO_2 in the gas phase, which occurs at ~350 °C in ~50 ms at near ambient pressures (Day et al., 2002). The timescale of evaporation/decomposition/ionization/detection for the AMS are on order tens of μs (Drewnick et al., 2015; Jimenez et al., 2016); however, at 600°C the dissociation rate coefficient for $pRONO_2$ is ~4 orders of magnitude larger (compared to 350 °C). That said, it is not clear what the pressures or temperatures of the gases are in the evaporation plume. Nevertheless, Farmer et al. note that thermal decomposition of $pRONO_2$ to NO_2 in the AMS would be consistent with the higher NO^+/NO_2^+ ratios observed for $pRONO_2$ than NH_4NO_3. Their reasoning is that reported ratios of NO_2 gas ionization (3.0) are substantially higher than those reported for HNO_3 (0.5) gas as well as their measurements of particle-phase NH_4NO_3. Using the simplest assumption that only NO_2 (from $RONO_2$ thermal decomposition) and HNO_3 (from NH_4NO_3 evaporation) are ionized would yield a *RoR* of 6, which is double that observed. Moreover, fixed values would be expected for $pRONO_2$ and NH_4NO_3 rather than

the observed range of ~4. Clearly, the behavior is more complicated than this simple model. Given that mass discrimination (ion transmission or detector efficiency differences) for the *m/z* range of the NO^+ and NO_2^+ ions is expected to be minor for the AMS (Hu et al., 2017b), the values and variability in NO_x^+ ratios likely originate in the vaporizer and/or ionizer region. As discussed in Hu et al. (2017b), the values and range of NO_x^+ ratios observed for NH_4NO_3 (combined with other observations) are consistent with EI from a combination of HNO_3, NO_2, and NO gases that are formed through thermal decomposition. They show the greatly-enhanced importance of such neutral gas-phase decomposition for measurements where a "capture vaporizer" is substituted for the standard AMS vaporizer. The capture vaporizer has a different geometry (optimized for limiting particle bounce) that results in longer gas-phase residence time near the hot vaporizer surfaces. Consequently, an order of magnitude lower NO_2^+/NO^+ ratio is observed for NH_4NO_3 (0.04–0.07), likely due to a shift in ionization toward primarily NO gas. Similar thermal decomposition processes would be expected for $RONO_2$. However, thermal decomposition to RO and NO_2 may occur much faster and always to near completion, given the thermal instability of the O-NO_2 bond and near absence of $C_xH_yO_zN^+$ fragments in AMS $pRONO_2$ spectra (Farmer et al., 2010). Hu et al. (2017a) report a large reduction in the NO_2^+/NO^+ ratios for $pRONO_2$ when using the capture vaporizer compared to the standard vaporizer (with a $pRONO_2$ ratio ten times lower than for NH_4NO_3 with the capture vaporizer).

As shown in Drewnick et al. (2015) and Jimenez et al. (2016), single-particle detection timescales for ions when sampling NH_4NO_3 show a range of a factor of two (and ~25 μs differences), primarily with NO^+ being longer than NO_2^+ and NH_x^+ ions. Those observations are interpreted as evidence for additional processes occurring at longer timescales than flash vaporization at the nominal temperature such as vaporization at lower effective temperatures, slower vaporization or thermal decomposition, and adsorption/desorption from ionizer surfaces. They also showed that the signal-particle detection timescales were insensitive to vaporizer temperatures above 300°C. On the other hand, Hu et al. (2017b) showed a small dependence of the R_{NH4NO3} on vaporizer temperature decreasing by 25% from 200°C to 800°C, consistent with more thermal decomposition to NO_2 and NO gases. Other studies have reported no dependence of NO_x^+ ratios on vaporizer temperature (~200–600°C) for $pRONO_2$-containing chamber SOA (Fry et al., 2009) or ambient (mixed nitrate) aerosol (Docherty et al., 2015). Overall, these observations point toward the timescales of interaction, and effects of spatial distribution of competing processes, playing a more important role in affecting observed ion ratios, rather than vaporizer temperature. In part, this relative insensitivity to vaporizer temperature may be because the physical process of particle vaporization occurs at lower temperature than the nominal vaporizer temperature due to evaporative cooling (Saleh et al., 2017). Another observation that Hu et al. reported for using the capture vaporizer was that the vaporization timescales (based on UMR PToF distributions) for NO^+ was much longer than for NO_2^+ for NH_4NO_3, but the reverse for $pRONO_2$. Such apparent spatiotemporal differences in thermal decomposition and ionization could potentially be used as another method for differentiating nitrates. However, low S/N of NO_2^+, differences in sizes and broader distributions for ambient aerosol nitrates, and the possibility that some of the differences Hu et al. observed were from $CH_2O_x^+$, may seriously limit such approach and would require further evaluation (using HR-PToF).

A few other evaluations of R_{NH4NO3}, described in Hu et al., (2017b) (using the standard vaporizer), showed dependencies of NO_x^+ ratios of only <20% including varying the location on which particles impact the vaporizer (by horizontally translating the aerodynamic lens position) and varying the vaporizer bias voltage over ranges expected for typical AMS operation. On the other hand, varying the vaporizer bias voltage over a wider range, such as slightly beyond the settings where the aerosol signal peaks and

where the gaseous "airbeam" signal peaks, can result in nearly a factor of two shift in the R_{NH4NO3} (Fig. S29). This behavior reflects the ability of the vaporizer bias voltage tuning to preferentially sample ions produced in different regions of the ionizer. It has also been shown for the signals of other ions, such as CO_2^+ (Jayne et al., 2015). While proper tuning of the AMS vaporizer bias voltage typically aims at optimizing the aerosol signal, that may not always be performed by AMS operators and likely in some cases the airbeam signal may be optimized instead (which can be different than the particle signal peak as in Fig. S29, although not always). Therefore, variability in this tuning parameter may explain a substantial fraction of the range in NH_4NO_3 (and possibly $pRONO_2$) NO_x^+ ratios shown in Fig. 1. Another effect that appears to be able to substantially alter the NO_x^+ ratios is related to exposure to high concentrations of OA for extended periods, possibly coating the vaporizer (and is possibly related to the "Pieber Effect" where nitrate aerosol produces CO_2^+ signal from interactions at the vaporizer surface), and will be discussed in a future publication. Taking all the evidence available at present, the range in NO_x^+ ratios for NH_4NO_3 and $pRONO_2$ among instruments, settings, and operating conditions appears to be driven by changes in the amount of chemical decomposition and the overlap of those products with the ionizing electron beam. This aspect highlights the importance of periodic measurement of the NO_x^+ ratios with a standard (i.e., NH_4NO_3), especially after making significant instrument changes, when quantifying $pRONO_2$ and NH_4NO_3 with the AMS.

7 Multisite survey of inorganic/organic nitrate fractionation

An overview of the inorganic vs organic nitrate apportionment for all of the campaigns discussed in this manuscript is shown in Fig. 5. The apportionment was conducted using the *RoR* method. The campaigns span: late-winter to summer across the northern hemisphere and wet/dry seasons near the equator; from ground level to the upper troposphere; and urban to remote locations. Overall, the f_{pRONO2} shows an inverse relationship with the pNO_3, approaching 100% at low pNO_3, primarily at rural/remote locations. At high pNO_3 and strongly urban-influenced locations, the nitrate is dominantly NH_4NO_3. However, urban and urban-influenced locations can often exceed 50% contributions from $pRONO_2$, when pNO_3 is lower (<1–2 μg m^{-3}). At the urban ground sites (MILAGRO, SOAR), the modulation of the variability in pNO_3 tended to be driven by large increases in NH_4NO_3 from photochemical production of HNO_3 during morning to early afternoon, followed by evaporation at higher temperatures during afternoon driving concentrations to minima that were generally sustained through nighttime (Aiken et al., 2009; Docherty et al., 2011). At the rural/remote sites, nitrate is nearly always dominated by $pRONO_2$ and with low concentrations. At the mid-latitude sites (BEACHON, SOAS), a large contribution to the variability in concentrations was attributed to nighttime production of $pRONO_2$ from BVOC (Fry et al., 2013; Xu et al., 2015b). For the Amazon studies, substantial variability was observed on sub-day and synoptic timescales, especially during the lower-concentration wet season measurements, with episodic elevated inorganic contributions (de Sá et al., 2018, 2019). Thus, variability may have largely been driven by transport changes and large-scale regional processes; however, the factors controlling particle-phase nitrate for those studies have not been thoroughly explored. For DAURE, an urban-downwind site with high pNO_3, consistent diurnal patterns were not observed, and pNO_3 variability was likely dominantly driven by variability in transport (Minguillon´ et al., 2011; Zhang and Jimenez, 2021).

The aircraft campaigns span the entire range of the urban and rural/remote sites combined, since they include urban and biomass burning sampling, as well as rural/remote and free tropospheric sampling. However, there are notable differences among them and compared to ground-based studies. A major difference is the shift toward lower f_{pRONO2} or pNO_3 in the intermediate ranges by factors of ~2 or ~10,

respectively. The large divergence as pNO_3 decreases from ~2 to ~0.2 μg m^{-3} coincides with the range where the aircraft measurements show NH_{4_Bal} transitions from balanced (NH_{4_Bal} ~ 1) to a modest deficit in ammonium (NH_{4_Bal} ~ 0.75–0.9) (see Fig. S30). Lower NH_{4_Bal} can be indicative of more acidic aerosol (Nault et al., 2021; Schueneman et al., 2021), making particle-phase NH_4NO_3 less thermodynamically stable. In comparison, the NH_{4_Bal} for the ground-based urban-influenced studies, (SOAR, MILAGRO, DAURE) were consistently near unity (Aiken et al., 2009; Docherty et al., 2011; this work for DAURE, not shown). However, such effects alone would result in higher f_{pRONO2} in the aircraft studies, not lower as observed, due to sulfate not balanced by ammonium and acidity making ammonium nitrate thermodynamically unstable. Therefore, other factors must be at play, such as very different sources being sampled, lower temperatures and higher RH for the aircraft measurements (making NH_4NO_3 more thermodynamically stable; see Sect. 5.1, Fig. S11), dilution shifting the curves, or higher acidity shortening the lifetime of $pRONO_2$ (such as accelerating hydrolysis). At the lower range of pNO_3 (<0.2 μg m^{-3}) the f_{pRONO2} is substantially different following the order KORUS < DC3 < SEAC^{4}RS. Considering again the NH_{4_Bal} (Fig. S30), for SEAC^{4}RS the aerosol inorganics are much less balanced by ammonium (NH_{4_Bal} ~ 0.08–0.75) compared to DC3 (NH_{4_Bal} ~ 0.5–0.8) and KORUS (NH_{4_Bal} ~ 0.5–0.9) at the lower pNO_3 range, suggesting a possible role of acidity and NH_3 availability. On the other hand, it does not appear that acidity plays a dominant role in favoring the high f_{pRONO2} at the rural/remote ground-based studies, as BEACHON tended to be fully balanced ($NH_{4\_Bal} \geq 0.9$) while SOAS was not (NH_{4_Bal} ~ 0.5–0.7) (Fry et al., 2013; Hu et al., 2016).

Many different chemical and physicochemical processes interplay to control the concentrations and relative proportions of NH_4NO_3 and $pRONO_2$ in the atmosphere. Fig. 6 shows a schematic of those key processes. The differentiation can be viewed as effectively beginning with the branching of the radical-radical reaction of NO_x with OH vs RO_2 or VOCs ($NO+RO_2$, $NO_2+RC(O)O_2$, $NO_3+RC=CR´$) to produce gas-phase HNO_3 vs $RONO_2$. The relative amount of these pathways can vary widely, in large part controlled by relative amounts of NO_x concentrations compared to VOC reactivity; the $RONO_2$ formation pathway can become dominant below modest NO_x concentrations, particularly at biogenically-influenced rural sites (e.g., Browne and Cohen, 2012; Romer, 2018). However, the partitioning of HNO_3 and $RONO_2$ into the particle phase can depend on numerous factors such as NH_3 availability, RH, temperature, particle acidity, $RONO_2$ volatility, or OA concentrations. Subsequent chemical, photochemical, evaporation, and deposition losses of gas and particle components will also exert controls on concentrations and lifetimes. In large part, the general trend shown in Fig. 5, over more than three orders of magnitude pNO_3, may be driven by the ability of HNO_3 formation in the presence of sufficient NH_3 at increasing pollutions levels (i.e., NO_x) to overwhelm more modest $pRONO_2$ formation, combined with the high volatility of NH_4NO_3 prone to evaporation upon dilution. In contrast, at rural and remote locations, the formation of $RONO_2$ becomes more favorable, producing $pRONO_2$ of which a substantial portion is not prone to rapid chemical or evaporative loss, thus dominating widespread background nitrate composition. However, this is a very simplified picture of the complex processes at play and more detailed investigations combining corresponding measurements with modeling to better understand the dominant processes controlling the trends shown in Fig. 5 are needed. In a recent study of eleven aircraft campaigns from throughout the globe, Nault et al. (2021) showed overall trends of decreasing pH and NH_{4_Bal} with remoteness (as indicated by decreasing total inorganic PM_1), which was not well-represented in many current models. While there may be some connections between that phenomena and the one shown in Fig. 5 (e.g., via acidity and NH_3 availability), inorganic PM_1 concentration is more closely related to remoteness than pNO_3, as it is often dominated by sulfate, which is less chemically reactive and

less volatile than $pRONO_2$ and NH_4NO_3, and its formation is less coupled to VOC conditions. For a ground-based study in a Chinese megacity during fall, a strong trend of increasing inorganic fraction of pNO_3 with increasing calculated aerosol pH (pH=1.5-3.5) was observed, which was attributed to numerous coincident factors during pollution episodes favoring NH_4NO_3 precursor availability and gas-to-particle partitioning (Chen et al., 2021).

We note that the data included in Fig. 5 are generally weighted toward warmer periods or regions. Xu et al. (2015a) reported wintertime (within Nov-Feb) measurements of organic and inorganic nitrate at two urban and one rural site in the southeast US. Campaign averages of pNO_3 ranged 0.8–1.4 μg m^{-3} (with 1σ variability of ±90–100%) and average f_{pRONO2} was 0–30% across the sites and the apportionment methods considered. pNO_3 and inorganic nitrate showed strong diurnal cycles, peaking mid-morning with minima mid-to-late afternoon. Nitrate apportionment vs pNO_3 was not reported, so it is unclear if similar trends to those in Fig. 5 were present (e.g., if f_{pRONO2} increased during afternoon pNO_3 minima). However, on average all three campaigns fell in the chemical coordinate space of the urban-influenced studies shown in Fig. 5. The fact that the rural site was similar to the urban sites may be due to the cooler winter temperature (and higher RH) as well as reduced biogenic influences, compared to warm rural studies shown in Fig. 5. A few other studies have shown AMS data as supplementary material, that suggest similar relationships to those in Fig. 5 for individual studies. Those include plots of NO^+ vs NO_2^+ ions which appear to have higher ratios of NO^+/NO_2^+ at lower signals (Docherty et al., 2015; Zhou et al., 2016) or decreasing NO_2^+/NO^+ ratios with decreasing pNO_3 (Kiendler-Scharr et al., 2016). Additionally, a recent analysis of three datasets in the North China Plain (urban summer/winter, rural winter), showed a strong decreasing trend in f_{pRONO2} vs PM_1 during the urban summer measurements and weak trends for the wintertime measurements (and lower overall f_{pRONO2}) (Xu et al., 2021). Those observations are generally consistent with the trends with pNO_3 during summer and with seasonality discussed above.

8 Further discussion of the efficacy and support for NO_x^+ ratio apportionment

From simply inspecting the relationships of f_{pRONO2} and NO_x^+ ratios vs pNO_3 in Figs. 5 and S9, or the variability of ratios shown in Fig. 2, it could be postulated that such trends could simply be driven by changing pNO_3 concentrations or some other confounding factor such as matrix effects. Thus, here we review several pieces of evidence presented in this manuscript and prior literature that, taken together, provide overwhelming support that the variability of measured $R_{ambient}$ between the calibrated R_{NH4NO3} and the *RoR*-derived R_{pRONO2} values is dominantly controlled by the continuum of inorganic/organic nitrate contributions. We emphasize that this discussion is relevant only to conditions where refractory nitrates ($NaNO_3$, $Ca(NO_3)_2$, e.g., from dust or seasalt) or nitrites are not substantial components of the aerosol, since they produce different NO_x^+ ratios and the apportionment equation becomes underconstrained.

Kiendler-Sharr et al., (2016) present laboratory data of NO_x^+ ratios for over a range of NH_4NO_3 concentrations and mixtures (Sect. S1, Fig. S1 in that paper). They conclude that "fragmentation behaviour as a function of mass concentration, composition of the particles and particle size of NH_4NO_3 and mixtures of NH_4NO_3 with $(NH_4)_2SO_4$ and glutaric acid, were observed to be constant, independent of mass concentration down to 0.1 μg/m^3 in the laboratory aerosol". We regularly generate scatterplots of the two NO_x^+ ions over a range of NH_4NO_3 concentrations recorded during calibrations. This is the typical method we use and recommend for quantifying the R_{NH4NO3} and inspecting for any irregularity in the relationships (such as non-linearity). The insensitivity of R_{NH4NO3} with concentration is a consistent feature. We have systematically explored concentration and matrix effects of NH_4NO_3 and $pRONO_2$ in the laboratory and with field data and show that under typical ambient conditions, effects, if present, are

small. This will be presented as part of a future manuscript exploring the uncertainties of these apportionment and quantifications methods. We note that this result contrasts with a similar study that assessed the viability of apportioning inorganic and organic sulfate using $H_ySO_x^+$ and SO_x^+ ion ratios (Schueneman et al., 2021). Strong dependencies on aerosol composition (i.e. acidity and nitrate mass fraction, but generally not OA concentration) were found for those ions, making sulfate apportionment not possible under a substantial fraction of conditions found in the atmosphere.

Inspection of the NO_x^+ ratios vs pNO_3 shown in Fig. S9a for the three urban field studies shows that ratios generally plateau at R_{NH4NO3} when the nitrate is only ~30% of the bulk aerosol — and thus still dominated by other compounds — supporting that mixing with other complex ambient components does not alter the NO_x^+ ratio produced from NH_4NO_3. Furthermore, at lower pNO_3, NO_x^+ ratios for all campaigns generally approach expected $pRONO_2$ ratios. While this certainly does not prove that at the lower pNO_3 range, the nitrates are primarily organic, and primarily NH_4NO_3 at the higher pNO_3 range, such consistent behavior would be highly coincidental. We also point to the comparisons of AMS-apportioned $pRONO_2$ with independent measurements of total $RONO_2$, shown in Figs. 3, S12a. There is a high level of tracking between the two independent organic nitrate components, while flying through intermittent elevated nitrate plumes, which were sometimes correlated with elevated OA while in other cases not (Figs. S11, S12b). This provides strong evidence that the use of NO_x^+ ratios are indeed effectively apportioning nitrate, and changing non-nitrate fractions are not hindering the method. Similarly, the apportioned NH_4NO_3 tracks well with estimates of NH_4 not associated with sulfate for those same aircraft flights (Figs. S11, S12b).

Finally, the exploration of NO_x^+ ratio apportionment with PMF, shows the distinct signature of $pRONO_2$ NO_x^+ ratios for secondary OA factors and that of NH_4NO_3 for the other components (Figs. S17, S25). That result would be highly unlikely if the continuum of NO_x^+ ratios in the total aerosol were dominantly controlled by concentration or matrix artifacts. While this preponderance of evidence strongly supports the effectiveness of this method, further laboratory and field data studies and analyses, including instrument comparisons, should be conducted to better constrain uncertainties and improve the method.

9~~8~~ Conclusions

We have explored the viability of using the NO_x^+ ion ratios produced in the AMS spectrum from nitrates to separate and quantify NH_4NO_3 and $pRONO_2$ concentrations in ambient aerosols. The use of NH_4NO_3 calibration NO_x^+ ratios and an inferred NO_x^+ ratio for $pRONO_2$ that tracks the NH_4NO_3 ratio ("Ratio-of-Ratios") is investigated and tested. An extensive range of data and approaches are utilized for this investigation including: a diverse collection of ambient field datasets, chamber studies, oxidation flow reactors, pure compounds, comparisons to AMS PMF methods and other $pRONO_2$ or related measurements, and a compilation of a broad literature survey.

It is shown that the method is robust and effective under typical ambient sampling conditions. Methods and practical considerations for calculating concentrations are described. The Ratio-of-Ratios NO_x^+ ratio method produced similar results to conducting PMF on the expanded mass spectra series (including both OA and NO_x^+ ions) to apportion nitrates. While using the PMF method may have advantages of improved signal-to-noise and can provide connections between $pRONO_2$ and OA sources, it is much more labor-intensive and can lead to substantial biases if not explored and applied carefully.

A broad survey of nitrate apportionment shows a pervasive relationship of increasing (decreasing) $pRONO_2$ relative contributions to nitrate with decreasing (increasing) total nitrate concentrations. Those

trends generally follow from urban-influenced to rural/remote regions. However, there are some clear differences in those trends between different sampling regions and conditions.

Previous studies reporting nitrate quantification using AMS NO_x^+ ratios (or PMF using NO_x^+ ions) have employed a range different approaches and assumptions, based on generally limited information. In some instances, likely substantial biases were present and rarely has the accuracy of the results been considered. This investigation will help provide a more consistent, accurate and transparent approach to quantification and exploration of bulk particle-phase nitrates in the atmosphere with AMS (and related instrumentation). Comparisons of this method to other instrumentation capable of quantifying bulk or speciated particle-phase organic nitrates, in the laboratory and field, should be an ongoing focus to help better constrain uncertainties, identify biases, and improve this method (and others).

Data availability

Data from the field campaigns are archived as follows: for the NASA airborne campaigns (DC3, SEAC^{4}RS, KORUS-AQ) at https://www-air.larc.nasa.gov/index.html (see "missions"); for SOAS at https://data.eol.ucar.edu/project/SAS; for BEACHON-RoMBAS at http://manitou.acom.ucar.edu/#data; for DAURE (and also for AMS data from other ground-based campaigns) at https://sites.google.com/site/amsglobaldatabase; for SOAR at http://cires.colorado.edu/jimenez-group/Field_Data/SOAR_1/SOAR%20data; for MILAGRO at https://www.eol.ucar.edu/field_projects/milagro; and for GoAmazon at https://www.arm.gov/research/campaigns/amf2014goamazon. All figures presented in the manuscript and data used to construct them are archived at http://cires1.colorado.edu/jimenez/group_pubs.html. Additional data used for or generated during intermediate stages of the analysis are archived on a data server at the University of Colorado and can be provided upon request by the corresponding authors.

Author contributions

DAD, PCJ, and JLJ designed the analysis; DAD, BAN, PCJ, and JLJ wrote the paper; All authors collected and analyzed data; All authors reviewed and provided comments for the paper.

Competing interests

The authors declare that they have no conflict of interest.

Acknowledgements

This research was supported by NASA grants 80NSSC18K0630 and 80NSSC19K0124, as well as US NSF grant NSF AGS-1822664, NOAA grant NA18OAR4310113. BBP acknowledges support from a US EPA STAR Graduate Fellowship (FP-91761701-0). This work has not been formally reviewed by the US EPA. The views expressed are solely those of the authors, and the US EPA does not endorse any products or commercial services mentioned in this work. We thank John Crounse and Paul Wennberg (Caltech) for use of nitric acid measurements in Figs. S11, S12.

Figures

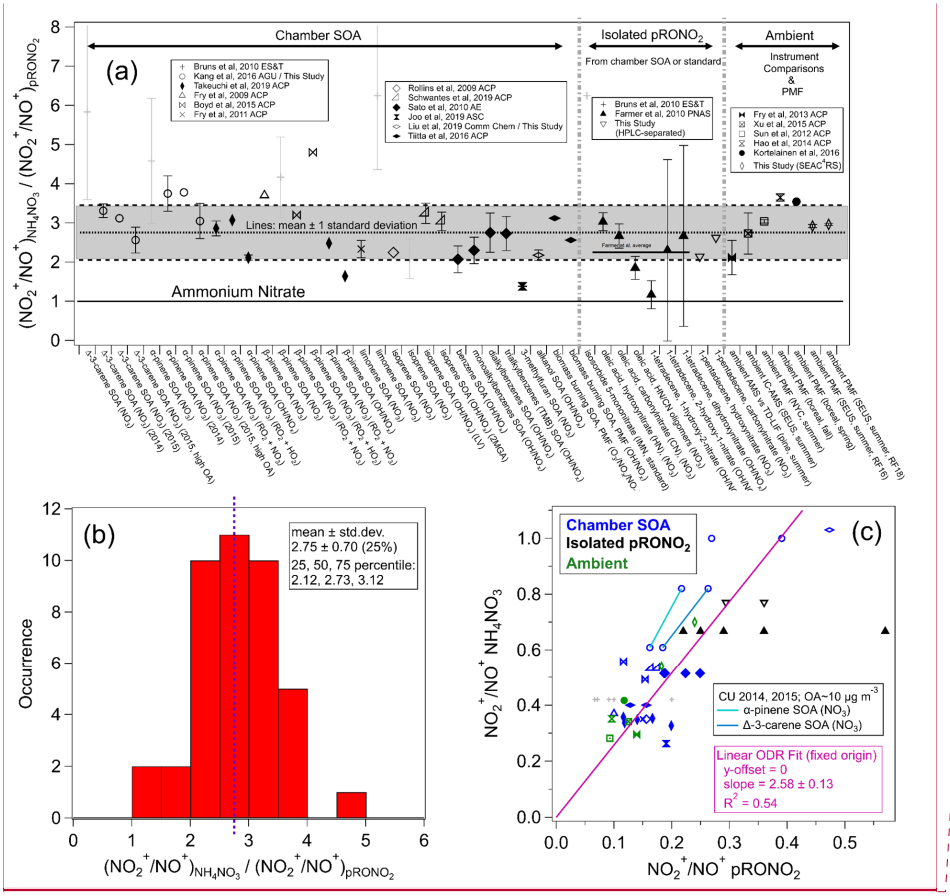

Figure 1. (a~~Top~~) Survey of "Ratio-of-Ratios" (*RoR*) computed from NO_2^+/NO^+ ratios reported for chamber studies, pure organic nitrates, and field observations (using instrument comparisons or PMF separation). The mean (2.75) and standard deviation (±0.70, ±25%) are also shown (standard error for n=41: ±0.11, ±4.0%). The light grey shading ("+" markers) indicates data that were not used in the average here, nor in the fits below (see Table S1 for rationale). Details of the values used to compute the ratios and uncertainties, data source, and any additional calculations for the information included in Figure 1 are provided in Table S1. (b~~ottom left~~) Histogram and statistics of *RoR*. (c~~bottom right~~) scatter plot of R_{NH4NO3} vs. R_{pRONO2}. Linear least-squares lines are shown with orthogonal distance regression ODR fit (with intercept constrained through the origin since offsets from unconstrained fits were not significant and for consistency with apportionment equation). The data connected by cyan and green lines are averages from experiments conducted in our lab with two different AMSs (with substantially different calibration R_{NH4NO3}) while sampling the same SOA particles produced using the same two precursors

Commented [7]: Panel letters added, some fonts increased and standardized

mixtures. See Fig. S3 for the equivalent scatter plot, instead using NO^+/NO_2^+ ratios and swapping the axes (R_{pRONO2} vs R_{NH4NO3}).

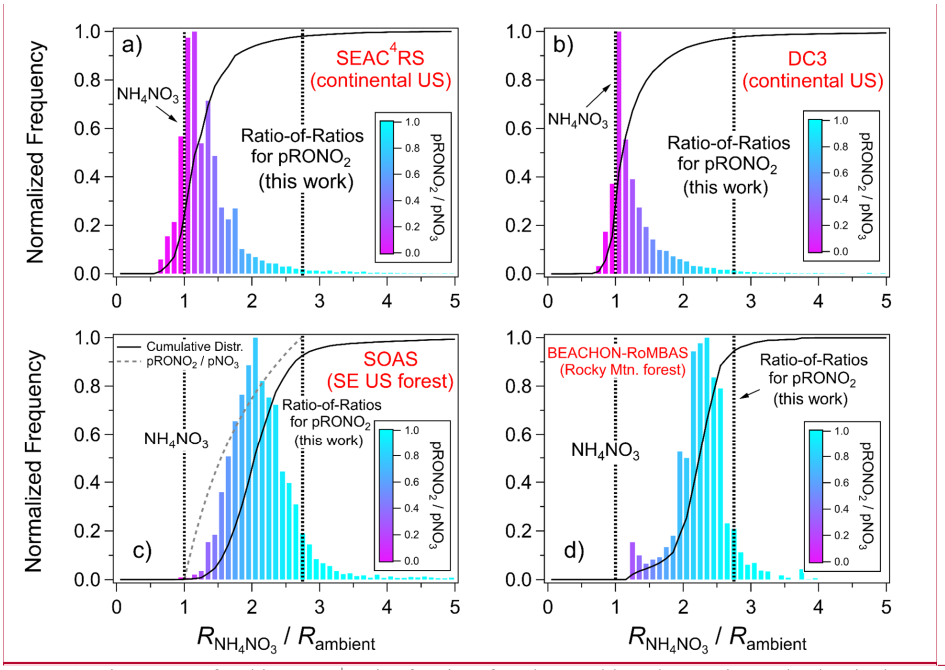

Figure 2. Histograms of ambient NO_x^+ ratios for aircraft and ground-based campaigns. The data is shown as the calibration R_{NH4NO3} divided by $R_{ambient}$, so that all data are on the same reference coordinates. The histograms are weighted by pNO_3 concentration. Cumulative distributions are shown in all plots and an additional curve only on the SOAS panel shows the f_{pRONO2} ($pRONO_2/pNO_3$) for these coordinates (would be identical on all panels). The data used were 1-minute averages and screened for pNO_3 detection limits for the aircraft campaigns (SEAC[4]RS, DC3), and 1-hour averages for the ground-based campaign (SOAS, BEACHON-RoMBAS). Measured R_{NH4NO3} for these studies were as follows: SEAC[4]RS (range 0.40–1.49, mean and stdev. 0.80±0.31); DC3 (0.71±0.04); SOAS (0.44±0.02); BEACHON-RoMBAS: (0.295±0.005). See Fig. S6 for equivalent plots where distributions are *not* weighted by mass concentration).

Commented [8]: Some fonts increased and standardized. Some duplicate axes removed.

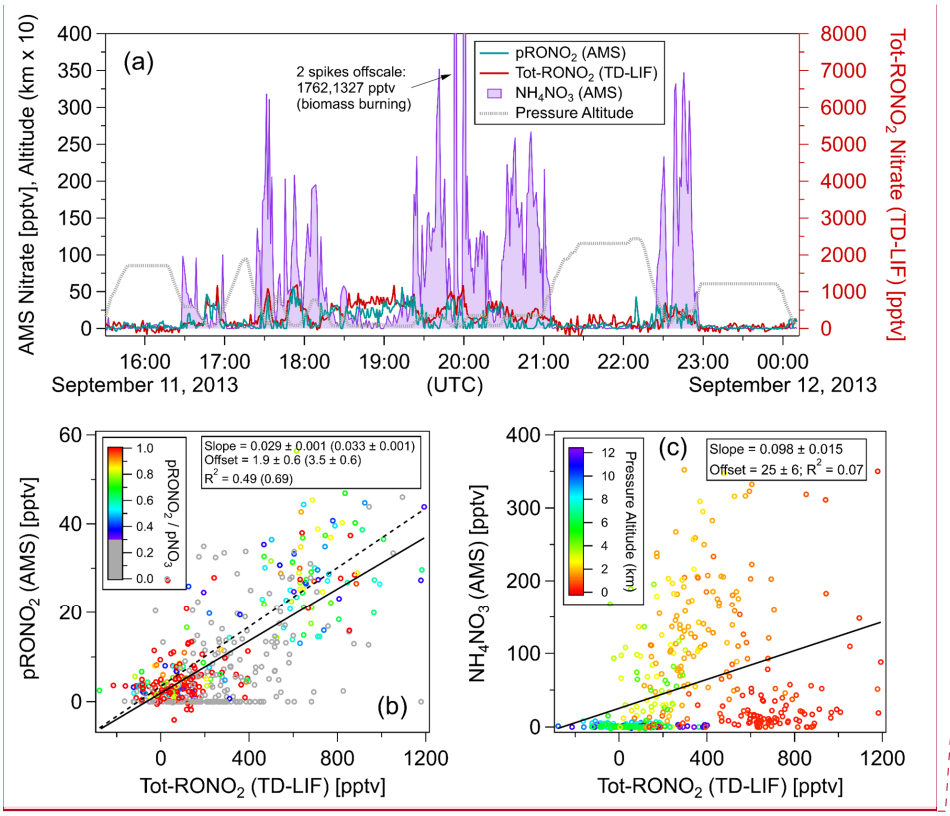

Figure 3. Comparisons of AMS $pRONO_2$ and NH_4NO_3 with TD-LIF total (gas+particles) organic nitrate (Tot-$RONO_2$) during a SEAC[4]RS flight (RF16) in the Southeast US (1-min averages). The time series (a~~top~~) and scatterplots of $pRONO_2$ (b~~ottom left~~) or NH_4NO_3 (c~~bottom right~~) vs Tot-$RONO_2$ are shown. Measured calibration R_{NH4NO3} (consistent with PMF results in Sect. 5.2.2), a *RoR* of 2.75, and Eqs. 2/3 were used to apportion the AMS nitrate. Linear least-squares lines are orthogonal distance regression (ODR). For the $pRONO_2$ vs Tot-$RONO_2$ plot (b~~ottom left~~), an additional line (dotted) and fits (parentheses) are shown for data including only when f_{pRONO2} ($pRONO_2/pNO_3$) is greater than 0.3 (and datapoints with f_{pRONO2}<0.3 are greyed). Figure S10 shows the flight track and timing of different source types sampled.

Commented [9]: Panel letters added, some fonts increased and standardized.

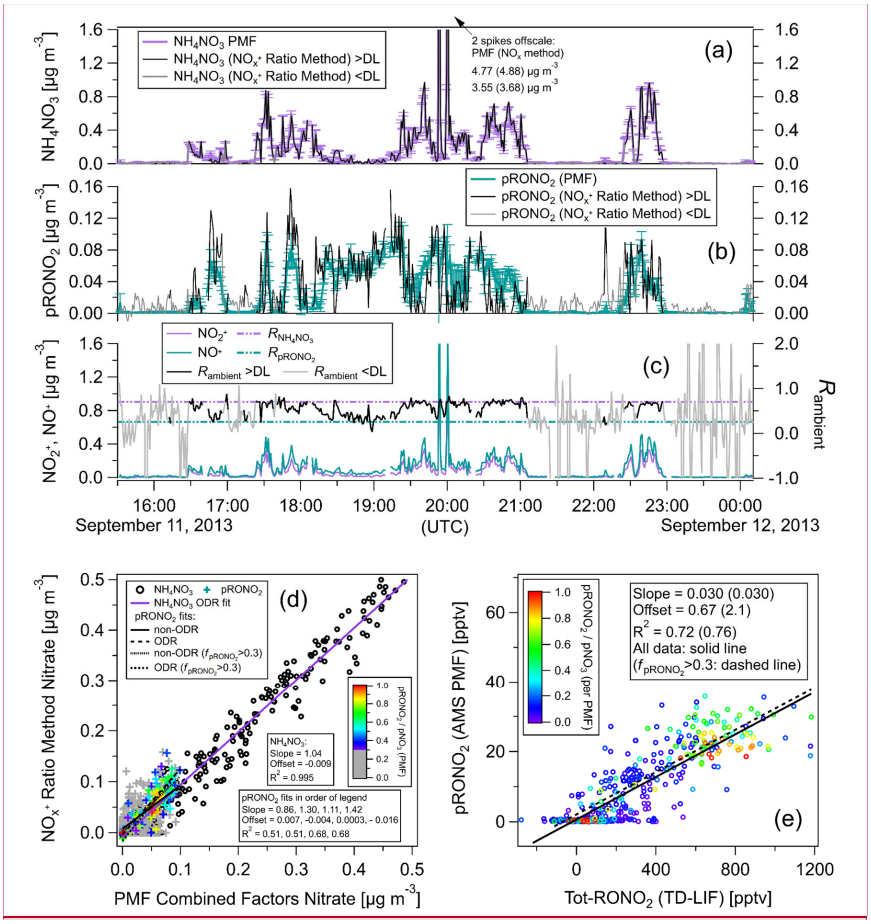

Figure 4. Comparison of NO_x^+ ratio vs PMF methods for calculation of NH_4NO_3 and $pRONO_2$ as time series (a-ctop three panels) and as scatter plots (dbottom left) for same flight shown in Fig. 3. Concentration time series calculated using the *RoR* method (as well as the measured NO_x^+ signals and ratios) are shown for all data as well as only when above the $R_{ambient}$ detection limit (DL; approximated as when both NO_x^+ ions are above standard AMS detection limits (Drewnick et al., 2009)). (e) Bottom right: PMF $pRONO_2$ vs TD-LIF Tot-$RONO_2$ (equivalent to Fig. 3bFig. 3 bottom left, which instead shows $pRONO_2$ from *RoR* method). $pRONO_2$ in scatterplots are colored by the f_{pRONO2} ($pRONO_2/pNO_3$) as computed using the PMF method. Regression line fits/slopes/offsets and correlation coefficients are shown using different fitting methods and criterion as indicated in legends (where "filt" indicates fits where data is limited to f_{pRONO2}>0.3). All PMF-derived concentrations are averages (and standard deviations) of 100 bootstrapping runs (similar results using seeding runs shown in Fig. S21).

Commented [10]: Panel letters added, some fonts increased and standardized.

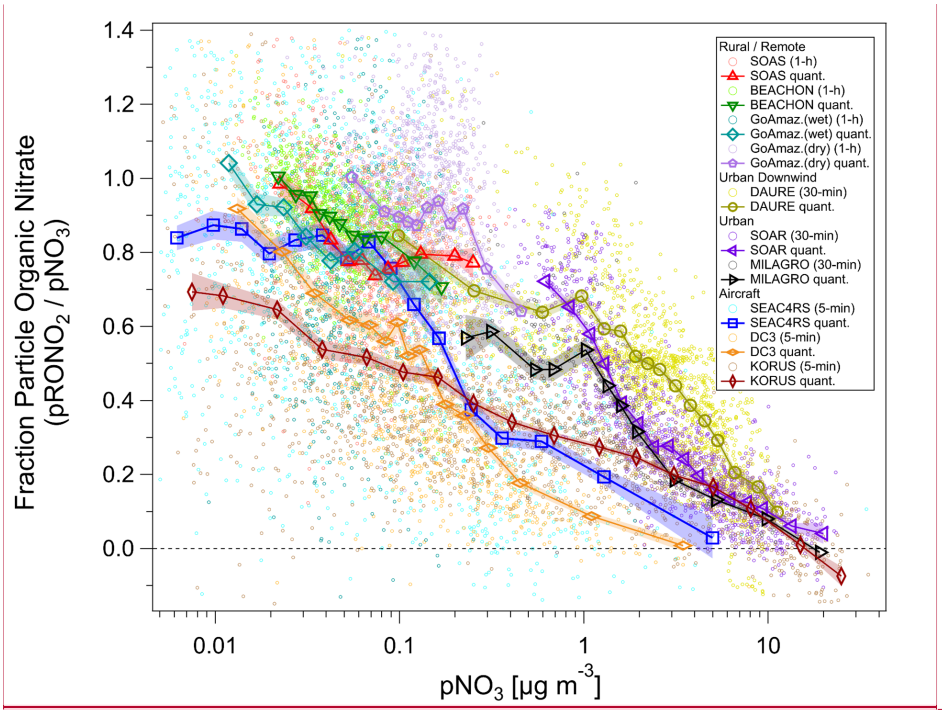

Figure 5. Fraction of total non-refractory submicron nitrate that is organic (f_{pRONO2}) vs. total nitrate concentration (pNO_3) for several ground and aircraft campaigns. Campaigns span: late-winter to summer across the northern hemisphere and wet/dry seasons near the equator; from ground level to the upper troposphere; and urban to remote locations. NO_x^+ ion signals were first averaged and then data was conservatively screened for detection limits (S/N>1-3) using both NO_x^+ ions (small circles). Quantile averages (means, 7–15 bins) are also shown for each campaign. Additionally, for all campaigns, one additional average was calculated and included with the quantile averages for the highest 1% (3%) of pNO_3 for urban/aircraft (rural/remote) campaigns in order to extend the pNO_3 by a factor of ~1.35–3 (undersampled chemical regime, but with sufficiently high S/N). The average of the lowest ~~1~~3% of pNO_3 for the MILAGRO campaign is also included. Shaded swaths indicate the standard error for the quantile averages. Many are no larger than the markers and thus may not be very apparent. See Fig. S31 for a simplified version, showing only binned averages and standard error bars.

Commented [11]: Revised to now show standard errors per explanation in responses to referees.

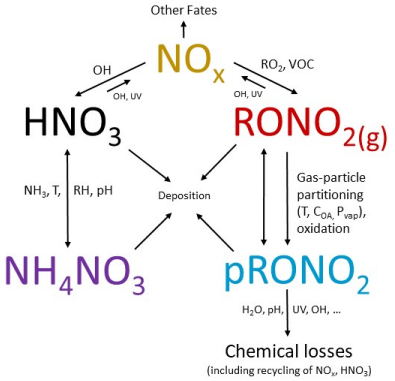

Figure 6. Schematic of key processes controlling particle-phase NH_4NO_3 and $pRONO_2$.

References

Aiken, A. C., Salcedo, D., Cubison, M. J., Huffman, J. A., DeCarlo, P. F., Ulbrich, I. M., Docherty, K. S., Sueper, D., Kimmel, J. R., Worsnop, D. R., Trimborn, A., Northway, M., Stone, E. A., Schauer, J. J., Volkamer, R. M., Fortner, E., de Foy, B., Wang, J., Laskin, A., Shutthanandan, V., Zheng, J., Zhang, R., Gaffney, J., Marley, N. A., Paredes-Miranda, G., Arnott, W. P., Molina, L. T., Sosa, G. and Jimenez, J. L.: Mexico City aerosol analysis during MILAGRO using high resolution aerosol mass spectrometry at the urban supersite (T0) – Part 1: Fine particle composition and organic source apportionment, Atmos. Chem. Phys., 9(17), 6633–6653, 2009.

Alfarra, M. R.: Insights into atmospheric organic aerosols using an aerosol mass spectrometer, PhD Thesis, University of Manchester Institute of Science and Technology., 2004.

Alfarra, M. R., Paulsen, D., Gysel, M., Garforth, A. a., Dommen, J., Prévôt, a. S. H., Worsnop, D. R., Baltensperger, U. and Coe, H.: A mass spectrometric study of secondary organic aerosols formed from the photooxidation of anthropogenic and biogenic precursors in a reaction chamber, Atmos. Chem. Phys., 6, 5279–5293, 2006.

Avery, A. M., Waring, M. S. and DeCarlo, P. F.: Seasonal variation in aerosol composition and concentration upon transport from the outdoor to indoor environment, Environ. Sci. Process. Impacts, 21, 528–547, 2019.

Ayres, B. R., Allen, H. M., Draper, D. C., Brown, S. S., Wild, R. J., Jimenez, J. L., Day, D. A., Campuzano-Jost, P., Hu, W., de Gouw, J., Koss, A., Cohen, R. C., Duffey, K. C., Romer, P., Baumann, K., Edgerton, E., Takahama, S., Thornton, J. A., Lee, B. H. H., Lopez-Hilfiker, F. D., Mohr, C., Wennberg, P. O., Nguyen, T. B., Teng, A., Goldstein, A. H., Olson, K. and Fry, J. L.: Organic nitrate aerosol formation via NO_3 + biogenic volatile organic compounds in the southeastern United States, Atmos. Chem. Phys., 15(23), 13377–13392, 2015.

Bottenus, C. L. H. H., Massoli, P., Sueper, D., Canagaratna, M. R., VanderSchelden, G., Jobson, B. T. and Vanreken, T. M.: Identification of amines in wintertime ambient particulate material using high resolution aerosol mass spectrometry, Atmos. Environ., 180(January), 173–183, 2018.

Boyd, C. M., Sanchez, J., Xu, L., Eugene, a. J., Nah, T., Tuet, W. Y., Guzman, M. I. and Ng, N. L.: Secondary organic aerosol formation from the β-pinene+NO_3 system: effect of humidity and peroxy radical fate, Atmos. Chem. Phys., 15(13), 7497–7522, 2015.

Brito, J., Freney, E., Dominutti, P., Borbon, A., Haslett, S. L., Batenburg, A. M., Colomb, A., Dupuy, R., Denjean, C., Burnet, F., Bourriane, T., Deroubaix, A., Sellegri, K., Borrmann, S., Coe, H., Flamant, C., Knippertz, P. and Schwarzenboeck, A.: Assessing the role of anthropogenic and biogenic sources on PM_1 over southern West Africa using aircraft measurements, Atmos. Chem. Phys., 18(2), 757–772, 2018.

Browne, E. C. and Cohen, R. C.: Effects of biogenic nitrate chemistry on the NOx lifetime in remote continental regions, Atmos. Chem. Phys., 12(24), 11917–11932, 2012.

Brown, S. S., Dubé, W. P., Bahreini, R., Middlebrook, A. M., Brock, C. A., Warneke, C., De Gouw, J. A., Washenfelder, R. A., Atlas, E., Peischl, J., Ryerson, T. B., Holloway, J. S., Schwarz, J. P., Spackman, R., Trainer, M., Parrish, D. D., Fehshenfeld, F. C. and Ravishankara, A. R.: Biogenic VOC oxidation and organic aerosol formation in an urban nocturnal boundary layer: Aircraft vertical profiles in Houston, TX, Atmos. Chem. Phys., 13(22), 11317–11337, 2013.

Bruns, E. A., Perraud, V., Zelenyuk, A., Ezell, M. J., Johnson, S. N., Yu, Y., Imre, D., Finlayson-Pitts, B. J., Alexander, M. L., Bruns, A. E., Perraud, V., Zelenyuk, A., Ezell, M. J., Johnson, S. N., Yu, Y., Imre, D., Finlayson-Pitts, B. J. and Alexander, M. L.: Comparison of FTIR and particle mass spectrometry for the measurement of particulate organic nitrates, Environ. Sci. Technol., 44(3), 1056–1061, 2010.

Canagaratna, M. R., Jayne, J. T., Jimenez, J. L., Allan, J. D., Alfarra, M. R., Zhang, Q. Q., Onasch, T. B., Drewnick, F., Coe, H., Middlebrook, A. M., Delia, A., Williams, L. R., Trimborn, A. M., Northway, M. J., DeCarlo, P. F., Kolb, C. E., Davidovits, P. and Worsnop, D. R.: Chemical and microphysical characterization of ambient aerosols with the Aerodyne Aerosol Mass Spectrometer, Mass Spectrom. Rev., 26(2), 185–222, 2007.

Canonaco, F., Tobler, A., Chen, G., Sosedova, Y., Slowik, J. G., Bozzetti, C., Daellenbach, K. R., El Haddad, I., Crippa, M., Huang, R.-J., Furger, M., Baltensperger, U. and Prévôt, A. S. H.: A new method for long-term source apportionment with time-dependent factor profiles and uncertainty assessment using SoFi Pro: application to 1 year of organic aerosol data, Atmospheric Measurement Techniques, 14(2), 923–943, doi:10.5194/amt-14-923-2021, 2021.

Cappa, C. D., Lim, C. Y., Hagan, D. H., Coggon, M., Koss, A., Sekimoto, K., de Gouw, J., Onasch, T. B., Warneke, C. and Kroll, J. H.: Biomass-burning-derived particles from a wide variety of fuels – Part 2: Effects of photochemical aging on particle optical and chemical properties, Atmos. Chem. Phys., 20(14), 8511–8532, 2020.

Chen, W., Ye, Y., Hu, W., Zhou, H., Pan, T., Wang, Y., Song, W., Song, Q., Ye, C., Wang, C., Wang, B., Huang, S., Yuan, B., Zhu, M., Lian, X., Zhang, G., Bi, X., Jiang, F., Liu, J., Canonaco, F., Prevot, A. S. H., Shao, M. and Wang, X.: Real-time characterization of aerosol compositions, sources and aging processes in Guangzhou during PRIDE-GBA 2018 campaign, J. Geophys. Res., doi:10.1029/2021jd035114, 2021.

Chen, Y., Takeuchi, M., Nah, T., Xu, L., Canagaratna, M. R., Stark, H., Baumann, K., Canonaco, F., Prévôt, A. S. H., Gregory Huey, L., Weber, R. J. and Ng, N. L.: Chemical characterization of secondary organic aerosol at a rural site in the southeastern US: insights from simultaneous high-resolution time-of-flight aerosol mass spectrometer (HR-ToF-AMS) and FIGAERO chemical ionization mass spectrometer (CIMS) measurements, Atmospheric Chemistry and Physics, 20(14), 8421–8440, doi:10.5194/acp-20-8421-2020, 2020.

Cubison, M. J., Ortega, A. M., Hayes, P. L., Farmer, D. K., Day, D. A., Lechner, M. J., Brune, W. H., Apel, E., Diskin, G. S., Fisher, J. A., Fuelberg, H. E., Hecobian, A., Knapp, D. J., Mikoviny, T., Riemer, D., Sachse, G. W., Sessions, W., Weber, R. J., Weinheimer, A. J., Wisthaler, A. and Jimenez, J. L.: Effects of aging on organic aerosol from open biomass burning smoke in aircraft and laboratory studies, Atmos. Chem. Phys., 11(23), 12049–12064, 2011.

Dai, Q., Schulze, B. C., Bi, X., Bui, A. A. T., Guo, F., Wallace, H. W., Sanchez, N. P., Flynn, J. H., Lefer, B. L., Feng, Y. and Griffin, R. J.: Seasonal differences in formation processes of oxidized organic aerosol near Houston, TX, Atmospheric Chemistry and Physics, 19(14), 9641–9661, doi:10.5194/acp-19-9641-2019, 2019.

Day, D. A., Wooldridge, P. J., Dillon, M. B., Thornton, J. A. and Cohen, R. C.: A thermal dissociation laser-induced fluorescence instrument for in situ detection of NO_2, peroxy nitrates, alkyl nitrates, and HNO_3, Journal of Geophysical Research-Atmospheres, 107(D5-6), 4046–4046, 2002.

Docherty, K. S., Aiken, A. C., Huffman, J. A., Ulbrich, I. M., DeCarlo, P. F., Sueper, D., Worsnop, D. R., Snyder, D. C., Peltier, R. E., Weber, R. J., Grover, B. D., Eatough, D. J., Williams, B. J., Goldstein, A.

H., Ziemann, P. J. and Jimenez, J. L.: The 2005 Study of Organic Aerosols at Riverside (SOAR-1): instrumental intercomparisons and fine particle composition, Atmos. Chem. Phys., 11(23), 12387–12420, 2011.

Docherty, K. S., Lewandowski, M. and Jimenez, J. L.: Effect of Vaporizer Temperature on Ambient Non-Refractory Submicron Aerosol Composition and Mass Spectra Measured by the Aerosol Mass Spectrometer Effect of Vaporizer Temperature on Ambient Non-Refractory Submicron Aerosol Composition and Mass Spectra Me, Aerosol Sci. Technol., 6826(March 2017), 00–00, 2015.

Drewnick, F., Hings, S. S., Alfarra, M. R., Prevot, a. S. H. and Borrmann, S.: Aerosol quantification with the Aerodyne Aerosol Mass Spectrometer: detection limits and ionizer background effects, Atmospheric Measurement Techniques, 2(1), 33–46, 2009.

Drewnick, F., Diesch, J.-M., Faber, P. and Borrmann, S.: Aerosol mass spectrometry: particle–vaporizer interactions and their consequences for the measurements, Atmos. Meas. Tech., 8(9), 3811–3830, 2015.

Farmer, D. K., Matsunaga, A., Docherty, K. S., Surratt, J. D., Seinfeld, J. H., Ziemann, P. J. and Jimenez, J. L.: Response of an aerosol mass spectrometer to organonitrates and organosulfates and implications for atmospheric chemistry, Proceedings of the National Academy of Sciences, 107(15), 6670–6675, 2010.

Fisher, J. A., Jacob, D. J., Travis, K. R., Kim, P. S., Marais, E. A., Chan Miller, C., Yu, K., Zhu, L., Yantosca, R. M., Sulprizio, M. P., Mao, J., Wennberg, P. O., Crounse, J. D., Teng, A. P., Nguyen, T. B., St. Clair, J. M., Cohen, R. C., Romer, P., Nault, B. A., Wooldridge, P. J., Jimenez, J. L., Campuzano-Jost, P., Day, D. A., Hu, W., Shepson, P. B., Xiong, F., Blake, D. R., Goldstein, A. H., Misztal, P. K., Hanisco, T. F., Wolfe, G. M., Ryerson, T. B., Wisthaler, A. and Mikoviny, T.: Organic nitrate chemistry and its implications for nitrogen budgets in an isoprene- and monoterpene-rich atmosphere: constraints from aircraft (SEAC^{4}RS) and ground-based (SOAS) observations in the Southeast US, Atmos. Chem. Phys., 16(9), 5969–5991, 2016.

Florou, K., Papanastasiou, D. K., Pikridas, M., Kaltsonoudis, C., Louvaris, E., Gkatzelis, G. I., Patoulias, D., Mihalopoulos, N. and Pandis, S. N.: The contribution of wood burning and other pollution sources to wintertime organic aerosol levels in two Greek cities, Atmos. Chem. Phys., 17(4), 3145–3163, 2017.

Fröhlich, R., Cubison, M. J., Slowik, J. G., Bukowiecki, N., Prévôt, a. S. H., Baltensperger, U., Schneider, J., Kimmel, J. R., Gonin, M., Rohner, U., Worsnop, D. R. and Jayne, J. T.: The ToF-ACSM: A portable aerosol chemical speciation monitor with TOFMS detection, Atmos. Meas. Tech., 6(11), 3225–3241, 2013.

Fry, J. L., Kiendler-Scharr, A., Rollins, A. W., Wooldridge, P. J., Brown, S. S., Fuchs, H., Dubé, W., Mensah, A., dal Maso, M., Tillmann, R., Dorn, H.-P., Brauers, T. and Cohen, R. C.: Organic nitrate and secondary organic aerosol yield from NO_3 oxidation of β-pinene evaluated using a gas-phase kinetics/aerosol partitioning model, Atmos. Chem. Phys., 9(4), 1431–1449, 2009.

Fry, J. L., Draper, D. C., Zarzana, K. J., Campuzano-Jost, P., Day, D. A., Jimenez, J. L., Brown, S. S., Cohen, R. C., Kaser, L., Hansel, A., Cappellin, L., Karl, T., Hodzic Roux, A., Turnipseed, A., Cantrell, C., Lefer, B. L. and Grossberg, N.: Observations of gas- and aerosol-phase organic nitrates at BEACHON-RoMBAS 2011, Atmos. Chem. Phys., 13(17), 8585–8605, 2013.

Fry, J. L., Brown, S. S., Middlebrook, A. M., Edwards, P. M., Campuzano-Jost, P., Day, D. A., Jimenez, J. L., Allen, H. M., Ryerson, T. B., Pollack, I., Graus, M., Warneke, C., de Gouw, J. A., Brock, C. A., Gilman, J., Lerner, B. M., Dubé, W. P., Liao, J. and Welti, A.: Secondary Organic Aerosol (SOA) yields

from NO_3 radical + isoprene based on nighttime aircraft power plant plume transects, Atmos. Chem. Phys., 18(16), 11663–11682, 2018.

Häkkinen, S. A. K., Äijälä, M., Lehtipalo, K., Junninen, H., Backman, J., Virkkula, A., Nieminen, T., Vestenius, M., Hakola, H., Ehn, M., Worsnop, D. R., Kulmala, M., Petäjä, T. and Riipinen, I.: Long-term volatility measurements of submicron atmospheric aerosol in Hyytiälä, Finland, Atmos. Chem. Phys., 12(22), 10771–10786, 2012.

Hao, L. Q., Kortelainen, A., Romakkaniemi, S., Portin, H., Jaatinen, A., Leskinen, A., Komppula, M., Miettinen, P., Sueper, D., Pajunoja, A., Smith, J. N., Lehtinen, K. E. J., Worsnop, D. R., Laaksonen, A. and Virtanen, A.: Atmospheric submicron aerosol composition and particulate organic nitrate formation in a boreal forestland–urban mixed region, Atmos. Chem. Phys., 14(24), 13483–13495, 2014.

Hogrefe, O., Schwab, J. J., Drewnick, F., Lala, G. G., Peters, S., Demerjian, K. L., Rhoads, K., Felton, H. D., Rattigan, O. V., Husain, L. and Dutkiewicz, V. a.: Semicontinuous PM2.5 sulfate and nitrate measurements at an urban and a rural location in New York: PMTACS-NY summer 2001 and 2002 campaigns, J. Air Waste Manag. Assoc., 54(9), 1040–1060, 2004.

Huang, W., Saathoff, H., Shen, X., Ramisetty, R., Leisner, T. and Mohr, C.: Chemical Characterization of Highly Functionalized Organonitrates Contributing to Night-time Organic Aerosol Mass Loadings and Particle Growth, Environ. Sci. Technol., 53(3), acs.est.8b05826–acs.est.8b05826, 2019a.

Huang, W., Saathoff, H., Shen, X., Ramisetty, R., Leisner, T. and Mohr, C.: Seasonal characteristics of organic aerosol chemical composition and volatility in Stuttgart, Germany, Atmos. Chem. Phys., 19, 11687–11700, 2019b.

Hu, W., Palm, B. B., Day, D. A., Campuzano-Jost, P., Krechmer, J. E., Peng, Z., de Sá, S. S., Martin, S. T., Alexander, M. L. L., Baumann, K., Hacker, L., Kiendler-Scharr, A., Koss, A. R., de Gouw, J. A., Goldstein, A. H., Seco, R., Sjostedt, S. J., Park, J.-H., Guenther, A. B., Kim, S., Canonaco, F., Prévôt, A. S. H., Brune, W. H. and Jimenez, J. L.: Volatility and lifetime against OH heterogeneous reaction of ambient isoprene-epoxydiols-derived secondary organic aerosol (IEPOX-SOA), Atmos. Chem. Phys., 16(18), 11563–11580, 2016.

Hu, W., Campuzano-jost, P., Day, D. A., Croteau, P., Canagaratna, R., Jayne, J. T., Worsnop, D. R., Jimenez, J. L., Hu, W., Campuzano-jost, P., Day, D. A., Croteau, P., Canagaratna, R., Jayne, J. T., Worsnop, D. R. and Jimenez, J. L.: Evaluation of the new capture vaporizer for aerosol mass spectrometers (AMS) through field studies of inorganic species, Aerosol Sci. Technol., 51(6), 735–754, 2017a.

Hu, W., Campuzano-Jost, P., Day, D. A., Croteau, P., Canagaratna, M. R., Jayne, J. T., Worsnop, D. R. and Jimenez, J. L.: Evaluation of the new capture vapourizer for aerosol mass spectrometers (AMS) through laboratory studies of inorganic species, Atmos. Meas. Tech., 10(6), 2897–2921, 2017b.

Jayne, J. T., Leard, D. C., Zhang, X. F., Davidovits, P., Smith, K. A., Kolb, C. E. and Worsnop, D. R.: Development of an aerosol mass spectrometer for size and composition analysis of submicron particles, Aerosol Sci. Technol., 33(1-2), 49–70, 2000.

Jayne, J. T., Croteau, P. L., Lambe, A. T., Xu, W., Onasch, T. B., Wolff, L. and Canagaratna, M. R.: Investigation of f44 variability in AMS and ACSM instruments, in 16th Aerosol Mass Spectrometer Users' Meeting, Milan, Italy. [online] Available from: http://cires1.colorado.edu/jimenez-group/UsrMtgs/UsersMtg16/Jayne_f44Intro.pdf (Accessed 11 August 2021), 2015.

Jimenez, J. L., Jayne, J. T., Shi, Q., Kolb, C. E., Worsnop, D. R., Yourshaw, I., Seinfeld, J. H., Flagan, R. C., Zhang, X. F., Smith, K. A., Morris, J. W. and Davidovits, P.: Ambient aerosol sampling using the Aerodyne Aerosol Mass Spectrometer, J. Geophys. Res., 108(D7), 8425–8425, 2003.

Jimenez, J. L., Canagaratna, M. R., Drewnick, F., Allan, J. D., Alfarra, M. R., Middlebrook, A. M., Slowik, J. G., Zhang, Q., Coe, H., Jayne, J. T. and Worsnop, D. R.: Comment on "The effects of molecular weight and thermal decomposition on the sensitivity of a thermal desorption aerosol mass spectrometer," Aerosol Sci. Technol., 50(9), i–xv, 2016.

Kiendler-Scharr, A., Mensah, A. A., Friese, E., Topping, D., Nemitz, E., Prevot, A. S. H., Äijälä, M., Allan, J., Canonaco, F., Canagaratna, M., Carbone, S., Crippa, M., Dall Osto, M., Day, D. A., DeCarlo, P., Di Marco, C. F., Elbern, H., Eriksson, A., Freney, E., Hao, L., Herrmann, H., Hildebrandt, L., Hillamo, R., Jimenez, J. L., Laaksonen, A., McFiggans, G., Mohr, C., O'Dowd, C., Otjes, R., Ovadnevaite, J., Pandis, S. N., Poulain, L., Schlag, P., Sellegri, K., Swietlicki, E., Tiitta, P., Vermeulen, A., Wahner, A., Worsnop, D. and Wu, H.-C.: Organic nitrates from night-time chemistry are ubiquitous in the European submicron aerosol, Geophys. Res. Lett., 43(14), 7735–7744, 2016.

Kim, H., Zhang, Q. and Heo, J.: Influence of intense secondary aerosol formation and long-range transport on aerosol chemistry and properties in the Seoul Metropolitan Area during spring time: Results from KORUS-AQ, Atmos. Chem. Phys., 18(10), 7149–7168, 2018.

Kortelainen, A., Hao, L., Tiitta, P., Jaatinen, A., Miettinen, P., Kulmala, M., Smith, J. N., Laaksonen, A., Worsnop, D. R. and Virtanen, A.: Sources of particulate organic nitrates in the boreal forest in Finland, Boreal Environ. Res., 22, 13–26, 2017.

Kostenidou, E., Florou, K., Kaltsonoudis, C., Tsiflikiotou, M., Vratolis, S., Eleftheriadis, K. and Pandis, S. N.: Sources and chemical characterization of organic aerosol during the summer in the eastern Mediterranean, Atmos. Chem. Phys., 15(19), 11355–11371, 2015.

Lee, A. K. Y., Adam, M. G., Liggio, J., Li, S.-M., Li, K., Willis, M. D., Abbatt, J. P. D., Tokarek, T. W., Odame-Ankrah, C. A., Osthoff, H. D. and Others: A large contribution of anthropogenic organo-nitrates to secondary organic aerosol in the Alberta oil sands, Atmos. Chem. Phys., 19(19), 12209–12219, 2019.

Lee, B. H., Mohr, C., Lopez-Hilfiker, F. D., Lutz, A., Hallquist, M., Lee, L., Romer, P., Cohen, R. C., Iyer, S., Kurtén, T., Hu, W., Day, D. A., Campuzano-Jost, P., Jimenez, J. L., Xu, L., Ng, N. L., Guo, H., Weber, R. J., Wild, R. J., Brown, S. S., Koss, A., de Gouw, J., Olson, K., Goldstein, A. H., Seco, R., Kim, S., McAvey, K., Shepson, P. B., Starn, T., Baumann, K., Edgerton, E. S., Liu, J., Shilling, J. E., Miller, D. O., Brune, W., Schobesberger, S., D'Ambro, E. L. and Thornton, J. A.: Highly functionalized organic nitrates in the southeast U.S.: Contribution to secondary organic aerosol and reactive nitrogen budgets, Proc. Natl. Acad. Sci., 113(6), 1516–1521, 2016.

Lin, C., Huang, R.-J., Duan, J., Zhong, H. and Xu, W.: Primary and Secondary Organic Nitrate in Northwest China: A Case Study, Environmental Science & Technology Letters, doi:10.1021/acs.estlett.1c00692, 2021.

Lopez-Hilfiker, F. D., Mohr, C., Ehn, M., Rubach, F., Kleist, E., Wildt, J., Mentel, T. F., Lutz, A., Hallquist, M., Worsnop, D. and Thornton, J. A.: A novel method for online analysis of gas and particle composition: description and evaluation of a Filter Inlet for Gases and AEROsols (FIGAERO), Atmos. Meas. Tech., 7(4), 983–1001, 2014.

Maria, S. F., Russell, L. M., Turpin, B. J. and Porcja, R. J.: FTIR measurements of functional groups and organic mass in aerosol samples over the Caribbean, Atmos. Environ., 36(33), 5185–5196, 2002.

McClure, C. D., Lim, C. Y., Hagan, D. H., Kroll, J. H. and Cappa, C. D.: Biomass-burning-derived particles from a wide variety of fuels – Part 1: Properties of primary particles, Atmos. Chem. Phys., 20(3), 1531–1547, 2020.

Minguillon´, M. C., Perron, N., Querol, X., Szidat, S., Fahrni, S. M., Alastuey, A., Jimenez, J. L., Mohr, C., Ortega, A. M., Day, D. A., Lanz, V. A., Wacker, L., Reche, C., Cusack, M., Amato, F., Kiss, G., Hoffer, A., Decesari, S., Moretti, F., Hillamo, R., Teinila, K., Seco, R., Penuelas, J., Metzger, A., Schallhart, S., Muller, M., Hansel, A., Burkhart, J. F., Baltensperger, U. and Prevot, A. S. H.: Fossil versus contemporary sources of fine elemental and organic carbonaceous particulate matter during the DAURE campaign in Northeast Spain, Atmos. Chem. Phys., 11(23), 12067–12084, 2011.

Nault, B. A., Garland, C., Wooldridge, P. J., Brune, W. H., Campuzano-Jost, P., Crounse, J. D., Day, D. A., Dibb, J., Hall, S. R., Huey, L. G., Jimenez, J. L., Liu, X., Mao, J., Mikoviny, T., Peischl, J., Pollack, I. B., Ren, X., Ryerson, T. B., Scheuer, E., Ullmann, K., Wennberg, P. O., Wisthaler, A., Zhang, L. and Cohen, R. C.: Observational Constraints on the Oxidation of NO_x in the Upper Troposphere, J. Phys. Chem. A, 120(9), doi:10.1021/acs.jpca.5b07824, 2016.

Nault, B. A., Campuzano-Jost, P., Day, D. A., Schroder, J. C., Anderson, B., Beyersdorf, A. J., Blake, D. R., Brune, W. H., Choi, Y., Corr, C. A., de Gouw, J. A., Dibb, J., DiGangi, J. P., Diskin, G. S., Fried, A., Huey, L. G., Kim, M. J., Knote, C. J., Lamb, K. D., Lee, T., Park, T., Pusede, S. E., Scheuer, E., Thornhill, K. L., Woo, J.-H. and Jimenez, J. L.: Secondary organic aerosol production from local emissions dominates the organic aerosol budget over Seoul, South Korea, during KORUS-AQ, Atmos. Chem. Phys., 18(24), 17769–17800, 2018.

Nault, B. A., Campuzano-Jost, P., Day, D. A., Jo, D. S., Schroder, J. C., Allen, H. M., Bahreini, R., Bian, H., Blake, D. R., Chin, M., Clegg, S. L., Colarco, P., Crounse, J., Cubison, M. J., DeCarlo, P. F., Dibb, J., Diskin, G. S., Hodzic, A., Hu, W., Katich, J. M., Kim, M. J., Kodros, J., Kupc, A., Lopez-Hilfiker, F. D., Marais, E. A., Middlebrook, A., Neuman, J. A., Nowak, J. B., Palm, B. B., Paulot, F., Pierce, J., Schill, G. P., Scheuer, E., Thornton, J. A., Tsigaridis, P. R., Wennberg, P. O., Williamson, C. J. and Jimenez, J. L.: Models underestimate the increase of acidity with remoteness biasing radiative impact calculations, Communications Earth & Environment, 2(93), doi:10.1038/s43247-021-00164-0, 2021.

Ng, N. L., Herndon, S. C., Trimborn, A., Canagaratna, M. R., Croteau, P. L., Onasch, T. B., Sueper, D., Worsnop, D. R., Zhang, Q., Sun, Y. L. and Jayne, J. T.: An Aerosol Chemical Speciation Monitor (ACSM) for Routine Monitoring of the Composition and Mass Concentrations of Ambient Aerosol, Aerosol Sci. Technol., 45(7), 780–794, 2011.

Ng, N. L., Brown, S. S., Archibald, A. T., Atlas, Elliot, Cohen, R. C., Crowley, J. N., Day, D. A., Donahue, N. M., Fry, J. L., Fuchs, H., Griffin, R. J., Guzman, M. I., Herrmann, H., Hodzic, A., Iinuma, Y., Kiendler-Scharr, A., Lee, B. H., Luecken, D. J., Mao, J., McLaren, R., Mutzel, A., Osthoff, H. D., Ouyang, B., Picquet-Varrault, B., Platt, U., Pye, H. O. T., Rudich, Y., Schwantes, R. H., Shiraiwa, M., Stutz, J., Thornton, J. A., Tilgner, A., Williams, B. J. and Zaveri, R. A.: Nitrate radicals and biogenic volatile organic compounds: oxidation, mechanisms, and organic aerosol, Atmos. Chem. Phys., 17(3), 2103–2162, 2017.

Pagonis, D., Campuzano-Jost, P., Guo, H., Day, D. A., Schueneman, M. K., Brown, W. L., Nault, B. A., Stark, H., Siemens, K., Laskin, A., Piel, F., Tomsche, L., Wisthaler, A., Coggon, M. M., Gkatzelis, G. I., Halliday, H. S., Krechmer, J. E., Moore, R. H., Thomson, D. S., Warneke, C., Wiggins, E. B. and Jimenez, J. L.: Airborne extractive electrospray mass spectrometry measurements of the chemical composition of organic aerosol, Atmos. Chem. Phys., 14(2), 1545–1559, 2021.

Palm, B. B., Campuzano-Jost, P., Day, D. A., Ortega, A. M., Fry, J. L., Brown, S. S., Zarzana, K. J., Dube, W., Wagner, N. L., Draper, D. C., Kaser, L., Jud, W., Karl, T., Hansel, A., Gutiérrez-Montes, C. and Jimenez, J. L.: Secondary organic aerosol formation from in situ OH, O_3, and NO_3 oxidation of ambient forest air in an oxidation flow reactor, Atmos. Chem. Phys., 17(8), 5331–5354, 2017.

Perring, A. E., Bertram, T. H., Wooldridge, P. J., Fried, A., Heikes, B. G., Dibb, J., Crounse, J. D., Wennberg, P. O., Blake, N. J., Blake, D. R., Brune, W. H., Singh, H. B. and Cohen, R. C.: Airborne observations of total $RONO_2$: new constraints on the yield and lifetime of isoprene nitrates, Atmos. Chem. Phys., 9(4), 1451–1463, 2009.

Pullinen, I., Schmitt, S., Kang, S., Sarrafzadeh, M., Schlag, P., Andres, S., Kleist, E., Mentel, T. F., Rohrer, F., Springer, M., Tillmann, R., Wildt, J., Wu, C., Zhao, D., Wahner, A. and Kiendler-Scharr, A.: Impact of NO_x on secondary organic aerosol (SOA) formation from α-pinene and β-pinene photooxidation: the role of highly oxygenated organic nitrates, Atmos. Chem. Phys., 20(17), 10125–10147, 2020.

Pye, H. O. T., Luecken, D. J., Xu, L., Boyd, C. M., Ng, N. L., Baker, K. R., Ayres, B. R., Bash, J. O., Baumann, K., Carter, W. P. L., Edgerton, E. S., Fry, J. L., Hutzell, W. T., Schwede, D. B. and Shepson, P. B.: Modeling the current and future roles of particulate organic nitrates in the southeastern United States, Environ. Sci. Technol., acs.est.5b03738–acs.est.5b03738, 2015.

Reyes-Villegas, E., Priestley, M., Ting, Y.-C., Haslett, S., Bannan, T., Le Breton, M., Williams, P. I., Bacak, A., Flynn, M. J., Coe, H., Percival, C., Allan, J. D., Breton, M. L., Attribution, Creative Commons, Reyes-Villegas, E., Reyes-Villegas, E. and By, C. C.: Simultaneous aerosol mass spectrometry and chemical ionisation mass spectrometry measurements during a biomass burning event in the UK : insights into nitrate chemistry, Atmos. Chem. Phys., 18(6), 4093–4111, 2018.

Rollins, A. W., Kiendler-Scharr, A., Fry, J. L., Brauers, T., Brown, S. S., Dorn, H.-P., Dubé, W. P., Fuchs, H., Mensah, A., Mentel, T. F., Rohrer, F., Tilmann, R., Wegener, R., Wooldridge, P. J. and Cohen, R. C.: Isoprene oxidation by nitrate radical: alkyl nitrate and secondary organic aerosol yields, Atmos. Chem. Phys., 9, 6685–6703, 2009.

Rollins, A. W., Pusede, S., Wooldridge, P., Min, K.-E., Gentner, D. R., Goldstein, A. H., Liu, S., Day, D. A., Russell, L. M., Rubitschun, C. L., Surratt, J. D. and Cohen, R. C.: Gas/particle partitioning of total alkyl nitrates observed with TD-LIF in Bakersfield, J. Geophys. Res. D: Atmos., 118(12), 6651–6662, 2013.

Romer, P. S.: Chemical removal of nitrogen oxides from the atmosphere: Impacts on air quality and effects of temperature, PhD Thesis, University of California, Berkeley. [online] Available from: http://digitalassets.lib.berkeley.edu/etd/ucb/text/Romer_berkeley_0028E_18182.pdf (Accessed 11 August, 2021), 2018.

Saleh, R., Robinson, E. S., Ahern, A. T., Donahue, N. M., Saleh, R., Robinson, E. S., Ahern, A. T. and Donahue, N. M.: Evaporation rate of particles in the vaporizer of the Aerodyne aerosol mass spectrometer, Aerosol Sci. Technol., 51(4), 501–508, 2017.

de Sá, S. S., Palm, B. B., Campuzano-Jost, P., Day, D. A., Hu, W., Isaacman-VanWertz, G., Yee, L. D., Brito, J., Carbone, S., Ribeiro, I. O., Cirino, G. G., Liu, Y. J., Thalman, R., Sedlacek, A., Funk, A., Schumacher, C., Shilling, J. E., Schneider, J., Artaxo, P., Goldstein, A. H., Souza, R. A. F., Wang, J., McKinney, K. A., Barbosa, H., Alexander, M. L., Jimenez, J. L. and Martin, S. T.: Urban influence on the concentration and composition of submicron particulate matter in central Amazonia, Atmos. Chem. Phys., 18(16), 12185–12206, 2018.

de Sá, S. S., Rizzo, L. V., Palm, B. B., Campuzano-Jost, P., Day, D. A., Yee, L. D., Wernis, R., Isaacman-VanWertz, G., Brito, J., Carbone, S., Liu, Y. J., Sedlacek, A., Springston, S., Goldstein, A. H., Barbosa, H. M. J., Alexander, M. L., Artaxo, P., Jimenez, J. L. and Martin, S. T.: Contributions of biomass-burning, urban, and biogenic emissions to the concentrations and light-absorbing properties of particulate matter in central Amazonia during the dry season, Atmos. Chem. Phys., 19, 7973–8001, 2019.

Schneider, J., Mertes, S., Van Pinxteren, D., Herrmann, H. and Borrmann, S.: Uptake of nitric acid, ammonia, and organics in orographic clouds: Mass spectrometric analyses of droplet residual and interstitial aerosol particles, Atmos. Chem. Phys., 17(2), 1571–1593, 2017.

Schroder, J. C., Campuzano-Jost, P., Day, D. A., Shah, V., Larson, K., Sommers, J. M., Sullivan, A. P., Campos, T., Reeves, J. M., Hills, A., Hornbrook, R. S., Blake, N. J., Scheuer, E., Guo, H., Fibiger, D. L., McDuffie, E. E., Hayes, P. L., Weber, R. J., Dibb, J. E., Apel, E. C., Jaeglé, L., Brown, S. S., Thornton, J. A. and Jimenez, J. L.: Sources and Secondary Production of Organic Aerosols in the Northeastern United States during WINTER, J. Geophys. Res. D: Atmos., 123(14), 7771–7796, 2018.

Schueneman, M. K., Nault, B. A., Campuzano-Jost, P., Jo, D. S., Day, D. A., Schroder, J. C., Palm, B. B., Hodzic, A., Dibb, J. E. and Jimenez, J. L.: Aerosol pH indicator and organosulfate detectability from aerosol mass spectrometry measurements, Atmos. Meas. Tech., 14(3), 2237–2260, 2021.

Schulz, C., Schneider, J., Holanda, B. A., Appel, O., Costa, A., de Sá, S. S., Dreiling, V., Fütterer, D., Jurkat-Witschas, T., Klimach, T., Knote, C., Krämer, M., Martin, S. T., Mertes, S., Pöhlker, M. L., Sauer, D., Voigt, C., Walser, A., Weinzierl, B., Ziereis, H., Zöger, M., Andreae, M. O., Artaxo, P., Machado, L. A. T., Pöschl, U., Wendisch, M. and Borrmann, S.: Aircraft-based observations of isoprene-epoxydiol-derived secondary organic aerosol (IEPOX-SOA) in the tropical upper troposphere over the Amazon region, Atmos. Chem. Phys., 18(20), 14979–15001, 2018.

Setyan, A., Zhang, Q., Merkel, M., Knighton, W. B., Sun, Y., Song, C., Shilling, J. E., Onasch, T. B., Herndon, S. C., Worsnop, D. R., Fast, J. D., Zaveri, R. A., Berg, L. K., Wiedensohler, A., Flowers, B. A., Dubey, M. K. and Subramanian, R.: Characterization of submicron particles influenced by mixed biogenic and anthropogenic emissions using high-resolution aerosol mass spectrometry: results from CARES, Atmos. Chem. Phys., 12(17), 8131–8156, 2012.

Sun, Y. L., Zhang, Q., Schwab, J. J., Yang, T., Ng, N. L. and Demerjian, K. L.: Factor analysis of combined organic and inorganic aerosol mass spectra from high resolution aerosol mass spectrometer measurements, Atmos. Chem. Phys., 12(18), 8537–8551, 2012.

Surratt, J. D., Murphy, S. M., Kroll, J. H., Ng, N. L., Hildebrandt, L., Sorooshian, A., Szmigielski, R., Vermeylen, R., Maenhaut, W., Claeys, M., Flagan, R. C. and Seinfeld, J. H.: Chemical composition of secondary organic aerosol formed from the photooxidation of isoprene, J. Phys. Chem. A, 110(31), 9665–9690, 2006.

Takeuchi, M. and Ng, N. L.: Chemical composition and hydrolysis of organic nitrate aerosol formed from hydroxyl and nitrate radical oxidation of α-pinene and β-pinene, Atmos. Chem. Phys., 19(19), 12749–12766, 2019.

Tiitta, P., Leskinen, A., Hao, L., Yli-Pirilä, P., Kortelainen, M., Grigonyte, J., Tissari, J., Lamberg, H., Hartikainen, A., Kuuspalo, K., Kortelainen, A.-M. M., Virtanen, A., Lehtinen, K. E. J., Komppula, M., Pieber, S., Prévôt, A. S. H., Onasch, T. B., Worsnop, D. R., Czech, H., Zimmermann, R., Jokiniemi, J. and Sippula, O.: Transformation of logwood combustion emissions in a smog chamber: formation of secondary organic aerosol and changes in the primary organic aerosol upon daytime and nighttime aging, Atmos. Chem. Phys., 16(20), 13251–13269, 2016.

Xu, L., Suresh, S., Guo, H., Weber, R. J. and Ng, N. L.: Aerosol characterization over the southeastern United States using high-resolution aerosol mass spectrometry: spatial and seasonal variation of aerosol composition and sources with a focus on organic nitrates, Atmos. Chem. Phys., 15(13), 7307–7336, 2015a.

Xu, L., Guo, H., Boyd, C. M., Klein, M., Bougiatioti, A., Cerully, K. M., Hite, J. R., Isaacman-VanWertz, G., Kreisberg, N. M., Knote, C., Olson, K., Koss, A., Goldstein, A. H., Hering, S. V., de Gouw, J., Baumann, K., Lee, S.-H., Nenes, A., Weber, R. J. and Ng, N. L.: Effects of anthropogenic emissions on aerosol formation from isoprene and monoterpenes in the southeastern United States, Proceedings of the National Academy of Sciences, 112(1), 37–42, 2015b.

Xu, L., Williams, L. R., Young, D. E., Allan, J. D., Coe, H., Massoli, P., Fortner, E., Chhabra, P., Herndon, S., Brooks, W. A., Jayne, J. T., Worsnop, D. R., Aiken, A. C., Liu, S., Gorkowski, K., Dubey, M. K., Fleming, Z. L., Visser, S., Prévôt, A. S. H. and Ng, N. L.: Wintertime aerosol chemical composition, volatility, and spatial variability in the greater London area, Atmos. Chem. Phys., 16(2), 1139–1160, 2016.

Xu, W., Takeuchi, M., Chen, C., Qiu, Y., Xie, C., Xu, W., Ma, N., Worsnop, D. R., Ng, N. L. and Sun, Y.: Estimation of particulate organic nitrates from thermodenuder–aerosol mass spectrometer measurements in the North China Plain, Atmospheric Measurement Techniques, 14(5), 3693–3705, doi:10.5194/amt-14-3693-2021, 2021.

Yu, K., Zhu, Q., Du, K. and Huang, X.-F.: Characterization of nighttime formation of particulate organic nitrates based on high-resolution aerosol mass spectrometry in an urban atmosphere in China, Atmos. Chem. Phys., 19(7), 5235–5249, 2019.

Zare, A., Romer, P. S., Nguyen, T., Keutsch, F. N., Skog, K. and Cohen, R. C.: A comprehensive organic nitrate chemistry: insights into the lifetime of atmospheric organic nitrates, Atmos. Chem. Phys., 18(20), 15419–15436, 2018.

Zaveri, R. A., Berkowitz, C. M., Brechtel, F. J., Gilles, M. K., Hubbe, J. M., Jayne, J. T., Kleinman, L. I., Laskin, A., Madronich, S., Onasch, T. B., Pekour, M. S., Springston, S. R., Thornton, J. A., Tivanski, A. V. and Worsnop, D. R.: Nighttime chemical evolution of aerosol and trace gases in a power plant plume: Implications for secondary organic nitrate and organosulfate aerosol formation, NO_3 radical chemistry, and N_2O_5 heterogeneous hydrolysis, J. Geophys. Res. D: Atmos., 115(12), 1–22, 2010.

Zhang, J. K., Cheng, M. T., Ji, D. S., Liu, Z. R., Hu, B., Sun, Y. and Wang, Y. S.: Characterization of submicron particles during biomass burning and coal combustion periods in Beijing, China, Sci. Total Environ., 562, 812–821, 2016.

Zhang, Q. and Jimenez, J. L.: Aerosol Mass Spectrometry (AMS) Global Database, [online] Available from: https://sites.google.com/site/amsglobaldatabase/urban-down-wind/montseny-spain (Accessed 11 August, 2021), 2021.

Zhang, Q., Stanier, C. O., Canagaratna, M. R., Jayne, J. T., Worsnop, D. R., Pandis, S. N. and Jimenez, J. L.: Insights into the chemistry of new particle formation and growth events in Pittsburgh based on aerosol mass spectrometry, Environ. Sci. Technol., 38(18), 4797–4809, 2004.

Zhao, D., Schmitt, S. H., Wang, M., Acir, I.-H., Tillmann, R., Tan, Z., Novelli, A., Fuchs, H., Pullinen, I., Wegener, R. and Others: Effects of NOx and SO2 on the secondary organic aerosol formation from photooxidation of α-pinene and limonene, Atmos. Chem. Phys., 18(3), 1611–1628, 2018.

Zhou, S., Collier, S., Xu, J., Mei, F., Wang, J., Lee, Y.-N., Sedlacek, A. J., Springston, S. R., Sun, Y. and Zhang, Q.: Influences of upwind emission sources and atmospheric processing on aerosol chemistry and properties at a rural location in the Northeastern U.S, J. Geophys. Res. D: Atmos., 121(10), 6049–6065, 2016.

Zhu, Q., He, L.-Y., Huang, X.-F., Cao, L.-M., Gong, Z.-H., Wang, C., Zhuang, X. and Hu, M.: Atmospheric aerosol compositions and sources at two national background sites in northern and southern China, Atmos. Chem. Phys., 16(15), 10283–10297, 2016.

Zhu, Q., Cao, L.-M., Tang, M.-X., Huang, X.-F., Saikawa, E. and He, L.-Y.: Characterization of Organic Aerosol at a Rural Site in the North China Plain Region: Sources, Volatility and Organonitrates, Adv. Atmos. Sci., 38(7), 1115–1127, 2021.

Supplement of

A Systematic Re-evaluation of Methods for Quantification of Bulk Particle-phase Organic Nitrates Using Real-time Aerosol Mass Spectrometry

Douglas A. Day,[1,2] Pedro Campuzano-Jost,[1,2] Benjamin A. Nault,[1,2,a] Brett B. Palm,[1,2,b] Weiwei Hu,[1,2,c] Hongyu Guo,[1,2] Paul J. Wooldridge,[3] Ronald C. Cohen,[3,4] Kenneth. S. Docherty,[5] J. Alex Huffman,[6] Suzane S. de Sá,[7] Scot T. Martin,[7,8] Jose L. Jimenez[1,2]

[1]Cooperative Institute for Research in Environmental Sciences, University of Colorado, Boulder, CO, USA
[2]Dept. of Chemistry, University of Colorado, Boulder, CO, USA
[3]Department of Chemistry, University of California Berkeley, Berkeley, CA, USA
[4]Department of Earth and Planetary Science, University of California Berkeley, Berkeley, CA, USA
[5]Jacobs Technology, Inc., Research Triangle Park, NC, USA
[6]Department of Chemistry and Biochemistry, University of Denver, Denver, CO USA
[7]School of Engineering and Applied Sciences, Harvard University, Cambridge, Massachusetts, USA
[8]Department of Earth and Planetary Sciences, Harvard University, Cambridge, Massachusetts, USA

[a]now at: Center for Aerosol and Cloud Chemistry, Aerodyne Research Inc., Billerica, MA, USA
[b]now at: Atmospheric Chemistry Observations and Modeling Laboratory, National Center for Atmospheric Research, Boulder, CO, USA
[c]now at: State Key Laboratory at Organic Geochemistry, Guangzhou Institute of Geochemistry, Chinese Academy of Sciences, Guangzhou, China

S1 Field and laboratory dataset descriptions and data processing methods

S1.1 Field datasets

Several AMS field datasets are used throughout this manuscript to refine and test the quantification methods, provide examples, and explore more advanced applications. The main datasets used here include and will be referred to as DC3, SEAC^{4}RS, KORUS-AQ, SOAR, MILAGRO, DAURE, BEACHON-RoMBAS, SOAS, and GoAmazon (IOP1/IOP2). All datasets were collected with a high-resolution time-of-flight AMS (HR-ToF-AMS) (DeCarlo et al., 2006). Table S3 provides a brief overview of the campaigns. Additional details are provided in this section.

Campaigns conducted onboard the NASA DC-8 research aircraft include: DC3 (Deep Convective Clouds & Chemistry (Barth et al., 2015; Nault et al., 2016)), SEAC^{4}RS (Studies of Emissions and Atmospheric Composition, Clouds and Climate Coupling by Regional Surveys (Fisher et al., 2016; Toon et al., 2016)), and KORUS-AQ (KORean-United States Air Quality mission; https://espo.nasa.gov/home/korus-aq; (Nault et al., 2018)). DC3 was conducted out of Salina, Kansas in spring 2012 and focused on investigating the effects of deep convective clouds on upper tropospheric composition and chemistry. SEAC^{4}RS was conducted out of Houston, Texas during late summer 2013, with a focus on effects of deep convection on pollution redistribution and chemistry and feedbacks, a regional survey of biogenic chemistry, and the evolution of anthropogenic and biomass burning emissions and effects on regional air quality. KORUS-AQ was conducted over South Korea and Seoul during spring 2016 to study the local and transport effects on air quality throughout the Korean Peninsula. Mass concentrations shown for aircraft campaigns are always reported in units of standard pressure and temperature (1013 mbar, 273K; often denoted as ng sm^{-3} or µg sm^{-3}, however usually omitting the "s" here as it is implied), while ground campaigns are reported under ambient conditions.

Ground-based campaigns include SOAR (Study of Organic Aerosols at Riverside (Docherty et al., 2011)), MILAGRO (Megacity Initiative: Local And Global Research Observations (Molina et al., 2010)), DAURE (Determination of the sources of atmospheric Aerosols in Urban and Rural Environments in the Western Mediterranean (Minguillon´ et al., 2011; Pandolfi et al., 2014), BEACHON-RoMBAS (Bio–hydro–atmosphere interactions of Energy, Aerosols, Carbon, H_2O, Organics and Nitrogen – Rocky Mountain Biogenic Aerosol Study (Ortega et al., 2014)), SOAS (Southern Oxidant and Aerosol Study (Carlton et al., 2018)), and GoAmazon (Martin et al., 2016, 2017). SOAR-1 (hereafter just SOAR) was conducted during summer 2005 in Riverside, California (eastern Los Angeles metropolitan region) to investigate chemical composition and sources of fine particles of inland Southern California. Details of the measurements used here can be found elsewhere (Docherty et al., 2011). MILAGRO was conducted during late winter / early spring 2006 in and around Mexico City and focused on understanding the emissions, transport, and transformation of pollution in a megacity. The measurements used here were collected at the "T0 urban supersite", 9 km NNE of the city center and are described in detail elsewhere (Aiken et al., 2009, 2010). DAURE was conducted during late winter / early spring and summer 2009 in the Western Mediterranean Basin to investigate urban and rural sources of aerosols in the region. Measurements used here were collected during the winter/spring intensive in Montseny, Spain, a rural location 50 km inland from Barcelona, and described elsewhere (Minguillon´ et al., 2011; Pandolfi et al., 2014). BEACHON-RoMBAS was conducted during summer 2011 at a mid-altitude pine forest in the Colorado Rocky Mountains with a focus on emissions of primary biological particles and SOA precursors, and their transformations and impacts in the atmosphere. Details of the measurements used here can be found elsewhere (Fry et al., 2013; Palm et al., 2017). SOAS was conducted during the

summer of 2013 at a semi-polluted rural mixed forest in central Alabama with a focus on understanding effects of BVOC on oxidants and aerosols and how anthropogenic emissions influences control those processes in the Southeast US. Details of the measurements used here can be found elsewhere (Hu et al., 2016). In addition to standard ambient AMS data, we use AMS measurements collected after ambient gases and aerosol were processed in an oxidation flow reactor (OFR) with OH or NO_3 radicals (Hu et al., 2016; Palm et al., 2017). GoAmazon was conducted during the 2014 wet season (IOP1) and dry season (IOP2) of central Amazonia (sometimes) downwind of a large urban city (Manaus). Details of the measurements used here can be found elsewhere (de Sá et al., 2018, 2019; Palm et al., 2018).

S1.2 Laboratory datasets

In addition to a range of field datasets used for this analysis, a smaller subset of laboratory measurements was included. AMS measurements were collected as part of a series of chamber studies investigating SOA (including $pRONO_2$) formed from reaction of terpenes (α-pinene and Δ-3-carene) with nitrate radicals under a range of seeds and oxidant-precursor ratios (Kang et al., 2016). Also, AMS measurements were made of HPLC-separated $pRONO_2$ products of SOA produced by reaction of 1-pentadecene + NO_3 radicals, according to the methods described in Farmer et al. (2010). Additionally, AMS measurements were made of SOA generated in a chamber from (high-NO) photooxidation of a series of n-alcohols (Liu et al., 2019). The terpene and alkanol SOA and HPLC-isolated products were included to provide additional data to a survey of R_{pRONO2} to that already reported in the literature (see Sect. 3). Specific details on the data used from those experiments are included in Table S1.

S1.3 Data collection and processing

Most details of the data collection and processing for each measurement dataset can be found in the references provided above. All HR-ToF-AMS data was analyzed with the latest standard ToF-AMS software packages available at the time (Squirrel, PIKA (DeCarlo et al., 2006; Sueper, 2021)). For ground-based and laboratory datasets the standard "MS" mode was used where the particle beam is alternately blocked ("closed") and transmitted ("open") with a chopper every ~5 s and data averaged and saved every 1–5 minutes. For aircraft measurements, data was collected in Fast MS mode (FMS (Kimmel et al., 2011)) where the chopper is open for most of a minute, collecting 1 Hz data and then backgrounds (closed) measured every minute for a few seconds - thus allowing for high-time resolution sampling required onboard fast-moving aircraft platforms. For some of the aircraft data presented here, data was analyzed as a 1-minute product, where the raw mass spectra are first averaged and then high-resolution peak fitting is done (which has improved signal-to-noise (S/N) over averaging 1-s peak-fitted data due to nonlinear effects associated with fitting less noisy spectra). The aircraft-based measurements were collected with a highly-customized aircraft version (Nault et al., 2018; Schroder et al., 2018). The only aspect of the aircraft sampling methods and configuration that may affect analysis of nitrates, other than possibly use of the FMS mode, is the presence of the cryopump-cooled shield surrounding the ionization region that substantially reduces backgrounds from some species, thus resulting in improved S/N of some species. For all datasets presented here, the lower spectral resolution (higher S/N) "V-mode" acquisition data (DeCarlo et al., 2006) was used except for SOAR and MILAGRO, where "W-mode" data was used.

Quantifying the NO^+ and NO_2^+ ion signals from ambient high-resolution AMS spectrum involves a few specific steps and assumptions, beyond the general HR peak-fitting methods described in DeCarlo et al. (2006). At *m/z* 30, where NO^+ is found, there are several other peaks that may be present in ambient aerosol such as CH_2O^+, CH_4N^+, $C_2H_6^+$, $H_2N_2^+$, $C^{18}O$, $^{13}CHO^+$, $^{13}C_2H_5^+$, $^{13}CHO_3N^+$, $^{30}Si^+$, $H^{29}Si^+$, $H^{15}NN^+$

(See Fig. S1 in Aiken et al. (2009); Farmer et al. (2010); Fig. S1 here). However, typically only CH_2O^+, $C^{18}O^+$, and $^{13}CHO^+$ would be expected to be close enough to the NO^+ peak or have appreciable signal to affect quantification of NO^+. The two isotope peaks are relatively small due to the ~1% and ~0.2% isotopic ratios, and thus are typically quantified by constraining to their isotopic parent ion peak. In contrast, CH_2O^+ can be of comparable signal to NO^+ and resides ~1.5 peak half-widths (in V-mode sampling) from NO^+; therefore, it can be precisely separated with HR peak fitting (Cubison and Jimenez, 2015).

At *m/z* 46, where NO_2^+ is found, there are several other peaks that may be present in ambient aerosol such as $CH_2O_2^+$, CH_4NO^+, $C_2H_6O^+$, CH_2S^+, NS^+, $C^{18}OO^+$, $^{13}CHO_2^+$, $^{13}CH_3NO^+$, $^{13}CCH_5O^+$, and ^{13}CHS (See Fig. S1 in Aiken et al. (2009); Farmer et al. (2010); Fig. S1 here). However, only $CH_2O_2^+$, $C^{18}OO^+$, CH_2S^+, ^{13}CHS, and $^{13}CHO_2^+$ have substantial overlap with the NO^+ peak, and only $CH_2O_2^+$ and $C^{18}OO^+$ would be expected to contribute substantial signal compared to NO_2^+ for typical ambient aerosol. The sulfur-containing peaks would not be expected from organosulfates, which are known to form in the atmosphere; however, they might be produced by other compounds, such as sulfides, thiols, sulfoxides, or sulfones if they were present in substantial concentrations (which to our knowledge have not been observed). Moreover, the isotopes peaks are often constrained to the parent peaks, minimizing any biases. $CH_2O_2^+$ is typically fit (and is ~1.2 peak half-widths separated from NO_2^+, in V-mode sampling) and $C^{18}OO^+$ is constrained to its isotopic parent ion (CO_2^+) which is precisely quantified. Uncertainties in quantification of the NO_x^+ peak ions will be systematically explored in a separate manuscript.

The standard process for constraining isotopic daughter peaks is to a) fit the parent peak at the lower *m/z*, b) fix the daughter peak according to the naturally occurring isotopic ratio (0.0108 for ^{13}C, 0.0216 for ^{13}CC, 0.00205 for ^{18}O, 0.00411 for ^{18}OO, etc.), and c) fit the remaining selected unconstrained peaks together with the constrained peaks. One exception related to NO_x^+ ion quantification is the $C^{18}O^+$, in the case that the CO^+ ion was not directly fit, which is typical for V-mode data and typical ambient concentrations. In that case, CO^+ is approximated as equal to the particle-phase CO_2^+ signal due to the difficulty of separating CO^+ from the large N_2^+ gas signal (Aiken et al., 2008). However, that step is part of the "fragmentation table" corrections and applied after the high-resolution peak fitting algorithm. Since the $C^{18}O^+$ almost exactly overlaps with the NO^+ peak (*m/z* 29.997990, 29.999161), the estimated $C^{18}O^+$ can simply be subtracted from the NO^+ signal without refitting the spectrum. Accounting for $C^{18}O^+$ interference in the NO^+ peak is typically not done in standard AMS processing. However, it was done for all datasets presented here except for the SOAR and MILAGRO datasets (where its effects are expected to be insignificant). Accounting for $C^{18}O^+$ interference has been standard practice in our $pRONO_2$ analyses since results presented in Fry et al. (2013), in order to most accurately account for organic ion interferences when nitrate concentrations are very low.

When nitrate concentrations are especially low (<10 ng m^{-3}, such as for the SOAS and BEACHON-RoMBAS datasets), it became clear that only "open-minus-closed" (OmC) peak fitting should be used (rather than "Diff"). In OmC fitting, the algorithm fits all peaks separately in the open and closed and then subtracts the integrated values ("sticks" in AMS parlance) to yield the aerosol signal. For "Diff", the background-subtracted high-resolution spectra are subtracted and then that "Diff" signal spectrum is peak fit. Using "Diff" at very low concentrations can result in the fits not converging which are assigned to zero. Including zeros or removing those points, when implementing further data averaging, would potentially bias the data. Use of OmC nearly always results in peak fitting convergence for open and closed spectral fitting, since even if aerosol concentrations are very low, some fitable signal is present in

the background. Thus OmC results for near or below detection limit data will yield noisy signal above/below zero, which can be averaged to derive unbiased concentrations.

S2 Further evaluation of calibration R_{NH4NO3} and *RoR* using ambient data (supporting Sect. 4)

Similar conclusions (to those presented in Sect. 4) can be inferred by inspection of the $R_{ambient}$ vs pNO_3 relationships for two campaigns that showed variable calibration R_{NH4NO3} as shown in Fig. S9d (DAURE) and Fig. S9e (SEAC[4]RS). For the five-week DAURE campaign, nine NH_4NO_3 calibrations were performed, and R_{NH4NO3} varied from 0.30 to 0.54 (Fig. S9d) for unknown reasons (no documented major instrumental changes). Calibration R_{NH4NO3} were linearly interpolated to the sampling data (as shown by coloring in Fig. S9d), and pNO_3-binned averages were computed for three calibration R_{NH4NO3} ranges. That treatment yields similar curves to those shown for studies with constant calibration R_{NH4NO3} values. The averaged curves do not appear to reach the average calibration R_{NH4NO3} at the highest concentrations sampled. It is not clear whether the highest observed fractions of NH_4NO_3 were not high enough to observe that behavior, or if possibly the approximation of interpolation of variable calibrations did not fully capture the true reference R_{NH4NO3} applicable to sampling periods. Nonetheless, the trends in $R_{ambient}$ are qualitatively consistent with average calibrations throughout the pNO_3 range.

Fig S9e presents a similar analysis for SEAC[4]RS; except NH_4NO_3 calibrations were performed more frequently, for every flight (R_{NH4NO3} ranged from 0.4–1.49). However, calibrations during the same day as the flight were not possible, and thus the instrument was shut down and restarted between flights and calibrations. pNO_3-binned averages were computed for eight calibration ranges (each including 1–6 flights) and yielded curves similar to other studies with many leveling remarkably close to the calibration ratios at higher pNO_3. Those that did not, tended to have low upper ranges of concentrations. For SEAC[4]RS, $R_{ambient}$ tended to reach calibration R_{NH4NO3} at much lower pNO_3 concentrations (in some cases as low as 1–3 μg m^{-3}), compared to other studies (~20 μg m^{-3}). See Sect. 7 for further discussion on these differences. Ratios at the lowest pNO_3 approximately grouped into two clusters, but mostly corresponded to their associated calibration R_{NH4NO3}. Estimating *RoR*s using each of the lowest pNO_3 bins yields an average value of 2.9 (±35%), while doubling the number of quantile averages (30 rather than 15 as shown in Fig. S9e) yields a *RoR* of 3.1 (±40%) — generally consistent with the studies summarized in Fig. 1.

An additional statistical test was performed for both the SEAC[4]RS and DAURE campaigns where f_{pRONO2} was calculated using Eq. 1 and the *RoR* value (2.75) to estimate the R_{pRONO2} and alternatively using a fixed R_{pRONO2} of 0.1 (as applied in Kiendler-Scharr, et al. (2016) and several subsequent papers). Correlations of the f_{pRONO2} vs the calibration R_{NH4NO3} were computed with the expectation that a (more) significant correlation for one method would indicate less suitable representation of R_{pRONO2}. However, for both campaigns no significant correlations were found which appears to be due to the high variability in sampling compositions from flight-to-flight (SEAC[4]RS) or the large synoptic-timescale trends in composition at similar timescales as the R_{NH4NO3} variability (DAURE). It appears that in order to glean information from this type of statistical test, the ideal scenario would include a large range of (well-captured) calibration R_{NH4NO3} while sampling air with similar composition. The differences in calculated apportionment and concentrations for using the *RoR* method vs fixed R_{pRONO2} will be discussed in a separate manuscript evaluating apportionment uncertainties, and can be quite substantial.

S3 Detailed summary of prior studies using PMF for $pRONO_2$ separation

As briefly introduced in Sect. 5.2.1, a few studies have reported results for using PMF of ambient AMS spectra including both the OA and NO_x^+ signals to quantify or investigate source associations of

$pRONO_2$. Below, we present details and interpretations of those analyses. Additionally, several aspects of the studies are summarized in Table S4.

In the first report of including nitrate ions in PMF, Sun et al. (2012) included HR ions from OA and the major nitrate, sulfate and ammonium ions for measurements collected in New York City during summertime. Eight PMF factors were resolved. Those included two factors which were dominated by $(NH_4)_2SO_4$ or NH_4NO_3 together with a mix of organic peaks. The NH_4NO_3 factor accounted for 79% of the nitrate; its spectrum was composed of 74% NH_4NO_3 with a NO_x^+ ratio within 5% of the value measured for pure NH_4NO_3, and the associated organic had a relatively low O/C (0.14). The NH_4NO_3 factor peaked during the early morning which was shown to be consistent with the temperature-controlled equilibrium of NH_4NO_3 with HNO_3 and NH_3 gases. Most of the NO_x^+ not in the NH_4NO_3 factor (12%) was apportioned to a factor characterized as the more oxidized (O/C of 0.48 vs 0.27) of two semi-volatile oxidized organic aerosol (SV-OOA) factors with a NO_x^+ ratio equivalent to a *RoR* of 2.6–2.7 (depending on if using the PMF NH_4NO_3 factor or pure calibration NH_4NO_3 NO_x^+ ratio for R_{NH4NO3}), indicative of organic nitrates. That factor was attributed to local photochemically-produced SOA, possibly from biogenic VOC (BVOC) oxidation, peaking mid-day. Alternatively, a *RoR* of 3.0–3.1 (depending on if using the PMF or pure calibration for R_{NH4NO3}) is calculated by combining the three OOA factors (see Table S1; the other two OOA factors contained only NO^+).

Hao et al. (2014) included the HR OA spectra and NO^+ and NO_2^+ ions in PMF analysis of measurements conducted in a rural forested region with urban influences during fall in Finland. Of the four factors resolved, one factor accounted for 63% of the nitrate, its spectrum was composed of 86% NO_x^+ ions with the rest composed of OA ions (O/C = 0.24), and the NO_x^+ ratio was within 5% of the value measured with pure NH_4NO_3. The rest of the NO_x^+ was split between an SV-OOA (28%; commonly referred to as less-oxidized OOA, LO-OOA, in the absence of volatility information; O/C: 0.41), a low-volatility OOA (LV-OOA; 9%; commonly referred to as more-oxidized OOA, MO-OOA, in the absence of volatility information; O/C: 0.74), and hydrocarbon-like OA (HOA; 0.5%) factor. The NO_x^+ ratio for the LV-OOA was similar to the R_{NH4NO3}, while the SV-OOA factor NO_x^+ was nearly all NO^+. The *RoR* for the combined non-NH_4NO_3 factors was 3.6–3.7 (depending on if using the PMF or pure calibration for R_{NH4NO3}). In that study, they explicitly separated the inorganic and organic nitrate concentration time series based on the PMF apportionment of NO_x^+ ions according to the NH_4NO_3 factor and sum of other factors, respectively. The NH_4NO_3 showed a highly-structured time series, on average peaking during morning (likely due in part to effects of temperature and RH) while the $pRONO_2$ was more slowly varying with a fairly flat average diurnal cycle (probably controlled by a combination of boundary layer dynamics, transport, and photochemical production). The strongly contrasting time series as well as similarity of PMF NH_4NO_3 NO_x^+ ratios to pure NH_4NO_3 and *RoR* of PMF $pRONO_2$ to typical values, suggests that the PMF method of separation of the two type of nitrates was likely effective.

In a study focused on $pRONO_2$ in a remote Finnish boreal forest in early spring, Kortelainen et al. (2017) used PMF to separate $pRONO_2$ and NH_4NO_3 from AMS measurements. Like Hao et al. (2014), they included the HR OA spectra and NO^+ and NO_2^+ ions in the PMF analysis. Of the three factors resolved, one was an NH_4NO_3 factor, composed of 88% NO_x^+ ions, with a NO_x^+ ratio identical to the pure NH_4NO_3 calibration, and accounting for 65% of the total nitrate on average. The remainder of the NO_x^+ was mostly apportioned to the SV-OOA (30%; a.k.a. LO-OOA, O/C: 0.44) with the remainder in the LV-OOA (~5%; a.k.a. MO-OOA, O/C: 0.87). Using the same method as Hao et al. (2014), they compute concentrations of NH_4NO_3 from the NH_4NO_3 factor time series and the $pRONO_2$ from the sum of the

other factors (both OOA). The $pRONO_2$ computed from both OOA factors combined had a NO_x^+ ratio equivalent to a *RoR* of 3.5. For the LV-OOA spectrum all the NO_x^+ was only present at NO^+ and therefore the *RoR* for the SV-OOA $pRONO_2$ would have been 3.0. They observed large $pRONO_2$ spikes from plumes from a nearby sawmill, associated with the SV-OOA factor, that they attributed to terpene emissions from the sawmill reacting with nitrate radicals (formed from the associated elevated gaseous NO_x concentrations). Otherwise, $pRONO_2$ was generally enhanced at night, attributed to BVOC reactions with nitrate radicals. They repeated the PMF analysis after removing the sawmill plumes and resolved similar spectra and time series with the same NO_x^+ ratios for the NH_4NO_3 factor and combined OOA factors; however, the spectra for the LV-OOA factor had only NO_2^+ and the spectra for the SV-OOA factor had only NO^+. That apparent poorer resolution of $pRONO_2$ NO_x^+ ratio signature may have been due to the decreased signal-to-noise in the NO_x^+ ions associated with $pRONO_2$ in the absence of the strong $pRONO_2$-containing plumes.

Xu et al. (2015a) performed PMF on seven AMS datasets collected at different locations and seasons in the Southeast US, including the HR OA and NO_x^+ ions. They compare NH_4NO_3 and $pRONO_2$ concentrations calculated with the PMF method (as applied by Hao et al. (2014)) with the NO_x^+ ratio method. For the NO_x^+ ion ratio method, they cite *RoR*s from isoprene+NO_3 SOA and β-pinene+NO_3 SOA experiments with *RoR* of ~2 and ~4 as limits, respectively, and then compute two fixed R_{pRONO2} (0.2 and 0.1) based on the average calibration R_{NH4NO3} of all the studies as upper/lower bounds. Given the evidence from our analysis presented in this paper, using fixed R_{pRONO2} that are not referenced to instrument-specific performance likely introduces biases in the apportionment. Such bias was likely substantial in the Xu et al. study, since the calibration R_{NH4NO3} for the campaigns spanned a factor of 1.7. Therefore, for this study, the upper/lower bounds used for the different measurement campaigns represent a wide range of *RoR*s from 1.7–3.4 up to 2.9–5.8. They show that the main uncertainty in the PMF nitrate apportionment was related to the separation of the NH_4NO_3 factor. For the two summertime studies, no NH_4NO_3 factors were resolved, while for the two "transition" season studies, the NO_x^+ ratio (NO_2^+/NO^+) for the NH_4NO_3 factor was 30–35% lower than for the NH_4NO_3 calibration ratio (toward that expected for $pRONO_2$). On the other hand, for wintertime studies, the NH_4NO_3 factors resolved had very similar NO_x^+ ratios to calibration R_{NH4NO3} (within 5–10%), which is not surprising since the nitrate was dominated by NH_4NO_3 during wintertime (as they calculated from both methods). They suggest that the NH_4NO_3 factors for the transition periods are likely partially contaminated with $pRONO_2$, thus causing $pRONO_2$ to be underestimated. They also show that the NH_4NO_3 factor spectra consisted of only 30–35% nitrate for transition periods and 60–80% in winter. The LO-OOA factors correlated with the $pRONO_2$ (calculated from the NO_x^+ ratio method) better than with pNO_3, especially for the warmer campaigns. Inspection of the spectra for the different factors shows that the LO-OOA factor had a substantially lower NO_2^+/NO^+ ratio than the NH_4NO_3 factor, in some cases near zero. Nitrate was distributed among multiple factors such as NH_4NO_3, HOA, COA (cooking OA), LO-OOA, OOA (but typically not IEPOX-SOA and MO-OOA) with a range of NO_x^+ ratios. BBOA tended to have NO_x^+ ratios similar to the NH_4NO_3 factor (in two out of three cases), which may be~~is likely~~ due to the ~~common~~ presence of NH_4NO_3 in aged biomass burning plumes. Inclusion of the nitrate from the BBOA factor in the $pRONO_2$ calculation, as done in that study, may lead to an overestimate in $pRONO_2$.

For the summer and transition period campaigns, the comparison of the NO_x^+ ratio method and PMF method showed large differences. Given the issues with separating a NH_4NO_3 factor that comparison provided little insights into further understanding of the NO_x^+ ratio method. Consequently, the NO_x^+ ratio method limits was used for their analyses. On the other hand, comparisons for the wintertime data

suggested that use of the fixed R_{pRONO2} of 0.1 (equivalent to *RoR*=3.4) was most consistent with the PMF results (compared to using R_{pRONO2}=0.2, *RoR*=1.7), so for those studies they used the PMF results or a combination of PMF and the NO_x^+ ratio method (with R_{pRONO2} of 0.1). In one of the winter studies, the performance of PMF appeared superior due to the often negative $pRONO_2$ concentration calculated with the NO_x^+ method — which is not unexpected when NH_4NO_3 dominates the nitrate (see later in this section, and Sect. 5.2). Finally, they conducted PMF separately with only OA ions and with both OA and NO_x^+ ions and overall the factor spectra and time series were very similar. That suggests that inclusion of NO_x^+ ions did not play a large role in factor determination, beyond of course resolving NH_4NO_3 factors in some cases.

In a study conducted in Beijing during a biomass burning (fall) and a coal combustion influenced (winter) period, Zhang et al. (2016) conducted PMF on combined HR OA and NO_x^+ ion spectra. PMF was run for the two periods, separately. For both datasets, an NH_4NO_3 factor was resolved with spectra comprised of 84–85% NO_x^+ ions, and NO_x^+ ratios that were within 4–7% of the calibration R_{NH4NO3}. Those factors accounted for 77–83% of the total nitrate, on average. Ranges quoted indicate results for the two periods. Four or five other factors were resolved including BBOA or CCOA (coal combustion OA), COA, HOA, OOA (or SV-OOA and LV-OOA). They follow the method of Hao et al. (2014) and calculated concentrations of NH_4NO_3 and $pRONO_2$ by equating the NO_x^+ in the NH_4NO_3 factor to NH_4NO_3 and the sum of the NO_x^+ in all other factors to $pRONO_2$, yielding average f_{pRONO2} of ~20% for both periods. However, that treatment appears potentially problematic since the NO_x^+ ratios in the spectra of the POA factors, that comprised a large amount of the calculated $pRONO_2$, are more similar to NH_4NO_3 than $pRONO_2$. For example, HOA has a NO_x^+ ratio roughly the same as the NH_4NO_3 factor; BBOA and CCOA appear to have only NO_2^+. The time series of those factors may have been tightly correlated with some NH_4NO_3 production, resulting in PMF apportioning part of the NH_4NO_3 to those factors. On the other hand, the OOA factor spectra showed NO_x^+ ratios much lower than NH_4NO_3, more consistent with $pRONO_2$. Thus, if all the NO_x^+ associated with the POA factors was instead assigned to NH_4NO_3, the average concentrations of $pRONO_2$ calculated would be a factor of ~2 and ~4 times lower for the biomass burning period and coal combustion periods, respectively.

Combined OA + NO_x^+ PMF (HR) was also conducted with data collected in an urban location in southern China (Shenzhen) during four separate seasons (Yu et al., 2019). During the spring, summer and fall seasons, four factors were resolved: HOA, LO-OOA, MO-OOA and a NH_4NO_3 factor. During the winter, the same factors and additionally BBOA and COA factors were resolved, however the $pRONO_2$ fraction was too small to accurately apportion, so their analysis focused on only the three warmer seasons. $pRONO_2$ was apportioned as the sum of all of the non-NH_4NO_3 factors, with the largest fraction in the LO-OOA factor for all seasons. The total $pRONO_2$ correlated best with the LO-OOA factor with stronger correlations in summer and also during nighttime, an aspect they focus on to support discussions of the importance of nighttime $pRONO_2$ formation processes. The NO_x^+ ratios for the NH_4NO_3 factors were similar to the calibration ratios (5–10% lower). The NO_x^+ ratios for the $pRONO_2$-apportioned factors were very low in most cases (nearly all NO^+) with a few cases where ratios were similar to that expected for $pRONO_2$ (see Table S4). They show that the NO_x^+ ion apportionment among factors was fairly insensitive (~10–20%) to changing FPEAK over a wide range (-1 to 1), and that increasing to 5 factors had little effect on overall inorganic/organic nitrate apportionment. Inorganic/organic nitrate was also apportioned with the NO_x^+ ratio method and compared to the PMF method. Following the method in Xu et al. (2015a), upper and lower limits (for $pRONO_2$) were estimated using *RoR*s of 2.08 and 3.99, respectively. The two methods correlated fairly well (R=0.82, 0.82, 0.72 for $pRONO_2$ and R=0.92, 0.87, 0.86 for NH_4NO_3, for

summer, spring, autumn), using the upper limit (*RoR* 3.99). However, they showed better average quantitative agreement with the lower limit assumption (*RoR* 2.08; correlations not reported). They suggest that may have been related to the modestly lower NO_x^+ ratios resolved for the NH_4NO_3 factors compared to the calibration ratio.

Tiitta et al. (2016) investigated the aerosol composition of logwood combustion in a chamber without aging (thus only POA) and with "dark" aging by O_3 (+NO_x, NO_3 radicals), and photochemical aging (UV light + HONO, thus OH/NO_x) (thus POA+SOA). They performed PMF on a combined AMS OA + NO_x^+ ions (NO^+, NO_2^+) spectra time series and observed two POA factors and three SOA factors. One of the two POA factors they identified as more associated with $pRONO_2$ (based on the contribution and ratio of NO_x^+ to the spectrum), however both showed prominent NO_x^+ peaks in the spectra and had substantially lower NO_x^+ ratios than the calibration NH_4NO_3 (equivalent *RoR* of 1.8, 2.5). Two of the SOA factors (from O_3/NO_x/NO_3 and from OH/NO_x oxidation) showed prominent NO_x^+ ion peaks with ratios consistent with $pRONO_2$ (equivalent *RoR* of 2.6 and 3.1, respectively) while the other (from O_3 oxidation) had only a little nitrate (consisting of only NO_2^+). While the *RoR*s were generally similar to the *RoR* of 2.75 derived in this study, it is difficult to compute the most representative overall $pRONO_2$ ratio for this study since: 1) an NH_4NO_3 factor was not separated (although NH_4 was low in POA: ~10% of nitrate in moles), 2) other inorganic nitrate may have been present (although the authors suggest it was negligible), and 3) the average mass contributions of PMF factors are not provided in order to compute combined mass-weighted NO_x^+ ratios. However, with dark (O_3/NO_x/NO_3) or UV (OH/NO_x) aging, the two SOA factors with *RoR*s of 2.6 and 3.1 grew in and typically dominated the overall contribution to OA mass (individually or combined), and thus provide an approximate range for log burning SOA for our survey (i.e., Fig. 1, Table S1). In that study, $pRONO_2$ concentrations were computed using the NO_x^+ ratio method with the measured calibration R_{NH4NO3} (0.4–0.6), and assuming a fixed R_{pRONO2} of 0.1 (thus a *RoR* of 4–6).

Reyes-Villegas et al. (2018) investigated OA sources during "Bonfire Night" and surrounding periods, and $pRONO_2$ concentrations were calculated using the NO_x^+ ratio method with the measured calibration R_{NH4NO3} (0.5), and assuming a fixed R_{pRONO2} of 0.1 for $pRONO_2$ (based on the lowest observed NO_x^+ ratio per Kostenidou et al. (2015), thus a *RoR* of 5). Since the data were collected with a UMR AMS (C-ToF-AMS), *m/z* 30 and *m/z* 46 were treated as equivalent to NO^+ and NO_2^+, respectively, which they justify based on the low contribution of other ions at *m/z* 30 in BBOA for prior HR AMS results. Subsequently, they used the calculated $pRONO_2$ time series, together with the standard UMR OA PMF matrix, for conducting constrained PMF (ME-2; (Paatero, 1999; Canonaco et al., 2013)). They separated two factors that they identify as primary and secondary $pRONO_2$ factors. They also show similar separation into primary and secondary $pRONO_2$ based on using the regression slope of total $pRONO_2$ with the BBOA factor during an intense biomass burning event. This hybrid method may have the advantage that separating $pRONO_2$ beforehand may allow for additional separation into primary and secondary $pRONO_2$. On the other hand, prior separation with the NO_x^+ method (as opposed to inclusion of the NO_x^+ ions in the PMF) may result in loss of some information since the NO_x^+ ratios of the resolved $pRONO_2$-containing factors, which can be useful for evaluation, are not determined.

Kim et al. (2018) conducted PMF including signals from OA as well as nitrate, sulfate and ammonium ions for investigation of sources and chemistry of aerosol in Seoul Korea as part of KORUS-AQ. They resolve six factors including four OA (two primary, two secondary) as well two inorganic (nitrate and sulfate, both with ammonium). Both inorganic factors show relatively small contributions from OA. However, they do not attempt to interpret the nitrate contributions to the OA factors, apportion

organic/inorganic nitrate, nor provide adequate information to evaluate the NO_x^+ ratios resolved for different factors or factor types.

Zhu et al. (2021) apportioned nitrate using both the OA + NO_x^+ PMF (HR) method and the NO_x^+ ratio method for a study at a rural site in the North China Plains during summer. BBOA, HOA, OOA, NIA factors were separated and the NIA apportioned to inorganic nitrate and the nitrate in the other three factors to $pRONO_2$. They report that two separate OOA factors (LO-OOA and MO-OOA) were resolved when using only OA ions, but not when including the NO_x^+ ions. Of the nitrate apportioned to $pRONO_2$, 11.8%, 85%, and 3.2% was contributed by the HOA, BBOA, and OOA factors, respectively. The NO_x^+ ratios for the resolved factors appear to be similar to the NH_4NO_3 calibration (~0.34 vs 0.43-0.47) for NIA, much lower for BBOA (~0.02), entirely NO^+ for HOA and possibly entirely NO_2^+ for OOA. For the NO_x^+ ratio method, *RoR*s of 1.4-4.0, based on four literature reports, were used to compute upper and lower limits. Comparison of $pRONO_2$ resolved using the NO_x^+ ratio (for the upper limit assumption) vs PMF method showed a slope of 1.2 and R^2=0.58. Average $pRONO_2$ concentrations and $fpRONO_2$ for the PMF method were in between the NO_x^+ ratio method limits. $pRONO_2$ concentrations computed with the NO_x^+ ratio method showed the strongest correlations with the BBOA factor (R^2=0.50) and the poorest with the LO-OOA factor (R^2=0.04), which they speculate could be due to $pRONO_2$ production from biomass burning VOC reactions.

Xu et al., (2021) also apportioned nitrate using PMF including OA and nitrate ion signals for measurements conducted in the North China Plain. They compared the results to using the NO_x^+ ratio method and newly-proposed method using thermal denuder measurements. However, $pRONO_2$ values computed with the PMF method were much lower than the other methods (which showed reasonable agreement with each other). Citing several possible sources of uncertainty of the PMF method for that analysis, they did not focus on further assessments of the PMF method, nor use it for their scientific analysis.

Lin et al. (2021) conducted PMF using only the NO_x^+ ions and 16 nitro-polycyclic aromatic hydrocarbon (NPAH, markers of combustion) ions fitted in the soot particle aerosol mass spectrometer (SP-AMS) spectrum for field measurements conducted in NW China during November. Three factors were resolved and assigned as inorganic nitrate, secondary organic nitrate, and primary organic nitrate. During a haze period the inorganic nitrate factor comprised 80% of the pNO_3, with 17% and 3% attributed to the secondary and primary organic nitrate factors, respectively. During the "reference period" (outside of haze events), those fractions were 47%, 36%, and 17%, respectively. The NO_x^+ ratios for the factor profiles resolved were 0.77 (0.72), 0.34 (0.28), and 0.15 (0.09) for two different approaches used (unconstrained and constrained PMF), respectively. Thus, taking the inorganic nitrate factor NO_x^+ ratio as equivalent to the R_{NH4NO3} (which was stated to be similar), the secondary organic nitrate factor ratio has a *RoR* of 2.3 (2.6), while the primary organic nitrate would be much higher (5.1, 8.0). It is not clear if the AMS nitrate signal from the factor assigned as primary organic nitrate is comprised of organic nitrates, nitroaromatics and/or other NO_x^+ ion-producing compounds. Combustion source studies conducted in the laboratory showed that NO_x^+ ratios for lubricant oil and coal were similar to the inorganic nitrate ratios, while biomass burning produced NO_x^+ ratios were similar to the secondary organic nitrate factor ratios. The constrained PMF approach involved constraining all the NPAH ion signals to the primary organic nitrate factor, and was used for the main scientific analyses. The NO_x^+ ratio method was also conducted to separate inorganic and organic nitrate using a range of R_{pRONO2}, 0.1-0.34 (0.1 per Kiendler-Scharr et al. (2016) and 0.34 representing the constrained PMF-resolved secondary

organic nitrate factor), representing *RoR* of 7.7-2.3. Organic nitrate concentrations calculated using R_{pRONO2} = 0.34 agreed well with the PMF apportionment (PMF vs NO_x^+ ratio method regression slope: 0.88), while using R_{pRONO2} = 0.1 did not (PMF vs NO_x^+ ratio method regression slope: 0.46), consistent with using a *RoR* values recommended in this manuscript.

S4 Expanded details and discussion of new results for PMF separation of $pRONO_2$ and comparison to *RoR* method (briefly summarized in Sect. 5.2.2).

We conducted PMF on the combined OA and $H_yNO_x^+$ family spectra time series for the same two flights from the SEAC[4]RS campaign as discussed in Sect. 5.1 (RF16, RF18). Unless otherwise specified, PMF analysis was conducted with unconstrained PMF using the PMF Evaluation Tool (PET, v3.01) (Ulbrich et al., 2009). Note that although all the $H_yNO_x^+$ ions that were fit were included in the PMF, the average contributions of all ions other than NO^+, NO_2^+ (and N^+ which is not fit and is fixed as 4% of NO^+ and therefore not included in PMF) were <1% of the $H_yNO_x^+$. Moreover, the apportionment of those ions did not show any clear patterns and spread fairly similarly among all factors, likely due to their low signal-to-noise. Therefore, discussions here focus only on the NO^+ and NO_2^+ ions and nitrate associated with PMF results was reported as the sum of NO^+ and NO_2^+ (plus 4% of NO^+).

Initially, PMF was conducted on 1-s data for both flights. NH_4NO_3 factors with NO_x^+ ratios similar to calibration R_{NH4NO3} were consistently resolved. However, neither individual factors nor the re-combined non-NH_4NO_3 factors showed NO_x^+ ratios similar to those expected for $pRONO_2$ (*RoR*~2.75) and in many cases several of the factors contained only NO^+ or NO_2^+. Generally, most of the non-NH_4NO_3 NO_x^+ concentrations were apportioned to one or two factors that were associated with biogenic OA for 5–6 factors solutions. Several iterations were conducted to test if better separation of individual factors or recombined factors with NO_x^+ ratios representing $pRONO_2$ was possible including: always exploring number of factors up to 12, always varying FPEAK from -1 to +1 (by 0.1 increments), upweighting the NO_x^+ ions by a factor of 2 or 10, downweighting the NO_x^+ ions by a factor of 2 or 1000 (essentially to remove any weight of the NO_x^+ ions in determining the overall OA factor spectra, while still keeping the ions present for assignment to factor spectra), and combining the upweighting/downweighting (or no reweighting) with excluding/including large biomass burning spikes (OA>10–20 μg m^{-3}). None of the iterations appeared to produce solutions with substantially improved separation of NO_x^+ ratios reflective of $pRONO_2$. Some general behavior included: 1) upweighting NO_x^+ ions tended to result in splitting of the NH_4NO_3 factor into factors with only NO^+ and only NO_2^+ at lower threshold of number of factors, 2) downweighting NO_x^+ ions by a factor of 2 generally had little effect on the NO_x^+ ion apportionment, while aggressive downweighting (×1000) resulted in NO_x^+ ions being apportioned among most factors with ratios similar to the average spectrum, 3) increasingly positive FPEAK values tended to result in separate and combined non-NH_4NO_3 factors with increasing relative amounts of NO^+ (often solely NO^+) and the NH_4NO_3 factor spectrum becomes an increasingly higher fraction NO_x^+ ions, 4) increasingly negative FPEAK values tended to progressively shift separate and combined non-NH_4NO_3 factors toward NH_4NO_3 NO_x^+ ratios, and 5) excluding biomass burning spikes resulted in a more mixed/aged BBOA factor (with smaller NO_x^+ contribution) or no BBOA factor at all. Finally, PMF with the 1 Hz data was conducted for OA ion matrix only (excluding $H_yNO_x^+$ ions) which produced very similar factor spectra and time series, as also reported in Xu et al. (2015a).

Additionally, *constrained* PMF was conducted on the 1-s data (ME-2; Paatero, (1999)) using the SoFi software package (Canonaco et al. (2013); v.6.3). One factor was constrained to be purely NO^+ and NO_2^+ at the ratio of the nearest calibration R_{NH4NO3} or the ratio for the NH_4NO_3 factor separated with

unconstrained PMF. No downweighting and upweighting of NO_x^+ ions was tested, rather only excluding and including large biomass burning plumes was tested. Overall results were similar to unconstrained PMF results, except that when a NO_x^+ ratio higher than that resolved with unconstrained PMF was used for the constrained NH_4NO_3 factor, all other factors contained only NO^+, suggesting that the prescribed NO_x^+ ratio for NH_4NO_3 was too high. The similarity of the results was not surprising since the unconstrained PMF already appeared to separate out a reasonable NH_4NO_3 factor. In situations where unconstrained PMF does poorly at separating an NH_4NO_3 factor, like described in Xu et al (2015a) discussed above, constrained PMF with a fixed NH_4NO_3 factor, based on offline calibrations, may be an effective approach to better separate nitrates using PMF.

S4.1 PMF of SEAC[4]RS RF16

Due to the inability of 1-s data to resolve separate or combined factors with NO_x^+ ratios similar to expected $pRONO_2$ ratios, PMF was conducted on 1-min data. Results from RF-16 are discussed here first. The main difference, compared to the 1-s analysis, was that the 1-min analysis was effective at separating factors (native individual factors and combined) with NO_x^+ ratios similar to a *RoR* of 2.75. Nearly the same iterations were performed as for the 1-s data (i.e. varying number of factors and FPEAK, upweighting (×2, ×10) / downweighting (×2, ×10) NO_x^+ ions, and including/excluding large biomass burning plumes). The effects of those iterations on the NO_x^+ apportionment (and ratios in profile spectra) and overall factors were generally similar to those described above for the 1-s runs, with results similar to the 1-min base run or degraded.

S4.1.1 Exploration of nitrate concentrations and NO_x^+ ratios apportionment using PMF (SEAC[4]RS RF16)

The results for the solutions for the FPEAK=0 runs with the standard NO_x^+ ions error weighting and unconstrained PMF (with biomass burning plumes included) are described in detail here. The results for the NO_x^+ ratios for different number of factors is shown in Fig. S14. For 3-factor solutions and higher, an "NH_4NO_3 factor" with a nearly constant NO_x^+ ratio (NO_2^+/NO^+=0.70 or NO_2^+/NO_x^+=0.41), and consistent with the NH_4NO_3 offline calibration ratios, is separated. A calibration was performed two days before RF16 and one day afterward with NO_x^+ ratios of 0.96 and 0.71, respectively. Given the variability in the NO_x^+ ratios measured in offline calibrations during the SEAC[4]RS campaign (Sects. 4 and S2, Figs. S8 and S9e), the PMF-resolved NO_x^+ ratio is consistent with the offline calibrations. Also for 3-factor solutions and higher, a biomass burning factor is resolved with a NO_x^+ ratio nearly identical to the NH_4NO_3 factor, up through the 7-factor solution. With increasing numbers of factors for the biomass burning factor, there is a decrease in the contribution of NO_x^+ to the factor spectrum as well as the NO_x^+ concentration attributed to the factor time series. This behavior of the NO_x^+ ions is consistent with nitrate aerosol in BBOA being dominantly NH_4NO_3 (Fig. 3), and PMF apportions it to either the NH_4NO_3 or BBOA factor with shifting proportions as the two factors evolve at higher factor solution numbers (e.g., the NH_4NO_3 factor spectrum has decreasing organic ion contributions). The remainder of the NO_x^+ is distributed among the non-NH_4NO_3/non-BBOA factors with a large range of NO_x^+ ratios (from all NO^+ to all NO_2^+), but with most of the NO_x concentration apportioned to LO-OOA factors. However, the NO_x^+ ratios of the non-NH_4NO_3/non-BBOA factor spectra combined (mass-weighted) for 5-factor solutions and higher is fairly similar to that predicted for a $pRONO_2$ for a *RoR* of 2.75 (NO_2^+/NO_x^+=0.203).

The 5-factor solution was identified as the most meaningful solution due to the overall factor solution spectra and time series. The factors separated include NH_4NO_3, BBOA, IEPOX-SOA, LO-OOA, and

MO-OOA. At higher numbers of factor solutions, in some cases factors split into very similar spectra and/or had time series that were very similar, noisy, or sometimes anticorrelated with each other at high frequency (yielding the results less meaningful). The 5-factor, FPEAK=0 solution spectra are shown in Fig. S15 and are very similar to the factors resolved for other summertime AMS measurements in the SE US (Xu et al., 2015a, 2015b) with the additional NH_4NO_3 factor. Like observed in other studies, the NH_4NO_3 factor spectrum had a substantial contribution from non-NO_x^+ ions. The contribution of NO_x^+ to the NH_4NO_3 spectrum increased from 19% to 36% from the 5-factor solution to the 12-factor solution (FPEAK=0; Fig. S14), and progressively with increasing FPEAK, up to 92% at FPEAK= +1.0 for the 5-factor solution (not shown). With those shifts, the NH_4NO_3 factor retained a similar NO_x^+ ratio; however, with increasing FPEAK, the NO_x^+ ratios for the combined non-NH_4NO_3 / non-BBOA factors shifted to values substantially below expected $pRONO_2$ *RoR*s and decreasing concentrations of NO_x^+. Also, with increasing numbers of factor solutions and FPEAK>0, the fraction of NO_x^+ attributed to BBOA shifted to the NH_4NO_3 factor. However, despite some potentially favorable, "cleaner", factor separations for the NH_4NO_3 and BBOA factors, the degradation in the overall factor separations and NO_x^+ ratios ruled out their use in this analysis.

The factor time series (including AMS OA and nitrate combined) and average mass fractions are shown in Fig. S16. In addition to the overall low concentrations associated with high altitudes (see Fig. 3), at lower altitudes, the MO-OOA tends to be least variable, the IEPOX-SOA was more variable, and the LO-OOA was the most variable of the secondary factors. Biomass burning was fairly pervasive at small concentrations at lower altitudes and showed very high spikes when intercepting a few concentrated plumes. The NH_4NO_3 factor times series was very different than the other factors, is similar to the NH_4NO_3 separated with the NO_x^+ method discussed in Sect. 5.1, and is further discussed below in this section.

In order to explore the robustness of the NO_x^+ ratios for individual and combined factors, 100 bootstrapping or starting seed iterations (Ulbrich et al., 2009) were run for the base case discussed above. Figure S17 shows histograms of the NO_x^+ ratios for the bootstrapping and seeding for each factor and the combined non-NH_4NO_3 / non-BBOA factors (therefore the three OOA/SOA factors combined). For the seeding runs, the distributions for the NH_4NO_3, BBOA, LO-OOA, and combined OOA/SOA factors are very narrow, while the bootstrapping distributions are a little broader for the NH_4NO_3 and BBOA factors and substantially broader for the LO-OOA and combined OOA/SOA factors. For both cases the BBOA was indistinguishable from the NH_4NO_3 and the IEPOX-SOA and MO-OOA highly variable. The ratios for the IEPOX-SOA are probably not meaningful since the amount of NO_x^+ in the spectra (Fig. S14) and the overall contribution to total NO_x^+ (Fig. S18) was very small. On the other hand, the MO-OOA spectra showed modest NO_x^+ contributions in the factor spectra (Fig. S15a, ~one-third that of LO-OOA) and to the average overall contribution to total NO_x^+ (Fig. S18a, half to two-thirds that of LO-OOA) for the bootstrapping runs (lower for seeding, Figs. S15b, S18b). The time series of the NO_x^+ concentration apportioned to each factor (Fig. S18a) shows that for the bootstrapping runs, the relative variability in the solution iterations for MO-OOA is quite high compared to the LO-OOA; while the variability for the total (OA + NO_x^+) concentrations of those factors is comparable (Fig. S16a). This may indicate that the more aged and mixed-source OOA has more variable $pRONO_2$ contribution and the PMF model of fixed factor profiles does not work well for the NO_x^+ ions apportionment. Nonetheless, it can be seen that the average NO_x^+ ratio for the combined OOA/SOA factors is similar to the LO-OOA factor (Fig. S17). For the bootstrapping, the average NO_x^+ ratios were equivalent to a *RoR* of 3.03 ± 0.54 for LO-OOA (for NO_2^+/NO_x^+ between 0.1 and 0.3) and 2.92 ± 0.43 for the combined OOA/SOA factors. For the seeding,

the average NO_x^+ ratios were equivalent to a *RoR* of 3.00 ± 0.19 for LO-OOA and 3.19 ± 0.14 for the combined OOA/SOA factors.

It is notable that, while the NO_x^+ ratios for the LO-OOA factor appear to be representative of $pRONO_2$, there are several bootstrapping runs with much lower NO_x^+ ratios and often with only NO^+. This may be largely due to the limited S/N in the NO_x^+ ions, particularly the lower NO_2^+, limiting the robustness of apportionment of those ions to and between OOA factors. However, the apportionment of NO_x^+ when considering the combined SOA/OOA factors appears to be substantially improved, as seen by the narrower NO_x^+ ratio distributions (Fig. S17) and variability in NO_x^+ concentrations time series (Fig. 4 vs Fig. S18).

In order to investigate the relationship between the NO_x^+ ratio in the factor profile and NO_x^+ concentrations apportioned to a factor time series, NO_x^+ concentrations for the LO-OOA from bootstrapping were compared for different NO_x^+ ratio ranges. Regression slopes were compared between the average concentrations using all solutions to those when $NO_2^+/NO_x^+ < 0.1$ or ≥ 0.1 (which were mostly ~0 and near 0.2, respectively; see Fig. S17). The scatterplots and regression fits are shown in Fig. S19. For $NO_2^+/NO_x^+ < 0.1$ (≥ 0.1), NO_x^+ concentrations were 69% (123%) that of the average of all solutions. Thus, the low NO_x^+ ratio solutions were 56% of the high NO_x^+ ratio solutions. This suggests that when the NO_x^+ ratio falls well below the expected $pRONO_2$ *RoR*, more total NO_x^+ signal is "lost" than just the NO_2^+, since a loss of only NO_2^+ would yield a value only ~20% lower (i.e. $NO_2^+/NO_x^+ = 0$ vs 0.2), not 44% lower. This exercise suggests that the NO_x^+ ratios resolved for factors may be indicative of substantial changes in nitrate apportionment. Consequently, care should be taken when interpreting individual or combined factor apportionment when NO_x^+ ratios diverge substantially from expected $pRONO_2$ ratios. This highlights the importance of exploring the variability and robustness of the resolved NO_x^+ ratios and apportionment (e.g., bootstrapping, FPEAK). In this particular example, a case could be made that nitrate apportionment to the LO-OOA factor is better represented by the average of the solutions with NO_x^+ ratios in an acceptable range (e.g., $NO_2^+/NO_x^+ > 0.1$ or 0.15–0.25).

While the average NO_x^+ ratios and the concentrations of nitrate apportioned to $pRONO_2$ vs NH_4NO_3 for bootstrapping vs seeding (Fig. S20) is very similar, by all metrics (Figs. S15, S16, S17, S18, S20), the variability of the seeded runs was substantially smaller than for the bootstrapping. This indicates that for this dataset, the starting point of the PMF algorithm had little influence on the resolved solutions. On the other hand, the substantial variability in the bootstrapping results suggests that those may be a better metric of overall robustness. Therefore, we focus the remainder of discussions and results on averages and variability from the bootstrapping analysis.

S4.1.2 Comparison of PMF method vs *RoR* method for apportionment (SEAC[4]RS RF16)

Comparisons of NH_4NO_3 and $pRONO_2$ concentrations using the *RoR* and PMF methods are shown in Fig. 4. As discussed above, for the PMF method NH_4NO_3 was calculated as the sum of the NH_4NO_3 and BBOA factors and $pRONO_2$ was calculated as the sum of the three SOA factors (LO-OOA, MO-OOA, IEPOX-SOA). Overall, the NH_4NO_3 agrees very well between the two methods, which is likely in large part due to the fact that NH_4NO_3 often dominated the nitrate. On average, the apportionment of $pRONO_2$ is similar but with notable differences. For much of the flight, NH_4NO_3 dominates the pNO_3 (~90%), and consequently the $pRONO_2$ computed with the NO_x^+ ratio method tends to be fairly noisy due to the measured NO_x^+ ratio being near or exceeding the pure NH_4NO_3 ratio line. Under those conditions, small variability in the measurement or uncertainties in the bounding ratios can lead to large relative uncertainties in $pRONO_2$. In contrast, under those conditions the PMF-computed $pRONO_2$ concentrations

appear to be less noisy in terms of the variability of the averages and standard deviations from the bootstrapping (Fig. 4). This may be due to the additional information and leverage that the other OA ions exert on the separation of the SOA factors which are not strongly affected by the large relative contributions of the NH_4NO_3 NO_x^+ ions. Similar behavior in NH_4NO_3 calculated with the NO_x^+ ratios occurs when $pRONO_2$ >> NH_4NO_3, such as around 18:45 during this flight (although not easily visible due to scaling in Fig. 4, top). Large relative variabilities in $pRONO_2$ calculated with the NO_x^+ ratios are also apparent when pNO_3 is very low, since the NO_x^+ ratio noise blows up. In the time series shown in Fig. 4, those points are screened as below detection limit (indicated by different shading) as determined by the detection limit of the NO_x^+ ratio. However, those points are mostly below the pNO_3 detection limit and thus still provide useful constraints on both the $pRONO_2$ and NH_4NO_3 concentrations, despite the large uncertainties in relative apportionment. During those periods, the PMF-apportioned concentrations show much less variability than the NO_x^+ ratio method and are near zero.

The scatterplots in Fig. 4 (bottom left) shows the correlations and regression fits for both nitrate types derived by the two methods. The slope for NH_4NO_3 is near unity (1.04) and highly correlated (R^2=0.995). For $pRONO_2$, the slopes vary, depending on the fitting method (ODR vs non-ODR), with slopes of 0.86 and 1.30 and R^2 = 0.49. The non-ODR fit may be more appropriate if uncertainties in the NO_x^+ method dominated over those for PMF. Limiting to data only when $f_{pRONO2} > 0.3$, the slopes are 1.11 and 1.42 (ODR, non-ODR) with an improved correlation (R^2 = 0.68). Figure 4 (bottom right) shows the PMF-computed $pRONO_2$ vs the TD-LIF Tot-$RONO_2$, similar to Fig. 3 (bottom left) with the NO_x^+ ratio method. The slope is very similar to when using the NO_x^+ ratio method, but the correlation is improved (0.72 vs 0.49) or similar to when the NO_x^+ ratios method was screened for $f_{pRONO2} > 0.3$ (0.76 vs 0.69). This suggests that the methods perform similarly when NH_4NO_3 does not dominate while the PMF method performs better when NH_4NO_3 dominates (in this case). However, it is not possible to assess the true accuracy of the PMF separation without an independent determination of $pRONO_2$. While the noise for the PMF method generally appears to be lower than for the NO_x^+ method, there may be factors dampening the noise or other biases such as the fact that the PMF model, by nature, apportions a fixed nitrate/OA ratio to each factor. A fixed chemical composition is an approximation since the chemical composition of sources may evolve (such as hydrolysis loss of $pRONO_2$ or gas-particle partitioning) or variable in different air masses sampled. In contrast, the NO_x^+ ratio method would not be prone to such effects since it only relies on the information contained in the nitrate ions time series. Scatterplots showing the same information as Fig. 4, except using the seeding results are shown in Fig. S21 with very similar results.

S4.2 PMF of SEAC^{4}RS RF18

Results from a similar analysis and comparisons for the SEAC^{4}RS RF18 flight (see Sect. 5.1) are shown in Figs. S22–S28. Overall, the results are similar, with similar factors resolved and similar comparisons between the PMF method and NO_x^+ method as well as compared to the Tot-$RONO_2$. However, there were a handful of notable differences in the analysis and results, compared to RF16. For example, the MO-OOA factor comprised a substantially smaller fraction of both OA and NO_x^+ concentrations at lower altitudes when OA concentrations were higher, but generally larger contributions when OA was lowest (Fig. S26, S27 vs S16, S18). Overall, NH_4NO_3 tended to comprise a smaller fraction and $pRONO_2$ a larger fraction of the nitrate compared to RF16 (Fig. S27 vs S18). Unlike RF16, for RF18 MO-OOA NO_x^+ ratios for the bootstrapping grouped around expected $pRONO_2$ ratios (Fig. S25 vs S17). Also unlike RF16, the IEPOX-SOA factor spectrum for RF18 contained a significant NO_x^+ contribution (Fig. S24 vs S15a; ~20% that of LO-OOA or MO-OOA, compared to 1% and 4% for RF16), and comprised a

substantial fraction of the overall NO_x^+ apportionment (Fig. S27 vs S18a; 5–9% compared to 0.3–0.4% for RF16 depending on weighting). While organic nitrate formation is not expected for the low-NO conditions that form IEPOX-SOA, this could be due to coincident presence or formation of isoprene, monoterpene or other VOC-derived nitrates in the presence of some NO_x that PMF cannot separate perfectly. The fact that a lot of the concentration variability is driven by aircraft movement in and out of the boundary and residual layers may hinder clean separation of some nuances of co-located sources. Finally, inspection of the NO_x^+ ratios for different numbers of factors resolved (Fig. S23) and bootstrapping results for the 5-factor solution (Fig. S25) for different FPEAK values showed that using FPEAK = -0.1 produced NO_x^+ ratios for the OOA factors much more representative of $pRONO_2$, thus all analysis and comparisons were conducted with the FPEAK = -0.1 (and 5-factor, bootstrapped) solution.

Some trends and statistics for the RF18 analysis that were reported for RF16 are summarized here. For the bootstrapping (FPEAK = -0.1), the average NO_x^+ ratios were equivalent to a *RoR* of 2.83 ± 0.64 for LO-OOA and 2.96 ± 0.28 for the combined OOA/SOA factor. As done for RF16, the concentrations of NO_x^+ apportionment were compared for bootstrap results when NO_x^+ ratios were low/high for the LO-OOA factor. This test was done for FPEAK=0 (rather than FPEAK = -0.1, which was selected for most analyses), since it has a broad range of NO_x^+ ratios (unlike FPEAK = -0.1, which is fairly narrow) — see Fig. S25. Using the same high/low criteria (NO_2^+/NO_x^+ ≥0.1 vs <0.1 for FPEAK = 0, on average 0.041 vs 0.134), resulted in NO_x^+ concentrations for low NO_x^+ ratios on average 74% that for high NO_x^+ ratios (Fig. S28). Thus, like for RF16, this suggests that solutions resolving lower NO_x^+ ratios tend to apportion substantially even less NO_x^+ concentration than the amount from the reduction of NO_2^+ signal apportionment alone (26% vs ~10%). Again, this results suggests that PMF solutions that do not show NO_x^+ ratios expected for $pRONO_2$ may also correspond to time series with biased concentrations, and emphasizes the importance of evaluating the variability and robustness of solutions. In this case, we chose the FPEAK = -0.1 solution instead, due to the narrower distributions in NO_x^+ ratios and values consistent with expected $pRONO_2$ ratios for LO-OOA, MO-OOA, and combined OOA/SOA.

Like for RF16, the NH_4NO_3 factor progressively "cleans up" with increasingly positive FPEAK. The fraction of the profile spectrum that is NO_x^+ ions increases from 21% at FPEAK= -0.1 to 88% at FPEAK= +1.0. However, at higher FPEAK (≥0.2–0.3) overall factor separation degrades, in addition to the loss of $pRONO_2$ NO_x^+ ratio signature at FPEAK other than -0.1 (see above and Fig. S25). Also, above FPEAK= +0.1, the amount of NO_x^+ concentration assigned to the sum of OOA factors progressively decreases substantially (from 23% at FPEAK= -0.1 to 9% at +1.0). In contrast, going to higher numbers of factors (for FPEAK= -0.1), the fraction of the profile spectra comprised by NO_x^+ ions for the NH_4NO_3 factor changes little, from 21% at 5 factors to no more than 27% at higher factor numbers (Fig. S23). Moreover, increasing factor numbers does not substantially change the amount of total NO_x^+ concentrations apportioned to NH_4NO_3 or non-NH_4NO_3 / non-BBOA factors. Notably, the NH_4NO_3 factor does tend to retain the same NO_x^+ ratio with these large variations in FPEAK and number of factors. However, these results suggest that increasing FPEAK to yield "cleaner" NH_4NO_3 factors does not appear to be an approach that yields anything meaningful, at least for these datasets. Also, the NH_4NO_3 factor resolved had a NO_x^+ ratio of 0.55, a bit lower than the calibration performed most closely in time (0.63), the day following the flight after the instrument was turned off and back on. Since the NH_4NO_3 calibration NO_x^+ ratios were highly variable over this campaign (see Sects. 4 and S2, Figs. S8 and S9e), we do not interpret this difference as meaningful, and thus use the PMF-resolved value for NO_x^+ ratio method apportionment for this flight.

S5 Detailed discussion of comparisons of $pRONO_2$ quantification with AMS and other instruments in the lab and field

In this section, quantitative comparisons of $pRONO_2$ concentrations, as measured by AMS vs other instrumental methods (alternate AMS-based methods, FTIR, TD-LIF/CRDS/CAPS, and FIGAERO-CIMS) are discussed. A few comparisons between non-AMS methods are also discussed. A brief summary is provided in Sect. 5.3 and key details summarized in Table S5.

Fry et al. (2013) compared bulk $pRONO_2$ concentrations measured by AMS (NO_x^+ ratio apportionment and *RoR*=2.25 per Farmer et al. (2010)) with those measured by TD-LIF (with a gas-phase denuder; Rollins et al. (2010b)) during the BEACHON-RoMBAS campaign. The two methods showed good agreement with a slope (AMS vs TD-LIF) of 0.94–1.16 (depending on averaging method) and fair correlation (R^2 = 0.53). The nitrate was typically dominated by $pRONO_2$; however, they show good inorganic/organic nitrate separation (as demonstrated by close tracking of $pRONO_2$) during an inorganic event.

In contrast, during the SOAS campaign, comparison of four different $pRONO_2$ measurements (AMS NO_x^+ ratio, AMS pNO_3 minus PILS inorganic nitrate, FIGAERO CIMS with iodide ionization, and gas-denuded TD-LIF) showed some substantial differences (Lee et al., 2016). The sum of the speciated CIMS $pRONO_2$ (nitrate functional groups only, 88 compounds) was correlated with the two bulk AMS-based methods (R^2=0.52, 0.67) with slopes of 0.63 and 0.90. However, the TD-LIF measurements were ~2–4 times higher than the AMS-based methods (depending on the period; i.e., TD-LIF/AMS NO_x^+ method slope 2.2 or 4.3, both periods with R^2=0.74). Possible explanations for the substantial differences between the AMS-based vs TD-LIF methods were investigated (e.g., particle size cut differences, gas-denuder breakthrough, bias in AMS collection efficiency or overall quantification); however, no plausible cause has yet been identified. Importantly, the AMS $pRONO_2$ measurements showed that particle nitrate during SOAS was dominated by $pRONO_2$; therefore, these large differences could not be related to the inorganic/organic apportionment — i.e., assuming all AMS nitrate was $pRONO_2$ would only slightly close the gap. A later modeling study of organic nitrates in the SE US estimated that $pRONO_2$ contributed ~20% to the total $RONO_2$ during SOAS (Zare et al., 2019), which is more consistent with the $pRONO_2$ concentrations measured by the AMS instruments (Ayres et al., 2015).

Similar measurements to Lee et al. (2016), of highly functionalized $pRONO_2$ with FIGAERO CIMS (iodide ionization) as well as with AMS and the NO_x^+ ratio method (using a fixed R_{pRONO2} of 0.1), were conducted in rural Germany (Huang et al., 2019a). It was shown that the FIGAERO $pRONO_2$ measurements accounted for 47% of the AMS $pRONO_2$ (R=0.52), similar to albeit a bit lower than the equivalent Lee et al. comparison. They note that their CIMS concentrations should be considered lower limits due to their calibration method used since: 1) a collisional limit sensitivity from literature was applied which itself is an upper limit on sensitivity, and 2) they suspected the collision limit applied may have also been too high for their instrument. Additionally, it appears that the mass concentrations of the total organic nitrate molecules measured by the CIMS (not just the nitrate functionality, as was done for Lee et al. (2016)) were compared to the AMS nitrate group only mass concentrations. Therefore, given that the average molecular weight of the CIMS-measured nitrates were ~250 g mol^{-1}, and di-nitrates were a small contribution, the CIMS-measured nitrate functional group mass concentration, may have been ~4 times smaller (250/62) than the total molecular concentration that was compared to AMS (thus accounting for ~10% of the AMS organic nitrate). Chen et al. (2020) also reported comparisons of FIGAERO-CIMS (I^-) and AMS field measurements (SE US). The fractions of the total organic signal that were organic

nitrate molecules were compared for each respective instrument, yielding 12.3±10.8% for the CIMS and 5-18% for the AMS. Assumptions required for the comparison included the average molecular weight of the AMS-measured organic nitrate molecules (220 g mol^{-1}), R_{pRONO2} fixed at 0.1-0.2, and constant sensitivity of all organic nitrates measured by CIMS. Additionally, the average N/C ratios for the CIMS total signal was shown to be in the center of the range estimated from the AMS total organic signal (including nitrate functional groups) across the diurnal cycle. However, comparison of the estimated O/C and H/C elemental ratios showed substantial differences (~10-20%), likely reflecting bias in the CIMS toward more oxygenated compounds.

Comparisons of AMS vs TD-LIF $pRONO_2$ observations in the boundary layer during the KORUS-AQ aircraft campaign are reported in Kenagy et al. (2021). TD-LIF measurements used in the analysis and comparisons were corrected for particle losses in the aircraft sampling inlet, including charge losses to non-conductive tubing as well as inertial and diffusion losses. Net inlet losses were typically ~20-60% by aerosol volume. AMS measurements used in the analysis and comparisons were screened for f_{pRONO2}>0.2 due to higher uncertainty and noise under those conditions. The inlet sampling corrections to the TD-LIF showed substantial improvements in agreement of the two methods, with an AMS vs TD-LIF slope without corrections, 3.12, decreasing to 1.89 after corrections.

Quantitative comparison of $pRONO_2$ concentrations formed during chamber experiments investigating SOA formed from reaction of terpenes (α-pinene and Δ-3-carene) with nitrate radicals (those described in Sect. S1.2) as measured by AMS and (gas-denuded) TD-CRDS (a similar method to TD-LIF but with cavity ring-down spectroscopy NO_2 detection (Paul et al., 2009; Thieser et al., 2016)) showed good average agreement, albeit with substantial scatter (Keehan et al., 2020) (AMS vs TD-CRDS slope = 1.06-1.14; R^2 = 0.73). In that analysis, specific *RoR* were determined for the α-pinene and Δ-3-carene SOA (3.12, 3.78, cf. Table S1 here) from dry experiments and used for apportionment, since experiments with elevated RH showed possible indications of inorganic nitrate formation (e.g. NH_3 gas from chamber walls reacting with HNO_3 generated from N_2O_5 injections). However, the apportionment of possible inorganic nitrate had a relatively small effect (~10%) on the average comparison slope (and slightly improved correlation), since $pRONO_2$ dominated the nitrate overall. Similarly, Eris et al. (2018) compared bulk $pRONO_2$ concentrations (for SOA formed from isoprene and monoterpenes reaction with OH, O_3, NO_3 in a chamber) measured with AMS and gas-denuded TD-CAPS (Cavity Attenuated Phase Shift Spectroscopy for NO_2 detection) and reported "quantitative agreement" which we assume to mean within combined instrumental uncertainties or within ~50%.

Bruns et al. (2010) compared the N/H elemental ratios as measured by FTIR vs AMS for SOA formed in a chamber from reaction of isoprene and monoterpenes with nitrate radicals and found ratios 3–4 times higher N/H for FTIR. They discuss some possible explanations for the difference including: 1) ionization of intact organic nitrates producing an organic cations and neutral NO_x fragments in the AMS, 2) evaporation of organic nitrate in the vacuum region of the AMS, or 3) artifacts from uptake of gas-phase organic nitrates as collected organic mass increases or volatilization of organic products that don't contain organic nitrates during collection for FTIR analysis (on an impactor). While such cation/neutral bias during electron ionization (EI) (1) may occur (as they show by performing AMS software-based elemental analysis on the NIST EI spectrum of hydroxy ethyl nitrate and compute a N/H 2.5 times lower than the elemental formula), the thermal lability of organic nitrates and propensity to decompose to NO_2 during vaporization in the AMS (as also pointed out by those authors) suggests that this would not have a major effect on organic nitrate quantification. Regarding large losses due to evaporation in the AMS vacuum chamber (2), such effects are likely too slow to be significant. For example, Shingler et al. (2016)

show that for liquid particles, losses as large as half the mass are expected to occur only for the highest volatility organic compounds expected to be present in OA on timescales of at least hundreds of milliseconds. In the AMS, the particles spend only a few milliseconds in the vacuum chamber prior to vaporization. The authors suggest the FTIR collection artifacts (3) did not appear to be a major factor based on an observation of invariant nitrate/carbonyl functional group ratios (as measured by FTIR) over a 2-hour collection period where SOA concentration varied 20-fold on the collection impactor.

Another possibility that may lead to an underestimate in the N/H (or N/C) ratio when N is dominated by organic nitrates, is application of an incorrect relative ionization efficiency for the organic component. While application of an RIE of 1.4 is recommended for ambient OA quantification, RIE for single species and simpler mixtures can be substantially larger (more than a factor of 2) (Jimenez et al., 2016; Xu et al., 2018). Thus, a factor of two larger RIE for organic and unchanged RIE for nitrate (assuming it largely decomposes prior to ionization) would lead to a factor of two underestimation of N/H, N/C, or nitrate fraction of OA if applying the default ambient RIE (which most likely was done for that study). Such an effect could explain their agreement of N/H between FTIR and AMS for the standard compound they analyzed (isosorbide 5-mononitrate, $C_6H_9NO_6$) if the ionization efficiency of that compound is similar to that of ambient OA.

Liu et al. (2012) showed a comparison of $pRONO_2$ as measured by FTIR vs AMS for SOA formed in a chamber experiment from photooxidation of 1,2,4-trimethylbenzene (TMB), with FTIR measuring 2.28 times AMS (R^2=0.98, with no dependence on humidity (for <1–85% RH). Speculating on the FTIR vs AMS differences, they state: "Possible explanation for the large slope include: (1) ON [organic nitrate] groups are fragmented by electron impact ionization and do not have a uniform probability of carrying the positive charge necessary for detection (Bruns et al., 2010), or the related point (2) the true relative ionization efficiency of ON molecules is lower than the value of 1.1 used to calculate nitrate mass, or (3) ON groups dissociated (during ionization processes) to form other nitrogen-containing fragments (e.g., $C_xH_yO_zN^+$ in Figure 2b) that were small (compared to NO^+ and NO_2^+) and caused the scatter in Figure 2c." Possibility 1 is discussed above and possibility 3 would not lead to large average differences. A comparison of the RIE for nitrate from $pRONO_2$ compounds vs NH_4NO_3 has not been directly tested (beyond the more convoluted instrument comparisons discussed in this section). However, again under the assumption that $RONO_2$ largely decomposes to NO_2 (and NO) upon vaporization, a much lower ionization efficiency does not seem likely. Possible reasons for a positive bias in FTIR quantification was not discussed. While a good agreement between total OA measured by FTIR and SMPS (R=0.9, slope 1.05) was observed, a similar comparison of AMS and SMPS is not reported (nor discussion of AMS calibration, collection efficiency applied, etc.), so it is difficult to assess the general quantification accuracy of AMS measurements within a factor of 2 during those experiments.

During a study in Bakersfield California, measurements of $pRONO_2$ using FTIR and (gas-denuded) TD-LIF were compared (Rollins et al., 2013). After applying an average correction factor for differences in particle sampling size cuts (1.0/2.5 μm = 0.83, based on FTIR OA measurements), the TD-LIF/FTIR linear fit showed a slope of 1.38 and offset of +0.068 μg m^{-3} (R=0.72). For concentrations measured (<0.2 μg m^{-3}), the offset was relatively large such that the average TD-LIF/FTIR ratio was substantially >2 and a fit line constrained through the origin was probably >2. As the authors note, possible reasons for the differences were scrutinized, yet the differences remain unexplained.

Abbreviations/Glossary/Nomenclature

NH_{4_Bal}	Ammonium Balance = molar ratio of $NH_4/(NO_3+2SO_4)$
ACSM	Aerosol Chemical Speciation Monitor (Aerodyne). UMR and lower sensitivity, typically used for routine or long-term air quality monitoring. Uses quadrupole MS (sometimes referred to as Q-ACSM).
AMS	Aerosol Mass Spectrometer. Refers to Aerodyne models cable of particle size-resolved chemical measurements.
BBOA	Biomass Burning OA (separated by PMF)
BVOC	Biogenic Volatile Organic Compounds; e.g., isoprene, monoterpenes
CIMS	Chemical Ionization Mass Spectrometry
Closed	Mode or signal observed in AMS when particle beam is blocked (background)
COA	Cooking OA (separated by PMF)
Collection Efficiency (CE)	The efficiency that particles are detected in the AMS (0–1). The dominant factor in reduced CE is due to particle bounce at the vaporizer.
C-ToF (AMS)	Compact Time-of-Flight AMS (Aerodyne). Nominal spectral resolution of ~600 and typically used only for UMR analysis.
Diff	Raw "closed" spectra subtracted from "open" spectra. HR fitting done after raw spectra subtraction.
EI	Electron Ionization (formally known as Electron Impact ionization)
FIGAERO	Filter Inlet for Gases and AEROsols.
FMS mode	Fast MS mode. Data acquisition mode where the particle beam is unblocked for an extended period (1+ minutes) to collect high-frequency data (1–10 Hz) and backgrounds (closed) measured intermittently for short periods. Used for aircraft studies discussed here.
f_{NH4NO3}	NH_4NO_3/pNO_3. I.e. fraction of AMS nitrate that is apportioned to particle-phase ammonium nitrate. Also denoted as $NH_4NO_{3,frac}$ in a few places per previous work. See Eq. 3
f_{pRONO2}	$pRONO_2/pNO_3$. I.e. fraction of AMS nitrate that is apportioned to particle-phase organic nitrate. Also denoted as $RONO_{2,frac}$ in other studies. See Eqs. 1,2
HOA	Hydrocarbon-like OA (separated by PMF)
HR	High-Resolution. Refers to AMS instrument models and peak-fitting with nominal spectral resolutions of ~2000–4000 (see "V-mode" and "W-mode").
HR-AMS,	High-Resolution (Time-of-Flight) AMS (Aerodyne)

HR-ToF-AMS	
IE	Ionization Efficiency. The efficiency of detection of ions from particles that vaporize on the AMS vaporizer.
IEPOX-SOA	IEPOX-derived SOA (separated by PMF). From low-NO oxidation of isoprene.
LO-OOA	Less-oxidized OOA (separated by PMF), sometimes equated with SV-OOA.
LV-OOA	Low-Volatility OOA (separated by PMF), sometimes equated with MO-OOA.
ME-2	Multi-linear Engine (2). PMF solver algorithm where factor time series and profiles can be constrained. Implemented with SoFi Software.
MO-OOA	More-oxidized OOA (separated by PMF), sometimes equated with LV-OOA.
MS mode	"Mass-Spec" mode. Data acquisition mode where particle beam is alternatively blocked (closed mode) and transmitted (open mode), typically every 5–10 s, in order to quantify non-size-resolved chemical composition.
NH_4NO_3	Always refers to particle-phase ammonium nitrate here.
NO^+, *m/z* 30	Aerosol signal from NO^+, sometimes approximated from *m/z* 30 for UMR.
NO_2^+, *m/z* 46	Aerosol signal from NO_2^+, sometimes approximated from *m/z* 46 for UMR.
NO_x^+ ratio	Ratio of aerosol-phase NO_2^+ and NO^+. Unless otherwise specified, the convention used here is always NO_2^+/NO^+.
O/C, H/C	Oxygen-to-carbon and hydrogen-to-carbon ratios for OA estimated with AMS.
OA	Organic Aerosol (particle-phase organic species)
OFR	Oxidation Flow Reactor. Flow reactor where gas/particle sample flow exposed to oxidants. Processed ambient outflow sampled by AMS here.
OmC	"Open" minus "Closed" signal (HR fitting done first and then subtracted).
OOA	Oxygenated OA (separated by PMF)
Open	Mode or signal observed in AMS when particle beam is not blocked.
PMF	Positive Matrix Factorization. Implemented with "PET" software.
$pRONO_2$	Particle-phase organic nitrate. Concentrations here are expressed in mass concentrations of the nitrate functional group ($-ONO_2$) only.
PToF mode	Particle-time-of-flight mode. Size-resolved chemical sampling mode.
Q-AMS	Quadrupole AMS (UMR).
$R_{ambient}$	NO_x^+ ratio measured for ambient mixed nitrate aerosol sampled with AMS. Applied in Eq. 1. Also referred to as R_{meas} or R_{obs} (measured, observed) in other studies.

R_{NH4NO3}	NO_x^+ ratio observed for calibration with pure NH_4NO_3. Applied in Eq. 1.
RIE	Relative Ionization Efficiency. The relative detection efficiency of a chemical species, referenced to that of nitrate (measure with NH_4NO_3 aerosol).
$RONO_2$	Organic nitrate (any organic molecule containing a nitrate functional group)
RoR	"Ratio-of-Ratios". R_{NH4NO3}/R_{pRONO2} for $pRONO_2$ (or more generally can be relative ratios of any other nitrate pairs).
R_{pRONO2}	NO_x^+ ratio observed for pure $pRONO_2$. Applied in Eq. 1. Measured in isolated studies or inferred as R_{NH4NO3}/RoR. Also referred to as R_{RONO2} in other studies.
S/N	Signal-to-Noise ratio
SOA	Secondary Organic Aerosol
SV-OOA	Semi-Volatile OOA (separated by PMF), sometimes equated with LO-OOA
TD-LIF	Thermal Dissociation – Laser Induced Fluorescence. Different classes of reactive nitrogen gas/aerosol (such as $RONO_2$) are separately quantified by selectively thermally decomposing molecules to NO_2 (which is detected).
ToF-ACSM	Time-of-Flight Aerosol Chemical Speciation Monitor. Higher sensitivity and spectral resolution (~600) than Q-ACSM. Uses compact ToF (Aerodyne).
pNO_3	Total nitrate (concentration) quantified by AMS.
Tot-$RONO_2$	Total $RONO_2$ concentration (gas + particle). Measured by TD-LIF here.
UMR	Unit-Mass-Resolution. Refers to AMS (or related) instrument models (or peak-fitting analysis) where only unit *m/z* can be (or are) resolved.
V-mode	Mode for HR-ToF-AMS with spectral resolution of ~2000 (higher-sensitivity)
W-mode	Mode for HR-ToF-AMS with spectral resolution of ~4000 (lower-sensitivity)

DC3, SEAC[4]RS, KORUS-AQ (or KORUS), SOAR, MILAGRO, DAURE, BEACHON-RoMBAS (or BEACHON), SOAS, GoAmazon (IOP1, IOP2) are field campaigns used in this analysis (see Sect. S1.1, Table S3).

SI Tables

Table S1. Summary of sources, values, calculations, and details for $pRONO_2$ and NH_4NO_3 NO_x^+ ratios and Ratio-of-Ratios included in Fig. 1. Numbers in bold indicate values directly reported in literature sources (or from this study) while otherwise the values were calculated here. Details relevant to specific calculations (beyond direct calculations using other numbers in each row of the table) are described in footnotes. For completeness, footnote "ee" lists a few earlier published studies that were not included in the characterization of the *RoR* in this study and the rationale (which includes the Bruns et al. (2010) data which are shown in Fig. 1 and this table but not included in averages or correlations).

$pRONO_2$ Source	**Reference**	***RoR***	***RoR* Uncertainty**	**$pRONO_2$**		**NH_4NO_3**	
				NO_2^+/NO^+	**NO^+/NO_2^+**	**NO_2^+/NO^+**	**NO^+/NO_2^+**
Chamber SOA							
Δ-3-carene SOA (NO_3)	Bruns et al. (2010)	5.8	2.2[g]	0.071	**14**	0.42	**2.4**
Δ-3-carene SOA (NO_3) (2014[y])	Kang et al. (2016)	**3.31**	**0.17[h]**	**0.184**	**5.4**	**0.61**	**1.64**
Δ-3-carene SOA (NO_3) (2015[y])	Kang et al. (2016)	**3.12**	N/A	**0.263**	**3.8**	**0.82**	**1.22**
Δ-3-carene SOA (NO_3) (2015[y], high OA[z])	Kang et al. (2016)	**2.56**	**0.33[i]**	**0.39**	**2.56**	**1.00**	**1.00**
α-pinene SOA (NO_3)	Bruns et al. (2010)	4.6	1.6[g]	0.091	**11**	0.42	**2.4**
α-pinene SOA (NO_3) (2014[y])	Kang et al. (2016)	**3.75**	**0.45[j]**	**0.162**	**6.2**	**0.61**	**1.64**
α-pinene SOA (NO_3) (2015[y])	Kang et al. (2016)	**3.78**	N/A	**0.217**	**4.6**	**0.82**	**1.22**
α-pinene SOA (NO_3) (2015[y], high OA[aa])	Kang et al. (2016)	**3.05**	**0.45[k]**	**0.269**	**3.71**	**1.00**	**1.00**
α-pinene SOA (NO_3) (RO_2+NO_3)	Takeuchi et al. (2019)	**2.86**	0.19[l]	0.118	**8.44**	0.337	**2.97**
α-pinene SOA (NO_3) (RO_2+HO_2)	Takeuchi et al. (2019)	**3.07**	N/A	0.116	**8.60**	0.357	**2.80**
α-pinene SOA (OH/NO_x)	Takeuchi et al. (2019)	**2.12**	0.065[m]	0.167	**6.00**	0.353	**2.84**
β-pinene SOA (NO_3)	Fry et al. (2009)	3.70	N/A	0.100	**10**	**0.37**	2.7
β-pinene SOA (NO_3)	Bruns et al. (2010)	4.2	1.0[g]	0.10	**10**	0.42	**2.4**
β-pinene SOA (NO_3) (RO_2+NO_3)	Boyd et al. (2015)	**3.2**	N/A	0.154	**6.5**	0.49	2.03
β-pinene SOA (NO_3) (RO_2+HO_2)	Boyd et al. (2015)	**4.8**	N/A	0.116	**8.6**	0.56	1.79

β-pinene SOA (NO_3) (RO_2+NO_3)	Takeuchi et al. (2019)	**2.48**	N/A	**0.140**	**7.13**	**0.348**	**2.87**
β-pinene SOA (OH/NO_x)	Takeuchi et al. (2019)	**1.64**	N/A	**0.199**	**5.02**	**0.327**	**3.06**
limonene SOA (NO_3)	Fry et al. (2011)	2.33	0.22[n]	**0.15**	6.7	**0.35**	2.9
limonene SOA (NO_3)	Bruns et al. (2010)	6.3	1.9[g]	0.067	**15**	0.42	**2.4**
isoprene SOA (NO_3)	Rollins et al. (2009)	2.24	N/A	**0.156**	6.41	**0.35**	2.86
isoprene SOA (NO_3)	Bruns et al. (2010)	2.1	0.50[g]	0.20	**5.0**	0.42	**2.4**
isoprene SOA (OH/NO_x), LV[bb]	Schwantes et al. (2019)	3.24	0.26[o]	0.164	6.1	0.53	1.88
isoprene SOA (OH/NO_x), 2MGA[bb]	Schwantes et al. (2019)	3.04	0.24[o]	0.175	5.7	0.53	1.88
benzene SOA (OH/NO_x)	Sato et al. (2010)	2.07	0.34[p]	0.249	**4.02**	0.514	**1.95**
monoalkylbenzenes SOA (OH/NO_x)	Sato et al. (2010)	2.30	0.34[p]	0.224	**4.47**	0.514	**1.95**
dialkylbenzenes SOA (OH/NO_x)	Sato et al. (2010)	2.75	0.50[p]	0.187	**5.35**	0.514	**1.95**
trialkylbenzenes (TMB) SOA (OH/NO_x)	Sato et al. (2010)	2.73	0.44[p]	0.189	**5.31**	0.514	**1.95**
3-methylfuran SOA (NO_3)	Joo et al. (2019)	**1.38**	0.01[q]	0.190	**5.25**	0.263	**3.8**
Alkanol SOA (OH/NO_x)	Liu et al. (2019)[cc]	**2.18**	**0.13**[r]	**0.473**	**2.11**	**1.03**	**0.97**
biomass burning SOA, PMF (O_3/NO_x /NO_3)	Tiitta et al. (2016)	3.12	N/A	0.128	**7.8**	**0.40**	**2.5**
biomass burning SOA, PMF (OH/NO_x)	Tiitta et al. (2016)	2.56	N/A	0.156	**6.4**	**0.40**	**2.5**
Isolated pRONO$_2$ (from chamber SOA or standard)							
isosorbide 5-mononitrate (standard)	Bruns et al. (2010)	6.3	N/A	0.067	**15**	0.42	**2.4**
oleic acid, hydroxynitrate (HN), (NO_3)	Farmer et al. (2010)	3.03	0.23[s]	0.220	**4.55**	0.68	**1.50**
oleic acid, carbonylnitrate (CN), (NO_3)	Farmer et al. (2010)	2.67	0.31[s]	0.250	**4.00**	0.68	**1.50**
oleic acid, HN/CN oligomers (NO_3)	Farmer et al. (2010)	1.85	0.30[s]	0.360	2.78	0.68	**1.50**

1-tetradecene, 1-hydroxy-2-nitrate (OH/NO_x)	Farmer et al. (2010)	1.17	0.36[s]	0.570	**1.75**	0.68	**1.50**
1-tetradecene, 2-hydroxy-1-nitrate (OH/NO_x)	Farmer et al. (2010)	2.30	2.32[s]	0.290	**3.45**	0.68	**1.50**
1-tetradecene, dihydroxynitrate (OH/NO_x)	Farmer et al. (2010)	2.67	2.31[s]	0.250	**4.00**	0.68	**1.50**
1-pentadecene, hydroxynitrate (NO_3)	This Study[dd]	**1.89**	N/A	**0.408**	**2.45**	**0.77**	**1.30**
1-pentadecene, carbonylnitrate (NO_3)	This Study[dd]	**2.62**	N/A	**0.294**	**3.41**	**0.77**	**1.30**
Ambient (instrument comparisons or PMF)							
ambient AMS NO_x^+ ratio method vs TD-LIF (pine forest, summer)	Fry et al. (2013)	**2.12[a]**	0.44[t]	0.139	7.17	**0.295**	3.39
ambient IC-AMS vs AMS NO_x^+ ratio method (SEUS, summer)	Xu et al. (2015a)	2.73[b]	0.53[u]	0.125	8.00[b]	0.341	**2.93**
ambient PMF (NYC, summer)	Sun et al. (2012)	3.04[c]	0.04[v]	0.093	10.8[c]	0.282	**3.55[c]**
ambient PMF (boreal, fall)	Hao et al. (2014)	3.65[d]	0.06[w]	0.096	**10.4[d]**	0.351	**2.85[d]**
ambient PMF (boreal, spring)	Kortelainen et al. (2017)	3.54	N/A	0.118	**8.5[e]**	0.42	**2.4[e]**
ambient PMF (SEUS, summer, RF16)	This Study	**2.92**	**0.04[x]**	**0.240**	**4.2**	**0.70[f]**	**1.43**
ambient PMF (SEUS, summer, RF18)	This Study	**2.96**	**0.03[x]**	**0.182**	**5.5**	**0.54[f]**	**1.85**

<u>*RoR* and $pRONO_2$ or NH_4NO_3 NO_x^+ ratio footnotes:</u>

(If no footnote, then values simply tabulated from reported NH_4NO_3 and pure $pRONO_2$ NO_x^+ ratios and RoR calculated or provided)

[a]Estimated by calculating *RoR* consistent with a 1:1 fit of AMS vs TD-LIF $pRONO_2$ (Fig. 11b in Fry et al. (2013)).

[b]Estimated by calculating R_{pRONO2} consistent with a 1:1 fit between AMS-PILS-IC vs AMS NO_x^+ ratio methods (Fig. 11 in Xu et al. (2015a)).

[c]Calculated from concentration-weighted combined PMF factors (three OOA factors only: LO-OOA, MO-OOA, LV-OOA) and NH_4NO_3 from offline NH_4NO_3 calibration and NH_4NO_3 PMF factor ("NO_3-OA") (Tables 1, 2 in Sun et al. (2012))

[d]R_{pRONO2} reported for concentration-weighted combination of the three non-NH_4NO_3 PMF factors (SV-OOA, LV-OOA, HOA although HOA contribution was very small) and average of R_{NH4NO3} from offline NH_4NO_3 calibration and NH_4NO_3 PMF factor ("NIA")

[e]R_{pRONO2} reported for combination of the two non-NH_4NO_3 PMF factors (SV-OOA, LV-OOA). Offline NH_4NO_3 calibration and NH_4NO_3 PMF factor ("NO-factor") NO_x^+ ratios were identical.

[f] R_{NH4NO3} from PMF NH_4NO_3 factor.

RoR Uncertainty footnotes:

(If N/A then RoR represents single measurement or statistics not available)

[g] Standard error (1σ) calculated by propagating 2σ values reported for repeat chamber experiments of $pRONO_2$ (n=2) and NH_4NO_3 (n=3) NO^+/NO_2^+ ratios.

[h] Standard error calculated for *RoR*s of 11 chamber experiments.

[i] Standard error calculated for *RoR*s of 2 chamber experiments.

[j] Standard error calculated for *RoR*s of 4 chamber experiments.

[k] Standard error calculated for *RoR*s for 3 chamber experiments.

[l] Standard error calculated for *RoR*s of 2 chamber experiments.

[m] Standard error calculated for *RoR*s of 2 chamber experiments.

[n] Standard error calculated from reported standard deviation of R_{pRONO2} for 2 chamber experiments.

[o] LV or 2MGA indicate experiments under conditions resulting in SOA formation via low-volatility or 2-methyl glyceric acid product formation pathways, respectively. All values used and calculated are taken from Fig. S8 in Schwantes et al. (2019) which contains values for four LV and six 2MGA experiments. NH_4NO_3 ratios were calculated from the five high RH experiments where large (and overwhelming) concentrations of inorganic nitrate were formed from HNO_3 partitioning to particles; these values were taken to be more representative of the corresponding instrument response in lieu of the typical instrument response quoted in the text for NH_4NO_3 NO^+/NO_2^+ (2.4).

[p] Standard error calculated from reported $pRONO_2$ and NH_4NO_3 *m/z*30-to-*m/z*46 ratios for 2–3 separate chamber experiments (and range of measured NH_4NO_3 values).

[q] Standard error calculated from reported range of 4 experiments and approximating standard deviation as one-fourth of the range.

[r] Standard error calculated from 3 experiments with different OA seeds (squalene, sucrose, and oleic acid)

[s] Standard error calculated from reported standard errors of $pRONO_2$ and NH_4NO_3 NO_2^+/NO^+ ratios for 3 or more repeat measurements.

[t] Calculated as combined accuracy for TDLIF (±25%) (Fry et al., 2013) and AMS (±34%) (Bahreini et al., 2009; Middlebrook et al., 2012) particle nitrate concentrations (accuracy uncertainties first divided by two to scale from 2σ to 1σ for consistency with other 1σ uncertainties reported here).

[u] Calculated as combined accuracy for PILS-IC (±10%) (Weber et al., 2001; Xu et al., 2015a) and AMS (±34%) (Bahreini et al., 2009; Middlebrook et al., 2012) particle nitrate concentrations (AMS accuracy uncertainty first divided by two to scale from 2σ to 1σ for consistency with other 1σ uncertainties reported here).

[v] Calculated as range for using NO_x^+ ratio from offline NH_4NO_3 calibration vs NH_4NO_3 PMF factor ("NO_3-OA").

[w] Calculated as range for using NO_x^+ ratio from offline NH_4NO_3 calibration vs NH_4NO_3 PMF factor ("NIA").

[x] PMF Bootstrapping standard error for 100 iterations.

Other footnotes:

[y] For Kang et al. (2016) values, 2014 and 2015 denote the year they were conducted which were done with two different AMS instruments, but with the same SOA production method.

[z] High OA: >200 μg m^{-3}. For other Kang et al. (2016) Δ-3-carene SOA (NO_3), concentrations of OA were 10–20 μg m^{-3}.

[aa]High OA: 25–75 μg m^{-3}. For other Kang et al. (2016) α-pinene SOA (NO_3), concentrations of OA were 5–10 μg m^{-3}.

[bb]Standard errors calculated from the 4 LV or six 2MGA experiments (including propagation of errors from 5 experiments representing NH_4NO_3 ratios).

[cc]Alkanol SOA was produced from a mixture of C6, C8, C9, C10, and C12 n-alcohols oxidized by OH at high-NO conditions according to the methods described in Krechmer et al. (2017), but with different organic seeds (Liu et al., 2019). Data included here are from the average (and standard error) of results for experiments with squalene, sucrose, and oleic acid seeds under dry conditions (RH<1%).

[dd]Measurements of isolated compounds separated by HPLC from SOA formed in a chamber from oxidation of 1-pentadecene by NO_3 radicals. Same chamber, separation, and sampling methods as described in Farmer et al. (2010). For the hydroxynitrate, the NO_x^+ ratio is from the period of the initial rise in concentrations when OA<20 μg m^{-3}, since OA concentrations reached ~500 μg m^{-3} at the peak concentration and the NO_x^+ ratio drifted up by 25%. OA concentration for the carbonylnitrate measurement was ~85 μg m^{-3}.

[ee]Published studies excluded from characterization of the *RoR* in this study and rationale: **Alfarra et al.** (2006) reported UMR *m/z* 46 / *m/z* 30 ratios for 1,3,5 trimethylbenzene (TMB) and α-pinene (+OH/NO_x) SOA (0.13, 0.20, respectively) but did not report corresponding R_{NH4NO3}. **Liu et al.** (2012) reported NO_x^+ ratios for 1,2,4 TMB +OH/NO_x SOA (0.11) but did not report corresponding R_{NH4NO3}. **Sato et al.** (2012) reported for 1,3,5 TMB (+OH/NO_x) SOA that "The NO^+/NO_2^+ ratio observed was 3.8–5.8, higher than that for inorganic nitrates", but R_{NH4NO3} was not explicitly reported, so is not clear what the "inorganic nitrate" refers to and if it was actually measured with their instrument. **Rollins et al.** (2010a) reported NO_x^+ ratios for hydroxy nitrates synthesized from butane, α-pinene, limonene, and caryophyllene and reported a large range of values (0.19–1.01), however associated R_{NH4NO3} was not reported. Additionally, two-thirds of the nitrogen observed in the AMS spectrum was at non-NO_x^+ peaks, mostly as reduced ions (NH_x^+, $C_xH_yN_z^+$), which is very atypical, since those ions are generally observed at no more than trace amounts for isolated organic nitrates or SOA containing organic nitrates (e.g., Farmer et al., 2010; Boyd et al., 2015). It is unclear if standards were impure, contaminants became concentrated in the aerosol during particle generation and evaporation/drying, possibly the AMS was functioning abnormally, or some other explanation for the atypical spectra. Consequently, we recommend interpretation of that large range in NO_x^+ ratios with caution. Finally, the **Bruns et al.** (2010) data were not included in reported averages or fitted lines reported in this table, the text, or figures due to the large range in variability of repeat measurements and also because the Particle Time-of-Flight (PToF) acquisition mode was used to conduct most experiments as a way to attenuate very large particle concentrations. It is not clear if using a different time sequence of impacting and blocking the particle beam on the vaporizer will affect the observed NO_x^+ ratios.

Table S2. Summary of sources, values, calculations, and details for inorganic nitrates and nitrites and NH_4NO_3 NO_x^+ ratios and Ratio-of-Ratios. Numbers in bold indicate values directly reported in literature sources (or measured in our laboratory), while otherwise the values were calculated here. See Fig. S4 for graphical representation and comparison to $pRONO_2$ of these *RoR*s.

Compound	Reference	*RoR*	*RoR* Uncertainty	Nitrate or Nitrite		NH_4NO_3	
				NO_2^+/NO^+	NO^+/NO_2^+	NO_2^+/NO^+	NO^+/NO_2^+
$NaNO_3$	Alfarra (2004)	10.8	N/A	0.0342	**29.2**	0.37	**2.7**
$NaNO_3$	Bruns et al. (2010)	33	8.1[a]	0.0125	**80**	0.42	**2.4**

$NaNO_3$	Hu et al. (2017b)	58	N/A	**0.006**	170	**0.35**	2.9
$NaNO_{-3}$	This study[b]	7.6	0.7	**0.0340 (0.0019)**	**29.4 (1.7)**	**0.2585 (0.0164)**	**3.88 (0.25)**
$Ca(NO_3)_2$	Alfarra (2004)	16.9	N/A	0.0219	**45.6**	0.37	**2.7**
$Mg(NO_3)_2$	Alfarra (2004)	3.93	N/A	0.0943	**10.6**	0.37	**2.7**
KNO_3	Drewnick et al. (2015)	9.7	N/A	0.036	**28**	0.35	**2.9**
KNO_3	This study[b]	40.7	4.9	**0.0141 (0.0014)**	**71.7 (7.85)**	**0.5694 (0.0281)**	**1.76 (0.09)**
$NaNO_2$	Bruns et al. (2010)	290	N/A	0.00142	**700**	0.42	**2.4**
KNO_2	This study[b]	28.9	4.9	**0.0103 (0.0016)**	**99.8 (15.4)**	**0.2913 (0.0200)**	**3.45 (0.23)**
4-nitrocatechol	This study[c]	3.783~~.35~~	0.150~~.81 (0.21)~~ (0.077)	**0.2190~~.246~~ (0.04552)**	**4.4225 (0.6084)**	**0.847795 (0.0821~~19~~)**	**1.1929 (0.123~~)~~**

[a]Standard error (1σ) calculated by propagating 2σ values reported for repeated chamber experiments of $NaNO_3$ (n=11) and NH_4NO_3 (n=3) NO^+/NO_2^+ ratios.

[b]Performed in our laboratory with the aircraft HR-AMS. Values in parentheses for the NO_x^+ ratios are standard deviations of ~5-20 minutes of 1 Hz resolution data for the duration of the one-time measurements, and reflect experimental/instrument noise and substantial drifts in some cases. The uncertainties for those *RoR* are the standard deviations from propagating standard deviations of the NO_x^+ ratios in quadrature.

[c]See Fig. S5 for details. The uncertainties for the NO_x^+ ratios (parenthesis) are standard deviations of the averages from each individual calibrations. Uncertainty~~ies~~ for the *RoR* is the standard deviation (1σ) and standard error (parenthesis) of the separately-calculated *RoR*s for each calibration (n=~~4~~15).

Table S3. Summary of field campaigns from which data is used in this analysis. See Sect. S1.1 for additional details.

Name	Location	Season, Year	Type	Reference(s)
SOAR-1	Riverside, California	Summer, 2005	Urban, ground	Docherty et al. (2011)
MILAGRO	Mexico City	Late winter / early spring, 2006	Urban (megacity), ground	Molina et al. (2010), Aiken et al. (2009, 2010)
DAURE	Montseny, Spain	Late winter / early spring, 2009	Rural, urban-influenced, ground	Minguillón et al. (2011), Pandolfi et al. (2014)
BEACHON-RoMBAS	Colorado Rocky Mts., pine forest	Summer, 2011	Rural, ground	Ortega et al. (2014), Fry et al. (2013), Palm et al. (2017)
DC3	Continental U.S.	Spring 2012	Focus on deep convective cloud chemistry, aircraft	Barth et al. (2015), Nault et al. (2016)
SOAS	Rural Alabama, mixed forest	Summer, 2013	Rural, semi-polluted, ground	Carlton et al. (2018), Hu et al. (2016)
SEAC^{4}RS	Continental U.S., especially SE US	Late summer, 2013. Special focus on RF16/18 (11/16 Sept) in SE US	Many foci, aircraft	Toon et al. (2016), Fisher et al. (2016)
GoAmazon	Central Amazonia	Wet season (IOP1), dry season (IOP2), 2014	Rural/remote. Sometimes urban downwind.	Martin et al. (2016, 2017), de Sá et al. (2018, 2019), Palm et al. (2018)
KORUS-AQ	South Korea and Seoul	Spring, 2016	Urban (megacity) + regional survey, aircraft	Nault et al. (2018)

Table S4. Summary of results for studies using PMF for $pRONO_2$ separation with AMS (using OA and nitrate ions as input). See Sects. 5.2.1, 5.2.2, and 5.2.3 for summaries and Sects. S3, S4 for details and discussions of these studies.

Reference	Sample description	No. fact.[a]	R_{NH4NO3} comp[b]	f_{pRONO2}[c]	$pRONO_2$ factors[d]	*RoR*[e]	NO_x^+ ratio meth.[f]
Sun et al. (2012)[g]	New York City, summer	8	3% lower	21%	MO-SV-OOA (12%)[h], NOA (4%)[h], LO-SV-OOA (2%)[h]	MO-SV-OOA (2.6-2.7), ∑OOA (3.0-3.1)	No
Hao et al. (2014)	Semi-polluted rural Finland, fall	4	3% lower	37%	SV-OOA (28%), LV-OOA (9%)	∑OA (3.6-3.7)	No
Xu et al. (2015a)	Southeast US, summer (2 sites)	3,4	Not resolved	100%	LO-OOA, possibly others	LO-OOA (~2.5)	Yes
Xu et al. (2015a)	Southeast US, winter (3 sites)	3,6,6	within 10%	10%, 11%, 19%	LO-OOA, possibly others	LO-OOA (>10, nearly all NO^+)	Yes
Xu et al. (2015a)	Southeast US, transition (2 sites)	6,7	30-35% lower	33%, 39%	LO-OOA, possibly others	LO-OOA (~5)	Yes
Zhang et al. (2016)	Beijing, fall, biomass burning-influenced period	6	4% lower	23%	SV-OOA (8%), HOA (6%)[i], LV-OOA (5%), BBOA (4%)[i]	SV-OOA (~5), LV-OOA (~2.5)	No
Zhang et al. (2016)	Beijing, winter, coal combustion – influenced period	5	7% lower	17%	HOA (10%)[i], OOA (4%), CCOA (2%)[i]	OOA (NO_x^+ was NO_2^+)	No
Kortelainen et al. (2017)	Remote Finnish boreal forest, spring	3	Same	35%	SV-OOA (30%), LV-OOA (5%)	SV-OOA (3.0), ∑OOA (3.5)	No
Yu et al. (2019)	Urban southern China (Shenzhen), spring	4	4% lower	12%	LO-OOA (6%) HOA (4%) MO-OOA (2%)	HOA (3.9), others (>10, nearly all NO^+)	Yes
Yu et al. (2019)	Urban southern China (Shenzhen), summer	4	9% lower	43%	LO-OOA (22%) HOA (12%) MO-OOA (9%)	LO-OOA (4.7), MO-OOA (2.1), HOA (>10, nearly all NO^+), ∑OA (5.0)	Yes

Yu et al. (2019)	Urban southern China (Shenzhen), fall	4	6% lower	16%	LO-OOA (7%) HOA (5%) MO-OOA (4%)	All (>10, nearly all NO^+)	Yes
Zhu et al. (2021)	North China Plains, summer	4	21-26% lower	9.3%	BBOA (8%) HOA (1.1%) OOA (0.3%)	BBOA (~20) Others all NO^+ or NO_2^+	Yes
Lin et al. (2021)	NW China, November	3	"within range"	20%, 53% (haze, non-haze)	Secondary $pRONO_2$ (17, 36%) Primary $pRONO_2$ + NPAH (3,17%) (haze, non-haze)	Secondary $pRONO_2$ (2.3-2.6) Primary $pRONO_2$ + NPAH (5.1-8.0)	Yes
This study	Southeast US, late summer (aircraft, RF16)	5	1% lower[j]	14%, (22%)[k]	LO-OOA (9, 12%)[k] MO-OOA (5, 9%)[k]	LO-OOA (3.03±0.54)[h], ∑OOA (2.92±0.43)[l]	Yes
This study	Southeast US, late summer (aircraft, RF18)	5	13% lower[j]	29%, (55%)[k]	LO-OOA (13, 18%)[k] MO-OOA (5, 28%)[k] IEPOX-SOA (5, 9%)[k]	LO-OOA (2.83± 0.64)[l], ∑OOA (2.96±0.28)[l]	Yes
Tiitta et al. (2016)	Wood burning emissions, oxidized with O_3, NO_3, OH, NO_x in laboratory	5	Not resolved	N/A[m]	N/A[m]	POA2 (2.5)[n], SOA2 (2.6)[n], SOA3 (3.1)[n]	No
Reyes-Villegas et al. (2018)[o]	Manchester UK, "Bonfire Night", fall	6	N/A	N/A	Primary and secondary $pRONO_2$	N/A	No[p]

[a]Number of factors resolved with PMF.

[b]Comparison of the NO_x^+ ratio (NO_2^+/NO^+) for NH_4NO_3 factor resolved with PMF vs the calibration NH_4NO_3 NO_x^+ ratio.

[c]Average fraction of total nitrate apportioned to $pRONO_2$ using PMF apportionment method.

[d]$pRONO_2$ factors comprising >85% of non-NH_4NO_3 nitrate concentration. % contributed to total nitrate indicated in parentheses when available.

[e]Ratio-of-Ratios for non-NH_4NO_3 factors where NO_x^+ ratios indicative of $pRONO_2$ were resolved. ∑OOA and ∑OA indicate the mass-weighted sum of all OOA (and other SOA) or OA (non-NH_4NO_3) factors, respectively.

[f]Was the NO_x^+ ratio method also used for nitrate apportionment and compared to PMF method apportionment?

Formatted Table

[g]Sulfate and ammonium ions also included.

[h]More-oxidized and less-oxidized of two SV-OOA factors; "Nitrogen-enriched" OA

[i]HOA NO_x^+ ratios very similar to NH_4NO_3. BBOA and CCOA factors had only NO_2^+ (no NO^+). However, nitrate from all OA factors were apportioned as $pRONO_2$. CCOA = Coal-Combustion OA

[j]NH_4NO_3 calibration NO_x^+ ratios were atypically variable during this campaign (see Sects. 4 and S2, Figs. S8, S9e). These comparisons are for the calibrations performed most closely in time, the day following the flight after the instrument was powered off and back on.

[k]Second % is the average fraction in the time series (not mass weighted). Other f_{pRONO2} in table are mass-weighted.

[l]"Uncertainties" for these *RoR* are the standard *deviation* of 100 bootstrapping runs (standard *error* is 10 times smaller)

[m]Not apportioned with PMF method. Apportioned with NO_x^+ ratio method.

[n]POA2 is a primary OA factor associated with $pRONO_2$. SOA2 and SOA3 are secondary factors from $O_3/NO_x/NO_3$ and OH/NO_x oxidation, respectively.

[o]$pRONO_2$ concentrations were separated first with the NO_x^+ ratio method. Then PMF performed with OA ions combined with $pRONO_2$ concentrations to separate different $pRONO_2$ sources.

[p]The secondary/primary $pRONO_2$ apportionment was compared between the combined $pRONO_2$ + OA PMF method (see footnote "o") and another apportionment method using ratios of $pRONO_2$ vs BBOA factor during distinct plume events. UMR data used (all other studies used HR).

Table S5. Summary of instrument comparisons of total $pRONO_2$ concentrations in the field and laboratory. A summary is presented in Sect. 5.3 and details and discussions of the comparisons are provided in Sect. S5.

Reference	Instruments compared	Sample description	Slope (R^2)	Notes
Field (outdoor ambient)				
Fry et al. (2013)	AMS (*RoR*) vs TD-LIF	Montane pine forest in US, summer	0.94-1.16 (0.53)	Typically nitrate was dominated by $pRONO_2$, however instruments tracked well during NH_4NO_3 plumes.
Lee et al. (2016)	AMS (*RoR*) vs AMS (AMS-IC)	Semi-polluted rural SE US, summer	1.15 (0.72)	Nitrate usually $pRONO_2$-dominated (same for following two entries).
Lee et al. (2016)	AMS (*RoR*) vs TD-LIF	Semi-polluted rural SE US, summer	0.23, 0.45 (0.74)	Two distinct slopes were observed for different periods (with same R^2).
Lee et al. (2016)	AMS (*RoR*) vs FIGAERO-CIMS (I^-)	Semi-polluted rural SE US, summer	1.11 (0.67)	FIGAERO-CIMS used iodide-adduct CI and was the sum of 88 compounds.
Huang et al. (2019a)	AMS (fixed R_{pRONO2}=0.1) vs FIGAERO-CIMS (I^-)	Rural Germany, summer	2.13 (0.27)	Reported as CIMS vs AMS (slope =0.47, R=0.52). CIMS considered lower limit, based on calibration assumptions. Considering only the nitrate functionality for the CIMS for direct comparison of nitrate functional group concentration, the CIMS vs AMS slope may have been ~0.1.
Chen et al. (2020)	AMS (fixed R_{pRONO2}=0.1-0.2) vs FIGAERO-CIMS (I^-); nitrate/organic fraction and N/C.	Rural SE US, late summer to mid-fall	5-18% vs 12.3±10.8%	Percents in slope column are the organic nitrate molecule fraction of total organic measured. Additionally, the N/C agreed ~1:1 ± ~30-50%, for the range of nitrate computed for the AMS (for assumed R_{pRONO2} range).
Kenagy et al. (2021)	AMS (*RoR*) vs TD-LIF	Korean Peninsula, spring (aircraft)	1.89	Screened for f_{pRONO2} (AMS) > 0.2 and TD-LIF corrected for particle losses in aircraft sampling inlet.
Rollins et al. (2013)	TD-LIF vs FTIR	Bakersfield, CA, summer	1.38 (0.52)	Relatively large offset in fit; average TD-LIF/FTIR ratio >2.

Laboratory				
Keehan et al. (2020)	AMS vs TD-CRDS	SOA from α-pinene and Δ-3-carene + NO_3 radicals	1.06-1.14 (0.73)	Range of slopes is for ODR fitting without and with y-intercept fixed to zero when plotting TD-CRDS vs AMS (0.88, 0.94) respectively; but reported here in the slope column as AMS vs TD-CRDS for consistency in this table.
Eris et al. (2018)	AMS vs TD-CAPS	SOA from terpenes and isoprene + OH, O_3, NO_3	"good quantitative agreement"	No peer-reviewed publication available at this time. Assumed to be within ~50%
Liu et al. (2012)	AMS vs FTIR	SOA from TMB + OH/NO_x	2.28 (0.98)	Inadequate information provided on AMS quantification and calibration to assess factor of 2 differences.
Bruns et al. (2010)	AMS (N/C ratio) vs FTIR (N/C ratio)	SOA from terpenes + NO_3 radical	FTIR N/C ~3–4 times AMS	Multiple possible factors may have led to large difference (see Sect. S5).

Supplementary Figures

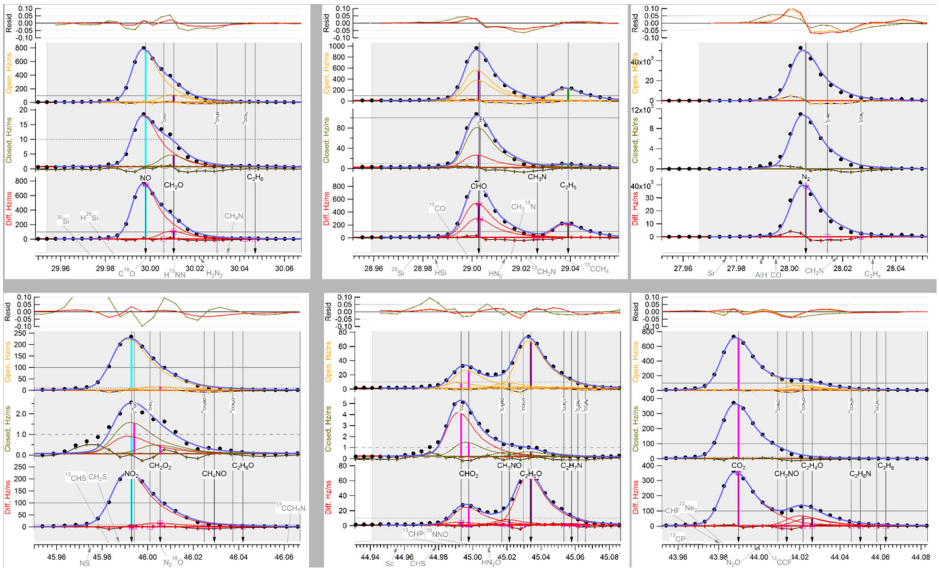

Figure S1. High-resolution peak fitting example for *m/z* 30, 29, 28, 46, 45, 44 for SOA produced from reaction of Δ-3-carene with nitrate radicals (see Sect. S1.2). Lower three panels (Open, Closed, Diff): acquired data (black dots), individual peak fits (red, gold, and orange curves), and sums of all ions fits (blue curves). Ion formulae in black were fit and grey formulae were not. Top panel: Residuals for Open, Closed, Diff color-coded according to the y-labels on the lower panel.

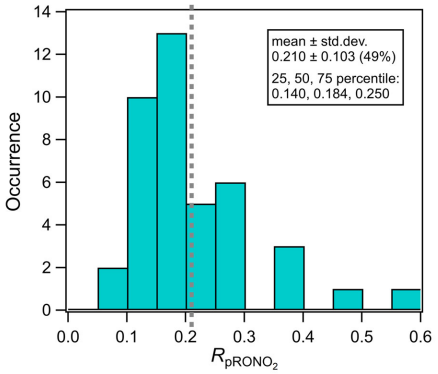

Figure S2. Histogram and mean of $pRONO_2$ NO_x^+ ratios (R_{pRONO2}) for studies in Fig. 1. The relative standard deviation (and interquartile range) is double that of the Ratio-of-Ratios (*RoR*) as shown in Fig. 1. The tighter distribution for the *RoR* in Fig. 1 than for R_{pRONO2} here reflects a substantial degree of correlation between R_{pRONO2} and R_{NH4NO3} and supports using the *RoR* method for estimating R_{pRONO2}.

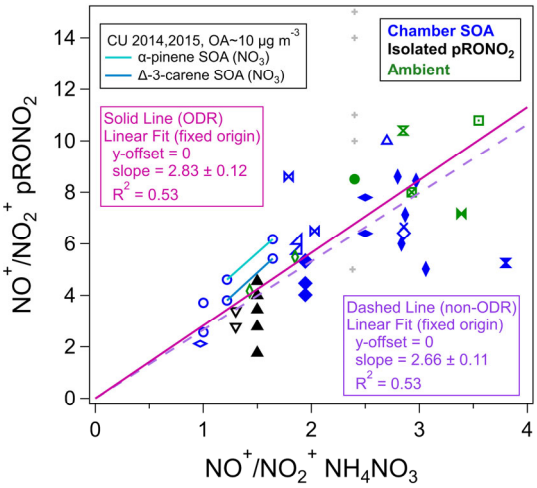

Figure S3. Same as lower right panel in Fig. 1, except axes are swapped and NO_x^+ ratios are inversed (NO^+/NO_2^+). Plotting this way (compared to Fig. 1), emphasizes slightly different data and outliers and gives more weight to points with higher NO^+/NO_2^+. In this representation the R_{NH4NO3} is placed on the x-axis, and thus a non-ODR fit may be appropriate under the assumption that most uncertainty is contributed by the $pRONO_2$ ratios. Thus both ODR and non-ODR fits are shown (constraining the y-intercept to zero since unconstrained intercept was not significant). Compared to Fig. 1, slopes (also equivalent to a *RoR*) are slightly higher (and bracket the average *RoR*, 2.75), and the degree of correlation is the same.

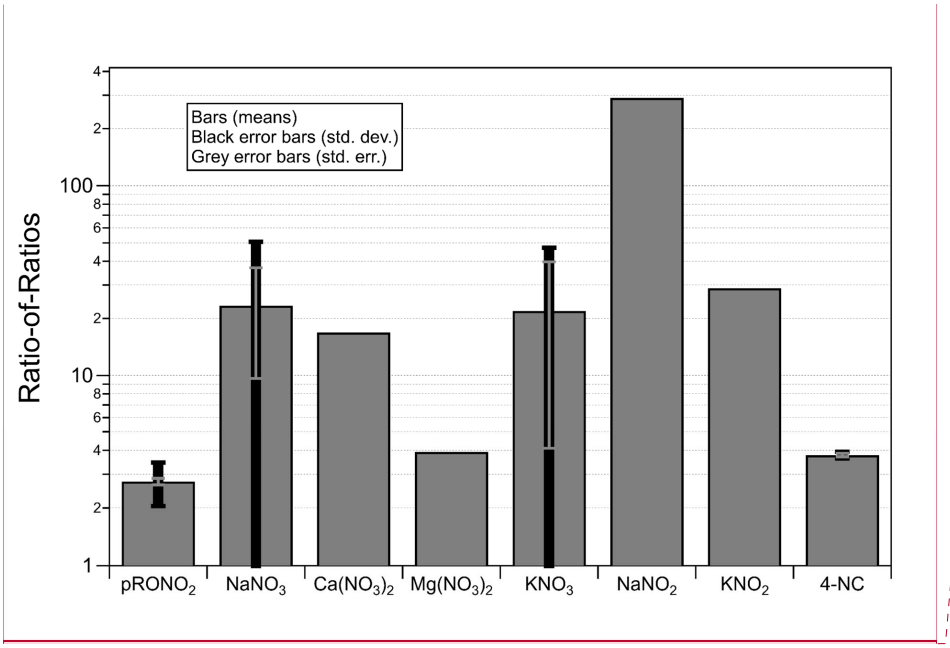

Figure S4. Ratios-of-Ratios (always referenced to the measured NH_4NO_3 ratio) reported for nitrate and nitrite compounds reported in the literature and this study. The value shown for $pRONO_2$ is from the survey conducted in this paper (as mean ± standard deviation/error). Sources and details for all other compounds are shown in Table S2. The values shown for $NaNO_3$ and KNO_3 are statistics for all values reported in different sources. Statistics for 4-nitrocatechol (4-NC) are for multiple measurements during a 2-month campaign with the same instrument.

Commented [12]: (replaced AMTD preprint version with this updated one with new 4-NC numbers)

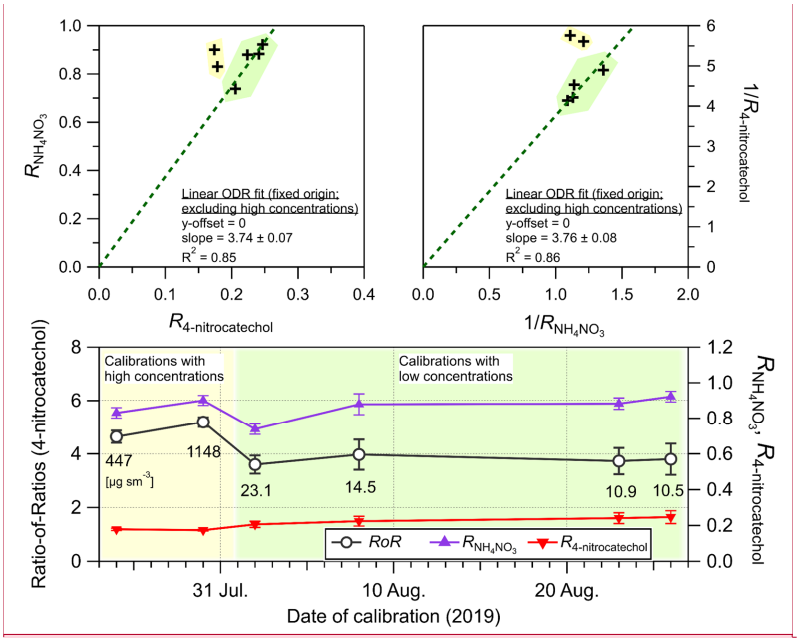

Figure S5. NO_x^+ ratios for 4-nitrocatechol (4-NC) and NH_4NO_3 and the corresponding *RoR* for ~~4-nitrocatechol~~ 4-NC measured on board the NASA DC-8 during the FIREX-AQ biomass burning study (Pagonis et al., 2021). Values listed below the *RoR* data points are the concentrations of 4-NC used to calibrate. ~~C~~While some calibrations were performed during pre-flight (4-NC only), post-flight (4-NC and NH_4NO_3), and ground-service days (4-NC and NH_4NO_3), only data for post-flight are shown. The reason for including only post-flight calibrations is: 1) due to the fact that typically the instrument had not been operating long enough (only a couple hours) to produce stable NO_x^+ ratios, which can be a sensitive parameter and require substantial time to stabilize shortly after starting up the AMS; 2) NH_4NO_3 calibrations were never conducted pre-flight (only 4-NC for cross calibration of sensitivity between the AMS and another chemical instrument, EESI — see Pagonis et al. (2021)); and 3) often the 4-NC and NH_4NO_3 calibrations were not conducted in close temporal proximity on ground-service days and/or too soon after startup for ratios to stabilize. ~~Pre-flight/post-flight calibrations pairs are shown on three days (Aug. 2, 8, 23), and with all cases post-flight *RoR* were measured higher due to higher measured $R_{4\text{-nitrocatechol}}$ values (since R_{NH4NO3} was only measured post-flight and applied to both calculations of the $RoR_{4\text{-nitrocatechol}}$). Therefore, it is not clear if that pattern was due to actual shifts in $RoR_{4\text{-nitrocatechol}}$ or if there were corresponding shifts in R_{NH4NO3}.~~ Scatter plots are shown for both the standard R_{NH4NO3} vs $R_{4\text{-nitrocatechol}}$ format (as NO_2^+/NO^+, top left) and as inverse ratios (top right), showing good correlation, over the limited range. Note that the calibrations conducted early in the campaign at very high 4-NC concentrations (indicated in yellow) are not included in the statistics here, nor for those in Fig. S4 and Table S2. This is because we have observed that when sampling very high OA concentrations (>50-200 µg m^{-3}), $NO_x^{\pm}$ ratios can be substantially skewed. This will be discussed in detail in a forthcoming manuscript exploring uncertainties of the nitrate apportionment methods. Similar behavior was also observed for $H_ySO_x^+$ and SO_x^+ ion ratios when sampling inorganic sulfate (Schueneman et al., 2021). ~~Linear fits with a y-intercept fixed to zero represent the average *RoR* (3.28 ± 0.19 and 3.37 ± 0.21, respectively). However there was no significant correlation, likely due to a combination of the limited range of R_{NH4NO3}, experimental uncertainty, and some variability in the *RoR* for nitrocatechol.~~ While this dataset suggests that a similar

Commented [13]: (replaced AMTD preprint version with this updated version with screening for relevant calibration data)

RoR relationship may be applicable to 4-NC and possibly other nitro organics or nitroaromatics, the number of datapoints (4), compounds (1), and instruments (1), as well as the range in R_{NH4NO3}, are very limited. Therefore it is not clear if NO_x^+ ratios for nitro compounds generally have a well-defined *RoR* and track NH_4NO_3 ratios. Further work would be required to draw any general conclusions, ideally including more compounds and mixtures, under different conditions, and with different instruments. To our knowledge, this provides the first example of repeated calibrations of a compound that produces $NO_x^{\pm}$ ions throughout a campaign, directly showing tracking of the NO_x^+ ratios with those of NH_4NO_3. Thus, it represents some indirect support for application of the *RoR* method to a single instrument throughout a campaign to apportion $pRONO_2$ and NH_4NO_3.

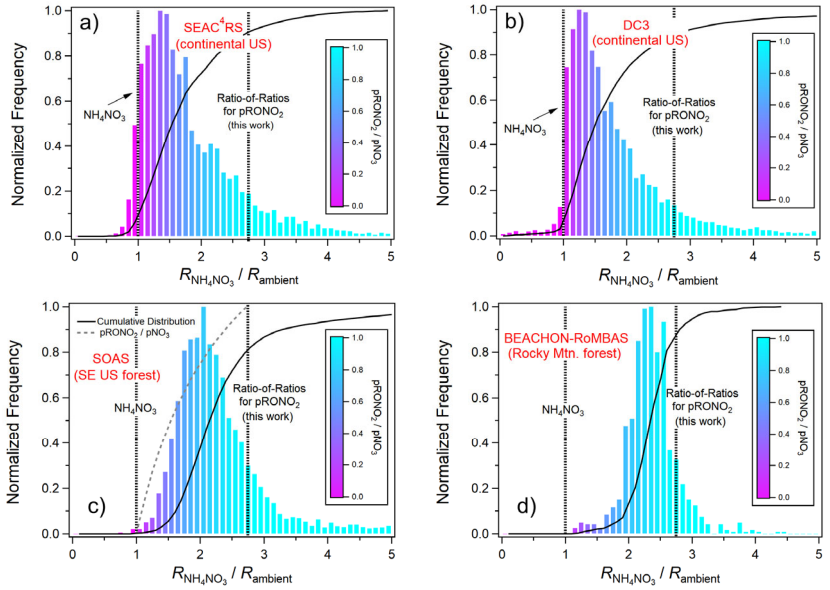

Figure S6. Standard frequency histograms (*not* weighted by mass concentration) for the same data as shown in Fig. 2. See Fig. 2 capture for additional details.

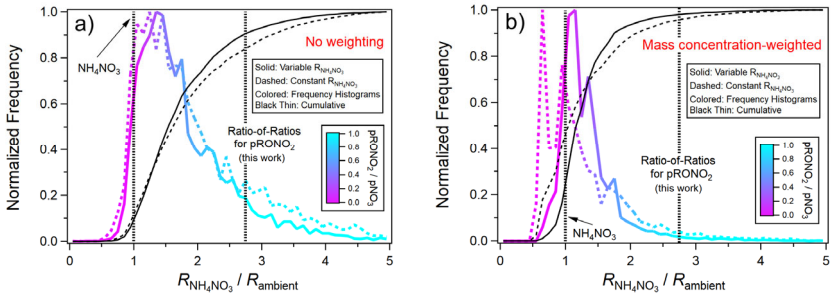

Figure S7. Histograms using the same data as shown in Figs. 2 and S6 for SEAC^{4}RS, except two versions of the histograms are shown: calculated with a campaign-average R_{NH4NO3} ("constant") vs flight-specific R_{NH4NO3} ("variable" as in Figs. 2 and S6). Panel a) shows standard frequency distributions and panel b) shows mass concentration-weighted distributions. The calibration R_{NH4NO3} for SEAC^{4}RS showed large variability between flights (Fig. S8 and S9e). There is substantial narrowing of the distributions using the flight-specific R_{NH4NO3} for the non-weighted distributions (panel a). The most prominent differences for the mass concentration-weighted distributions are largely due to data with high NH_4NO_3 concentrations where the $R_{ambient}$ were beyond the campaign-averaged R_{NH4NO3} ("constant"), resulting in much more of the distribution below 1. These differences support the importance of applying time-varying calibration ratios, when applicable (see Sect. 4)

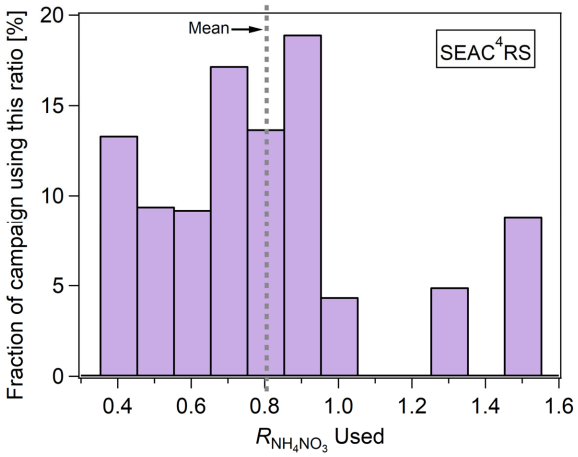

Figure S8. Frequency distribution of NH_4NO_3 calibration NO_x^+ ratios (R_{NH4NO3}) applied to ambient nitrate apportionment for SEAC^{4}RS campaign. Mean value is also shown, which was used for the "constant" R_{NH4NO3} calculation shown in Fig. S7.

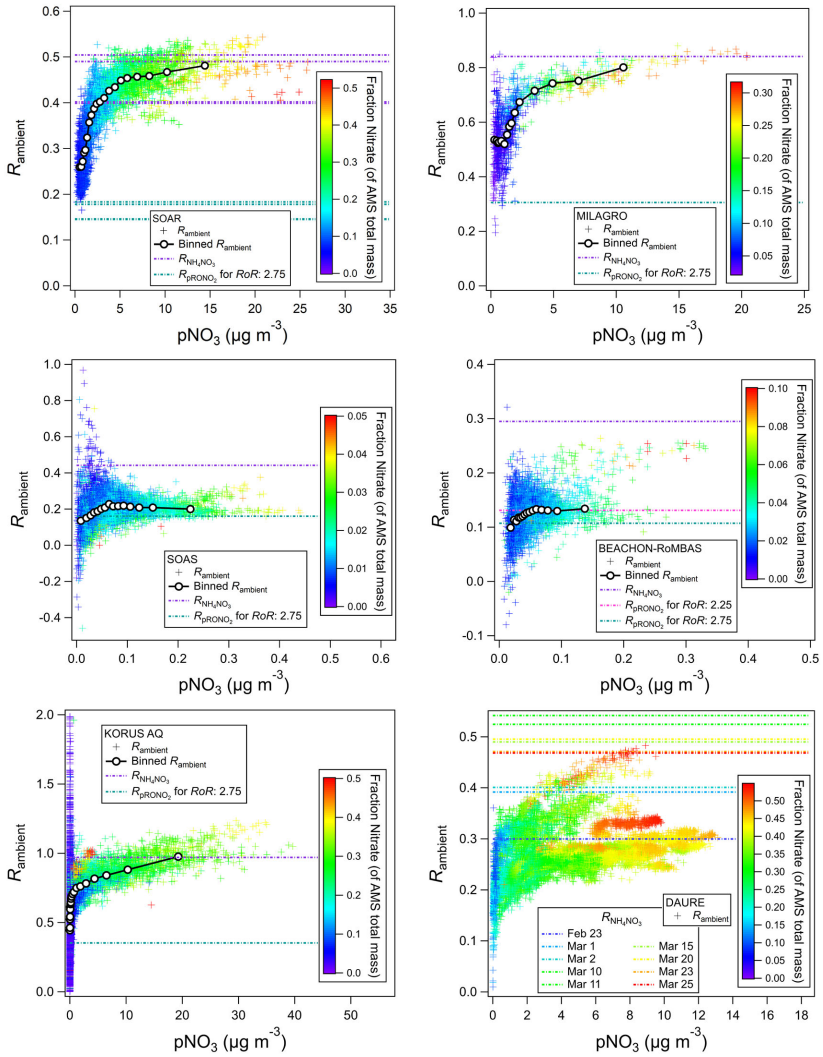

Figure S9a. $R_{ambient}$ vs pNO_3 for six different campaigns (indicated in legends), colored by mass fraction nitrate, and overlaid with quantile averages. Horizontal lines are shown for calibration R_{NH4NO3} (multiple in some cases) and the corresponding estimated R_{pRONO2} ratios (using RoR = 2.75). Data is not detection limit thresholded, and quantiles are means except for BEACHON-RoMBAS and KORUS-AQ which are medians (to reduce impact of outliers). Where only one R_{NH4NO3} is shown, only one value was available for the data period shown (MILAGRO) or they are averages of several stable values (see Fig. 2 for averages and standard deviations for SOAS and BEACHON, and KORUS-AQ was 0.97 ± 0.04).

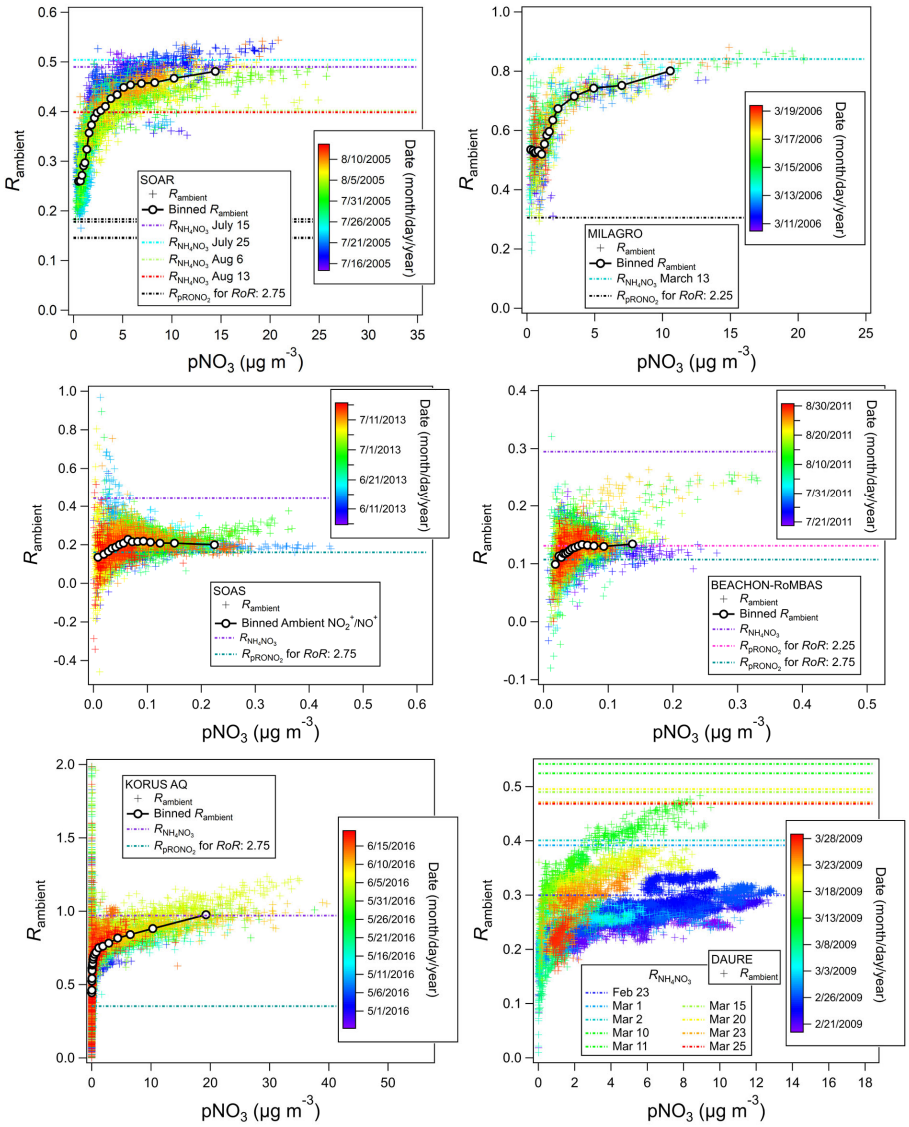

Figure S9b. Same as Fig. S9a except colored by data collection time during campaign.

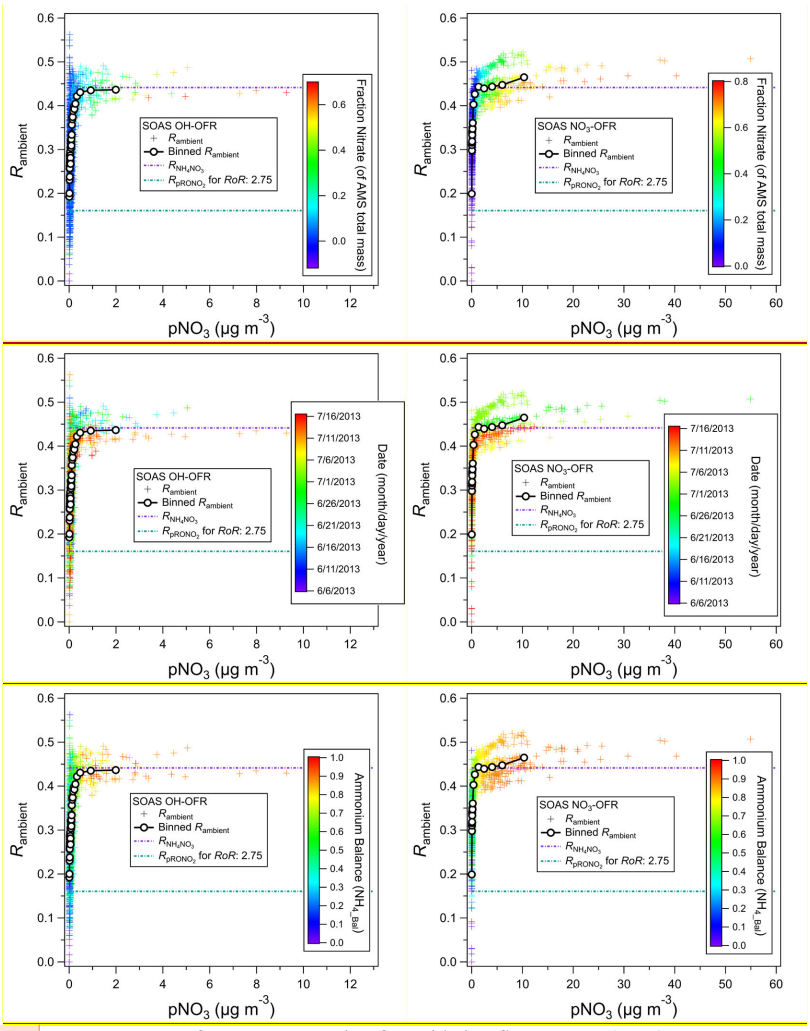

Figure S9c. $R_{ambient}$ vs pNO_3 for SOAS campaign for oxidation flow reactor (OFR) measurements using OH (left column) and NO_3 (right column) radicals as oxidants. Each of the three rows contains the same data, but colored by different measures: mass fraction of AMS mass that is aerosol nitrate (top row), time (middle row), and NH_{4_Bal} (bottom row) as indicated in colorbar legends. Data is overlaid with quantile averages (medians). NH_{4_Bal} is calculated as the molar ratio of $NH_4/(NO_3+2\times SO_4)$. Values approaching unity suggests full ion balance of sulfate and nitrate by ammonium and little contribution of organic nitrate or organic sulfate. Lower values suggest acidic particles and/or the presence of substantial organic nitrate or organic sulfate. Horizontal lines are shown for calibration R_{NH4NO3} and corresponding estimated R_{pRONO2} (from RoR = 2.75).

Commented [DD14]: y-axes rescaled to all be same in all panels per discussion in response to referee comments.

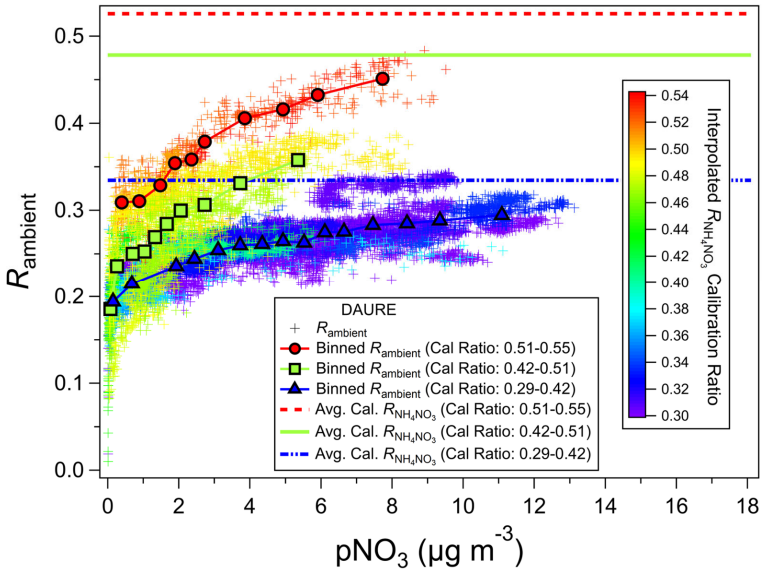

Figure S9d. $R_{ambient}$ vs pNO_3 for DAURE campaign, colored by time-dependent calibration R_{NH4NO3} (calculated by linear interpolation of measured ratios during NH_4NO_3 calibrations). Binned averages (means) for three calibration ratio ranges are shown as well as corresponding averages of applied calibration R_{NH4NO3} (horizontal lines).

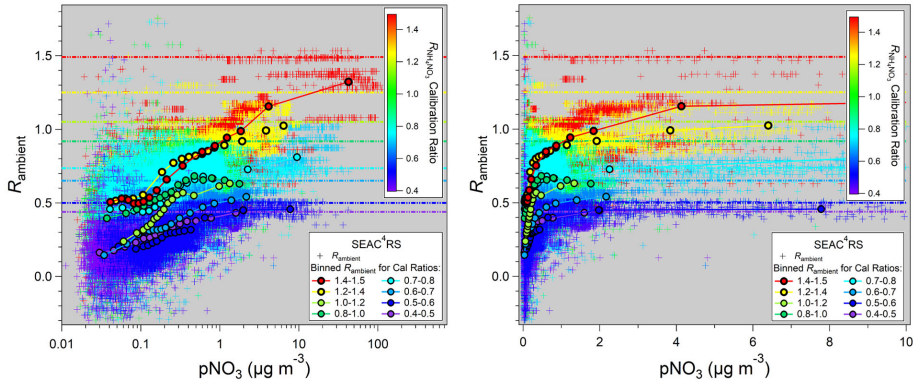

Figure S9e. $R_{ambient}$ vs pNO_3 for SEAC^{4}RS campaign (log left, linear right), colored by flight-dependent calibration R_{NH4NO3}. Binned averages (means; 15 quantiles & 98–100% by pNO_3) for seven R_{NH4NO3} calibration ratio ranges are shown, as well as corresponding averages of applied calibration ratios (horizontal lines, in color matching binning). Grey background is used for better contrast of light colors.

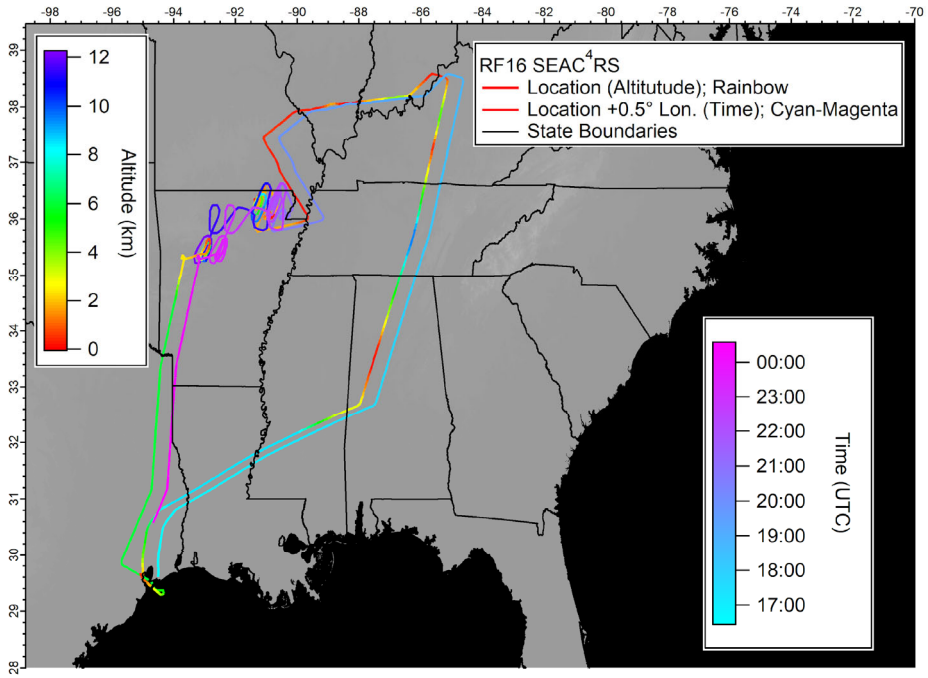

Figure S10. Flight track for SEAC4RS RF16 (11 Sept, 2013) over the SE US, colored by altitude and time (offset +0.5 degrees in longitude). Flight description (locations and sources sampled): The aircraft flew from Houston northeast to the Ohio River Valley partly at higher altitude with dips to low altitude in the region where the SOAS campaign was conducted in west-central Alabama, in central Kentucky, and at the Ohio River Valley, then flew to western Missouri (Ozark Mts) and the Mississippi River Valley (low altitudes), then northern Arkansas (range of altitudes), then returned south to Houston (at altitude). A range of source influences were sampled during different periods of the flight and can be approximately separated as follows for the low-level legs (<500 m) when $pRONO_2$ tended to be elevated: 16:40–17:00: (biogenic including isoprene-related and especially monoterpenes, low anthropogenic); 17:30 (biogenic and anthropogenic such as NO_x, NO_y, CO, aromatics); 17:45–18:00 (biogenics and anthropogenics; 18:20–19:30 (mixed anthropogenic and biogenic with varying proportions); 19:45–20:00 (mixed biogenic and anthropogenic with two large agricultural biomass burning spikes at 19:53–19:54 and 19:59–20:00 showing large spikes in NH_4NO_3, acetonitrile, and f_{60}); 20:15–20:30 (mixed biogenic and anthropogenic); 22:25–22:55 (mixed biogenic, anthropogenic). During low-level legs, OA was typically ~7-15 μg m^{-3}, but exceeded 80 μg m^{-3} during the biomass burning plumes, and was 0.1–0.3 μg m^{-3} in the free troposphere (see Fig. S11, top).

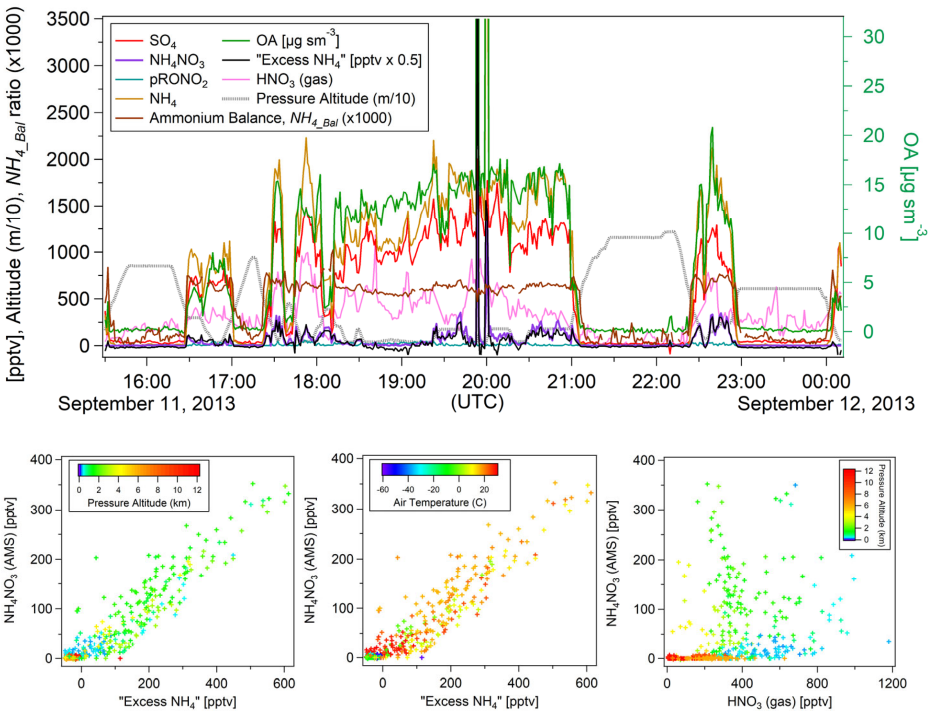

Figure S11. (top) Time series of SO_4, NH_4, NH_4NO_3, $pRONO_2$, "Excess NH_4", OA, HNO_3(gas), altitude, and ammonium balance (NH_{4_Bal}, molar ratio of NH_4/ (NO_3+2SO_4)) for SEAC^{4}RS RF16 flight (same flight as shown in Fig. 3). "Excess NH_4" was calculated by subtracting the AMS-measured molar concentrations of NH_4 - 1.2 x SO_4 as an indicator of possible changes in the NH_4 related to NH_4NO_3 concentrations (see Sect. 5.1). All concentrations shown are in parts-per-trillion (pptv) mixing ratio unless otherwise indicated (i.e., OA). (bottom) Scatterplots of NH_4NO_3 vs. "Excess NH_4" (colored by altitude or air temperature) and vs HNO_3 gas (colored by altitude).

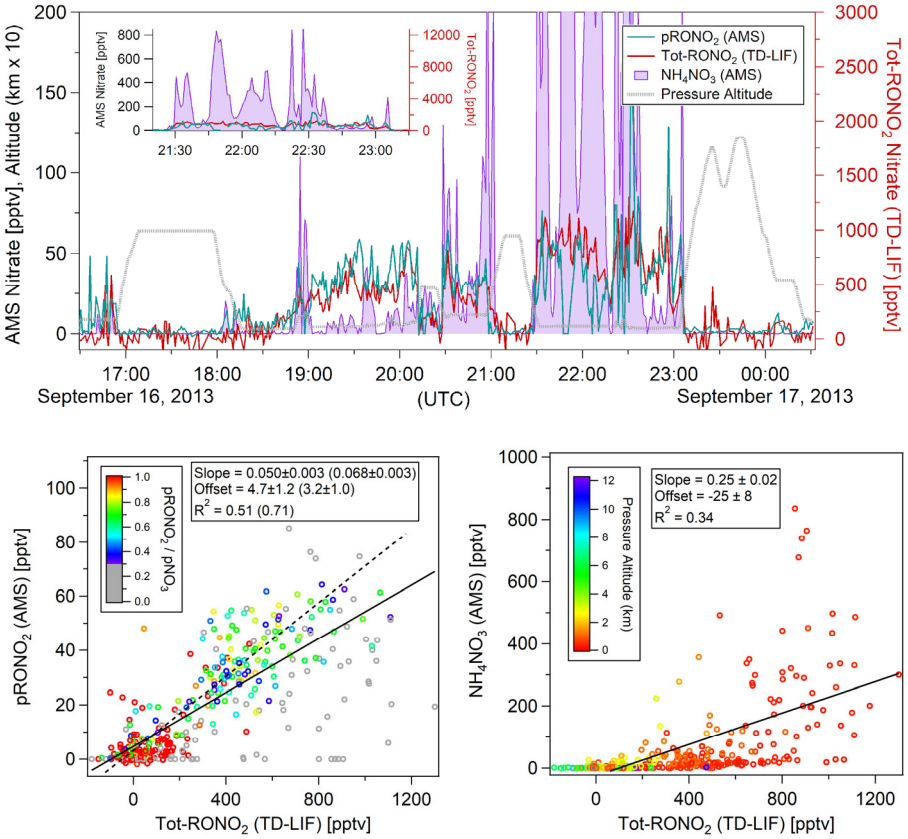

Figure S12a. Comparisons of AMS $pRONO_2$ and NH_4NO_3 with TD-LIF total (gas+particles) organic nitrate (Tot-$RONO_2$) during a SEAC[4]RS flight (RF18) in the Southeast US (1-min averages). The time series (top) and scatterplots of $pRONO_2$ (bottom left) or NH_4NO_3 (bottom right) vs Tot-$RONO_2$ are shown. R_{NH4NO3} (constrained by calibrations and PMF), a *RoR* of 2.75, and Eqs. 2/3 were used to apportion the AMS nitrate. Linear least-squares lines are orthogonal distance regression (ODR). For the $pRONO_2$ vs Tot-$RONO_2$ plot (bottom left), and additional line (dotted) and fits (parentheses) are shown for data including only when f_{pRONO2} is greater than 0.3 (and datapoints with f_{pRONO2}<0.3 are greyed). Figure S13 shows the flight track and timing of different source types sampled.

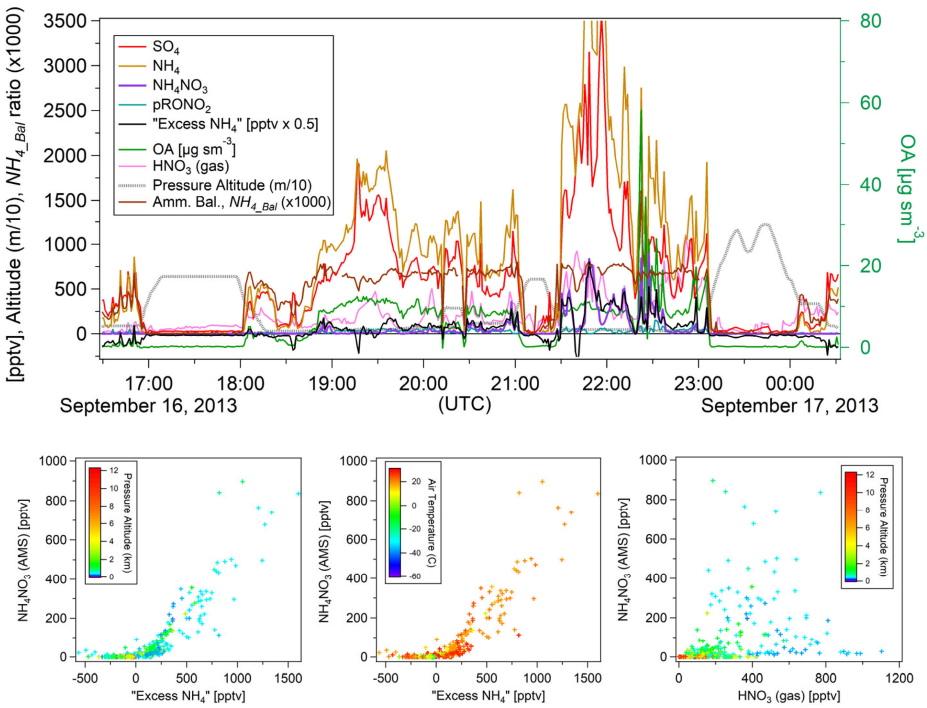

Figure S12b. Same as Fig. S11, except for RF18 (same flight as shown in Fig. S12a).

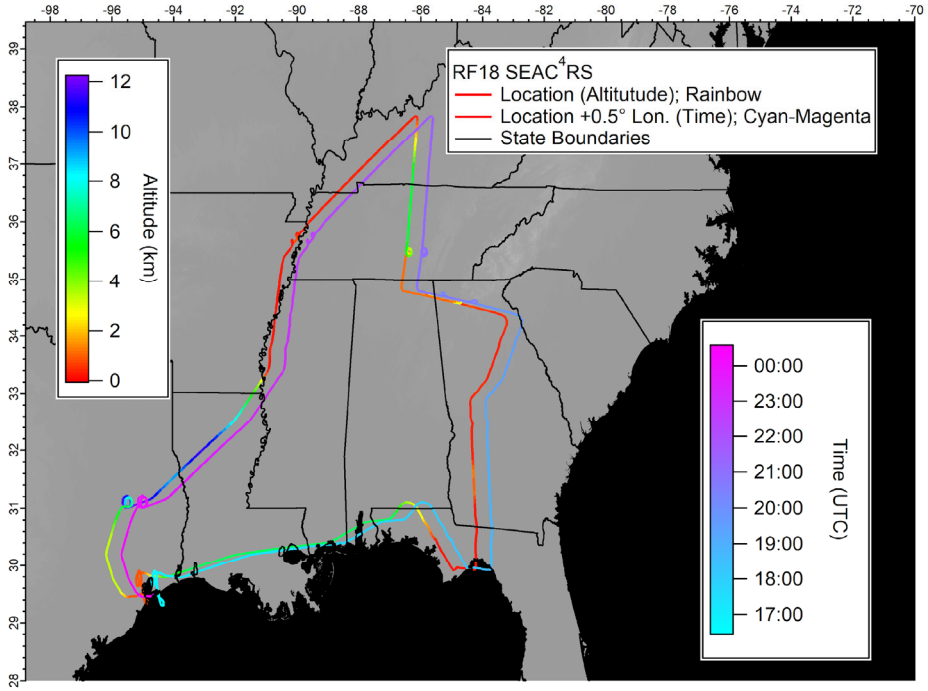

Figure S13. Flight track for SEAC4RS RF18 (16 Sept, 2013) over the SE US, colored by altitude and time (offset +0.5 degrees in Longitude). Flight description (locations and sources sampled): The aircraft flew from Houston east just inland along the Gulf Coast to the Florida panhandle (mostly at high altitude), north and northwest to the Ohio River Valley (mostly at low altitude), southwest to and south along the Mississippi River Valley (at low altitude), and then returned to Houston (mostly at high altitude). A range of source influences were sampled during different periods of the flight and can be approximately separated as follows for the low-level legs: 18:00–19:00 (strongly biogenic including isoprene-related and especially monoterpenes, low anthropogenic); 19:00–20:15 (elevated/decreasing monoterpenes, increasing isoprene-related, elevated anthropogenic such as aromatics, NO_x, NO_y); 20:30–21:00 (elevated isoprene-related biogenics and anthropogenics); 21:30–22:10 (lower biogenics, elevated anthropogenics); 22:20–23:10 (episodic concentrated agricultural biomass burning). During low-level legs, OA was typically ~5–10 μg m^{-3}, but exceeded 50 μg m^{-3} during the biomass burning plumes, and was 0.1–0.3 μg m^{-3} in the free troposphere (see Fig. S12b, top).

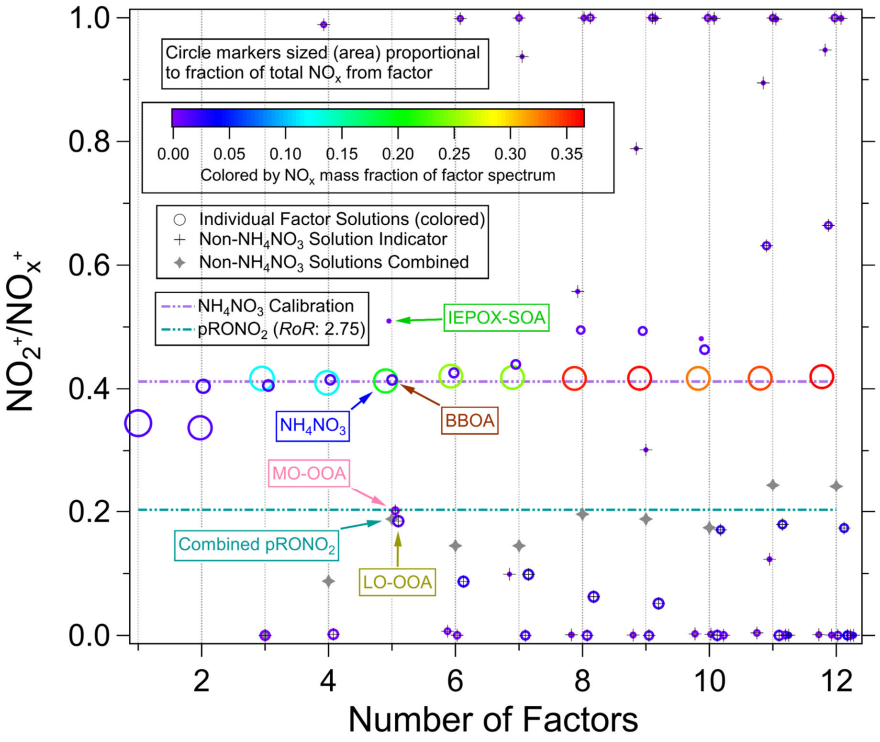

Figure S14. NO_x^+ ratios for individual and combined factors for PMF solutions for SEAC[4]RS RF16 vs number of factor solutions (FPEAK=0). Circles are sized by the fraction of the total NO_x^+ concentration apportioned to each individual factor and colored by the fraction of the spectrum from NO_x^+ ions. The individual factors that are not associated with NH_4NO_3 (generally a "NH_4NO_3 factor" and BBOA-related factors are and those not are defined as outside -20%/+50% of the calibration NH_4NO_3 NO_2^+/NO_x^+ for this plot) are indicated and their combined (mass-weighted) ratio is also shown. The largest circles with high NO_x^+ fraction in the spectrum are the NH_4NO_3 factors and generally the factors with similar NO_x^+ ratio are BBOA. The points not associated with NH_4NO_3 that have the largest contribution to total NO_x^+ concentration are typically LO-OOA. Factor assignments are indicated for the 5-factor solution, which was used in the analyses discussed in the manuscript. Note that in this figure rather than represent NO_x^+ ratios as used throughout this paper (NO_2^+/NO^+), instead NO_2^+/NO_x^+ is used. This allows the full range from entirely NO^+ to entirely NO_2^+ to be shown on a compact scale, since NO_2^+/NO^+ blows up as the limit of entirely NO_2^+ is approached. The relationship between the two ratios is: $NO_2^+/NO_x^+ = 1/(1+1/(NO_2^+/NO^+))$ or $NO_2^+/NO^+ = 1/(1/(NO_2^+/NO_x)-1)$.

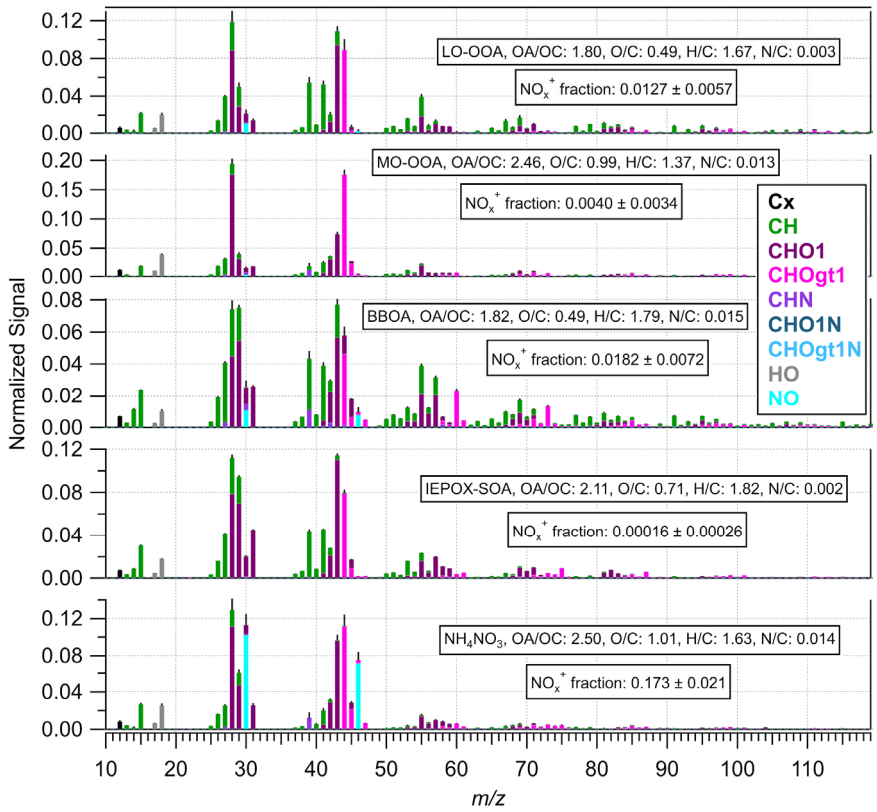

Figure S15a. PMF factor spectra for SEAC[4]RS RF16 (FPEAK=0). The spectra are averages from 100 *bootstrapping* (Ulbrich et al., 2009) iterations (with standard deviations propagated to the UMR sum shown in thin black vertical lines). The contributions from different ion families are colored and stacked at nominal *m/z*. The "1" or "gt1" denote that one or greater-than-one nitrogen or oxygen is associated with an ion family. The "NO" ion family contains all $H_yNO_x^+$ calculated in the HR analysis, although ions other than NO^+ and NO_2^+ are too small to be visible. "NO_x^+ fraction" is the fraction of the total signal from NO^+ and NO_2^+ ions. Elemental ratios (Aiken et al., 2008; Canagaratna et al., 2015) are also indicated where N/C ratios do not include $H_yNO_x^+$ ions (as is typically reported for AMS analysis).

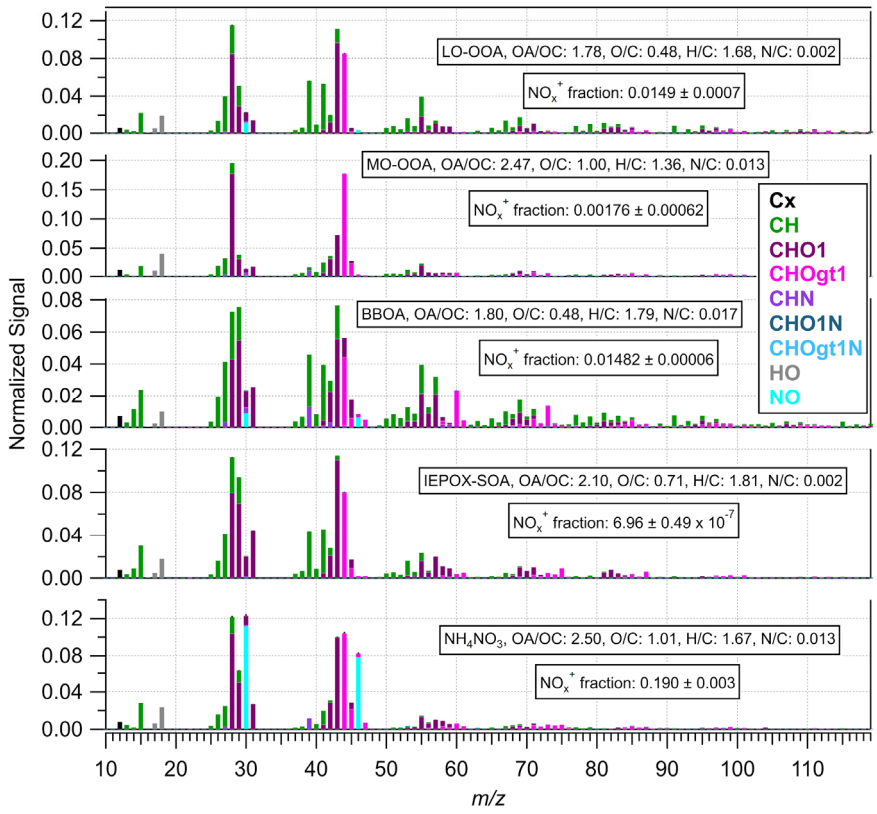

Figure S15b. Same as Fig. S15a except averages and standard deviations are from 100 starting *seed* iterations (Ulbrich et al., 2009).

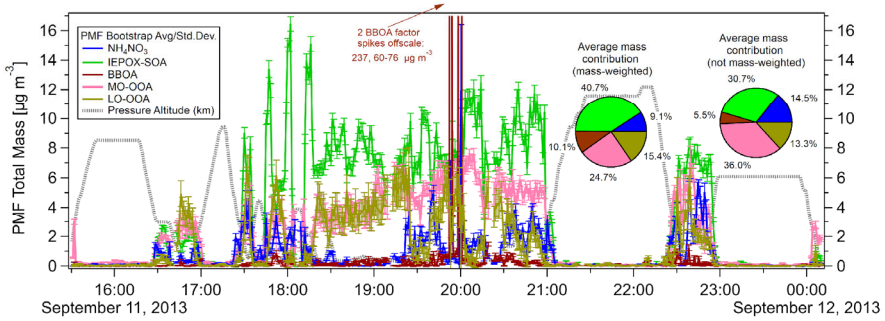

Figure S16a. Time series of PMF factors (total signal: OA + nitrate) for SEAC[4]RS RF16 (FPEAK=0). Averages and standard deviations for each point in the time series as well as the all-flight averages (shown as pies) were computed from 100 *bootstrapping* run

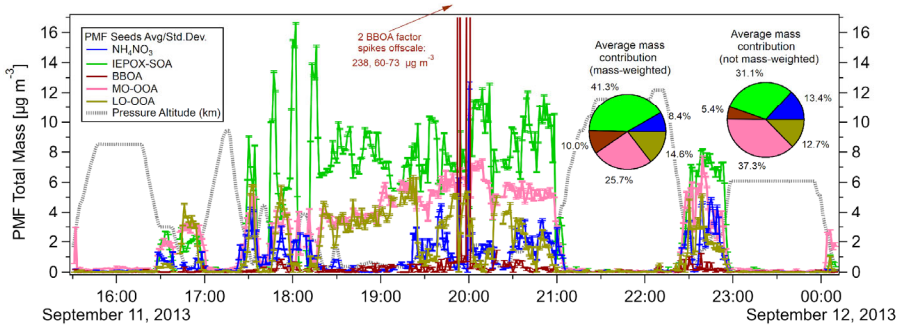

Figure S16b. Same as Fig. S16a, except using 100 *seed* runs (rather than *bootstrapping*)

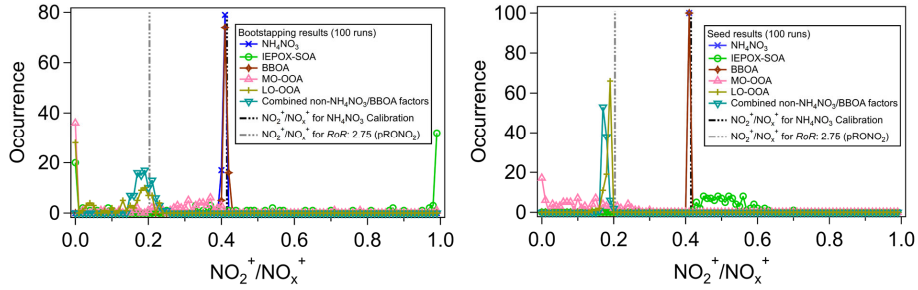

Figure S17. Histograms of NO_x^+ ratios for individual and combined PMF factors for SEAC[4]RS RF16 (FPEAK=0) for 100 bootstrapping (left) or seeding (right) iterations. Vertical lines are shown for the calibration R_{NH4NO3} and the R_{pRONO2} using a *RoR* referenced to the NH_4NO_3 factor ratio. Note that in this figure rather than represent NO_x^+ ratios as used throughout this paper (NO_2^+/NO^+), instead NO_2^+/NO_x^+ is used in order that the full range from all NO^+ to all NO_2^+ can be displayed on a compact scale (see Fig. S14 caption for more details).

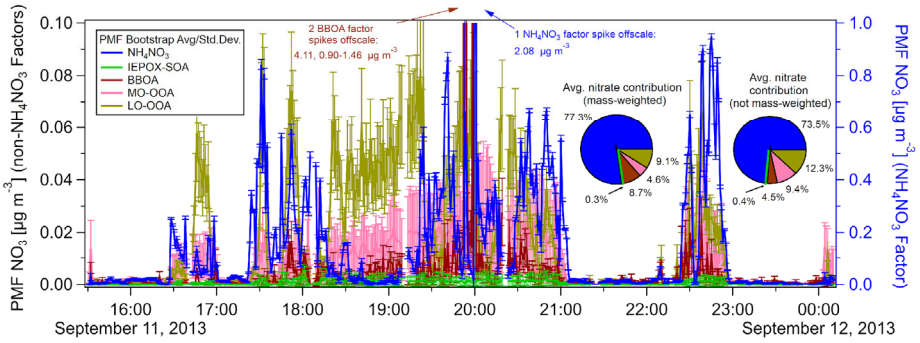

Figure S18a. Time series of nitrate component of PMF factors for SEAC[4]RS RF16 (FPEAK=0). Averages and standard deviations for each point in the time series as well as the all-flight averages (shown as pies) were computed from 100 *bootstrapping* runs. For aircraft sampling altitude see Fig. S16.

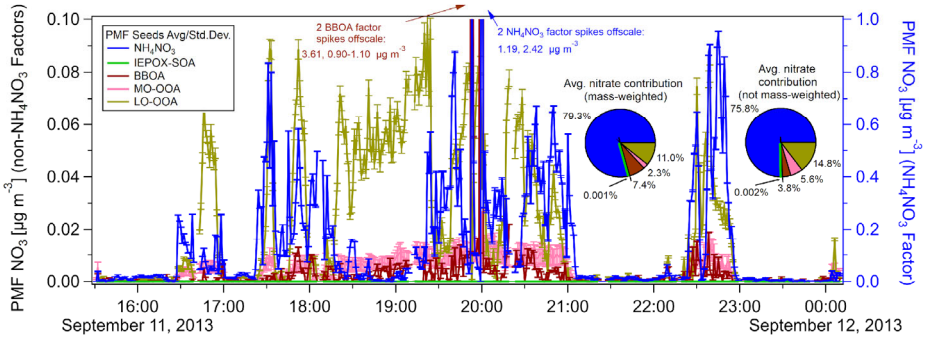

Figure S18b. Same as Fig. S18a, except using 100 *seed* runs (rather than *bootstrapping*). For aircraft sampling altitude see Fig. S16.

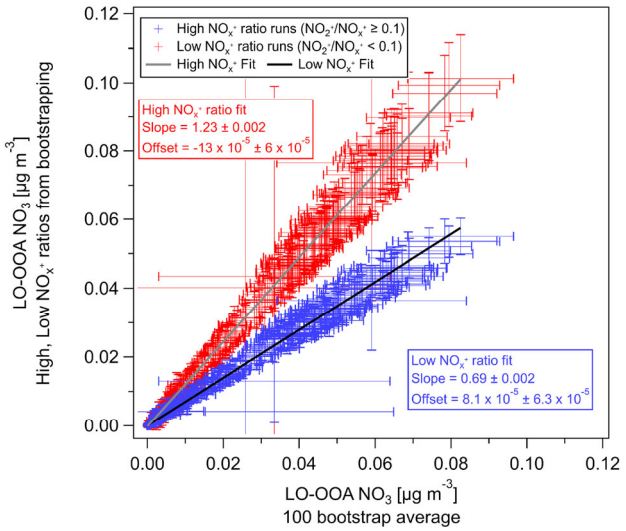

Figure S19. Nitrate concentrations apportioned to the PMF LO-OOA factor for different ranges of NO_x^+ ratios (in the factor spectra) vs the average of all runs for 100 bootstrapping runs (SEAC[4]RS RF16). The averages and standard deviations for the different subsets are shown for each time point.

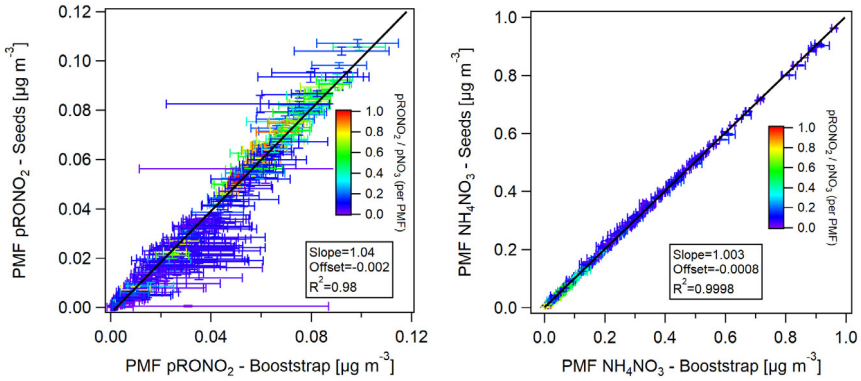

Figure. S20. Comparison of bootstrapping vs seeding nitrate apportionment concentrations for SEAC[4]RS RF16 (averages and standard deviations for 100 runs shown for each time point).

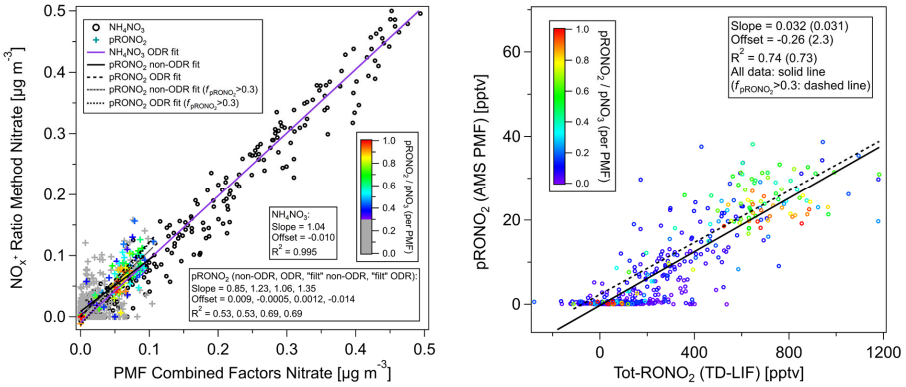

Figure S21. Equivalent plots to bottom panels in Fig. 4 except averages of seed runs (rather than bootstrapping).

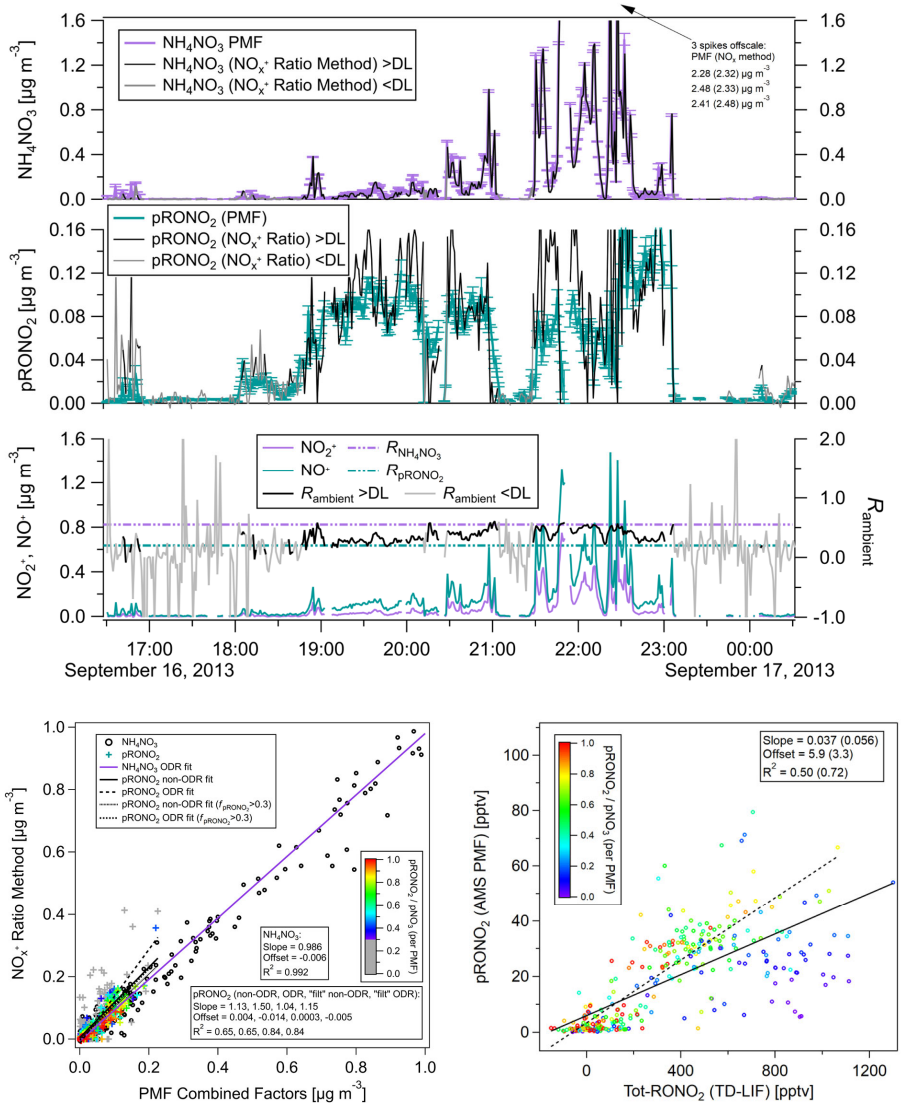

Figure S22. Same as Fig. 4 except for SEAC[4]RS RF18 (rather than RF16).

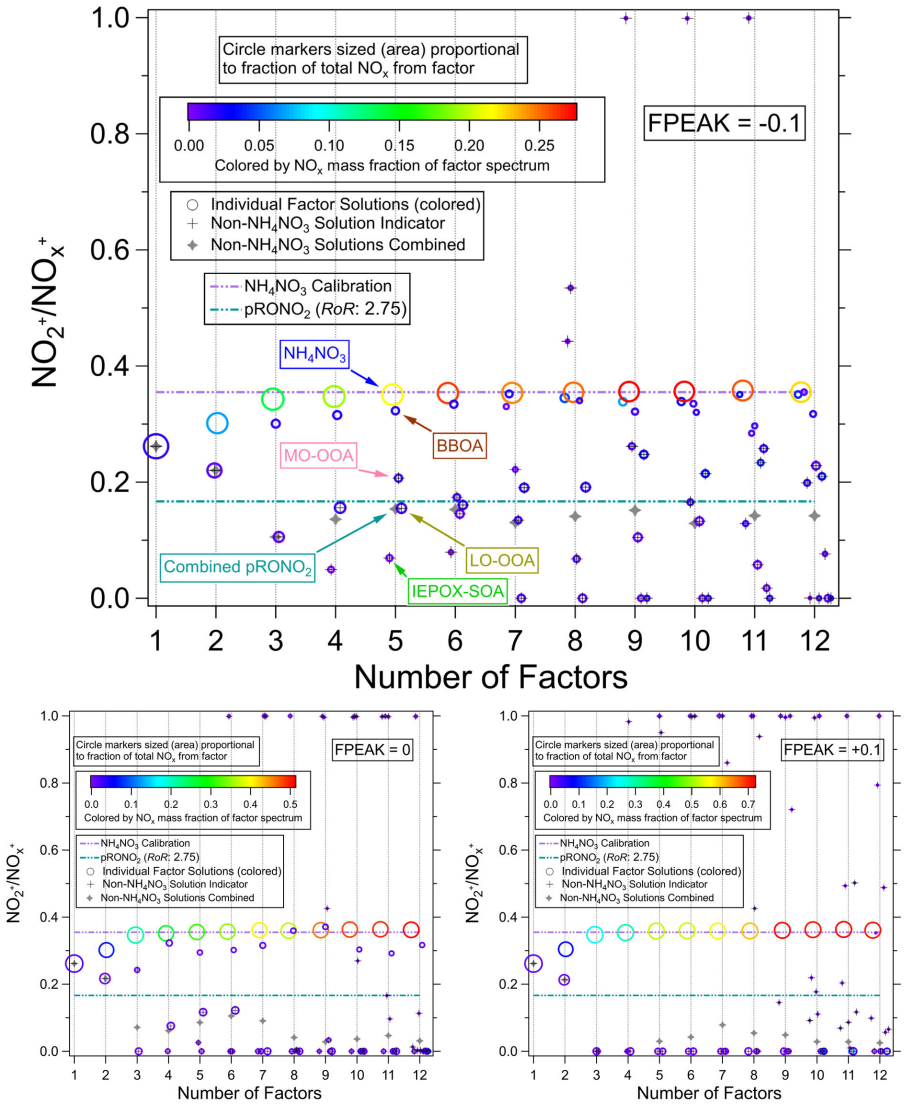

Figure S23. Same as Fig. S14 except for SEAC[4]RS RF18 (instead of RF16) and also showing results for three different FPEAK (-0.1, 0, +0.1), since the FPEAK = -0.1 (5-factor) solution was used all for analyses and comparisons (see Sect. S4.2). Factor assignments are indicated for the 5-factor solution with FPEAK = -0.1.

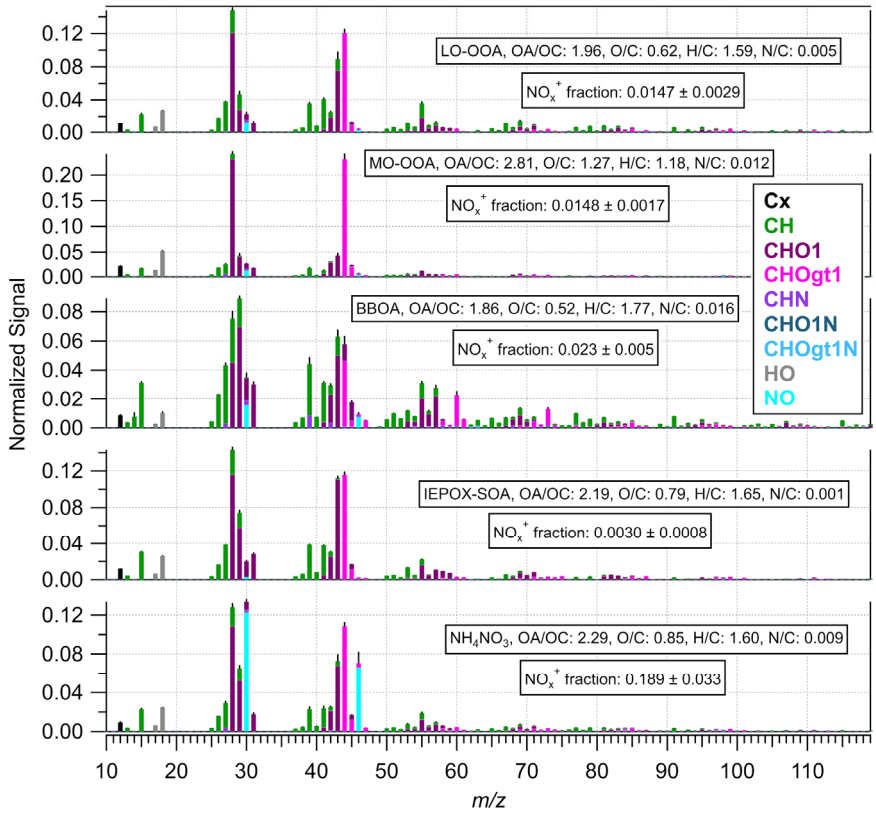

Figure S24. PMF Factor spectra for SEAC[4]RS RF18 (FPEAK= -0.1). The spectra are averages and from 100 bootstrapping iterations. See caption for Fig. S15a (showing same results for RF16) for additional details.

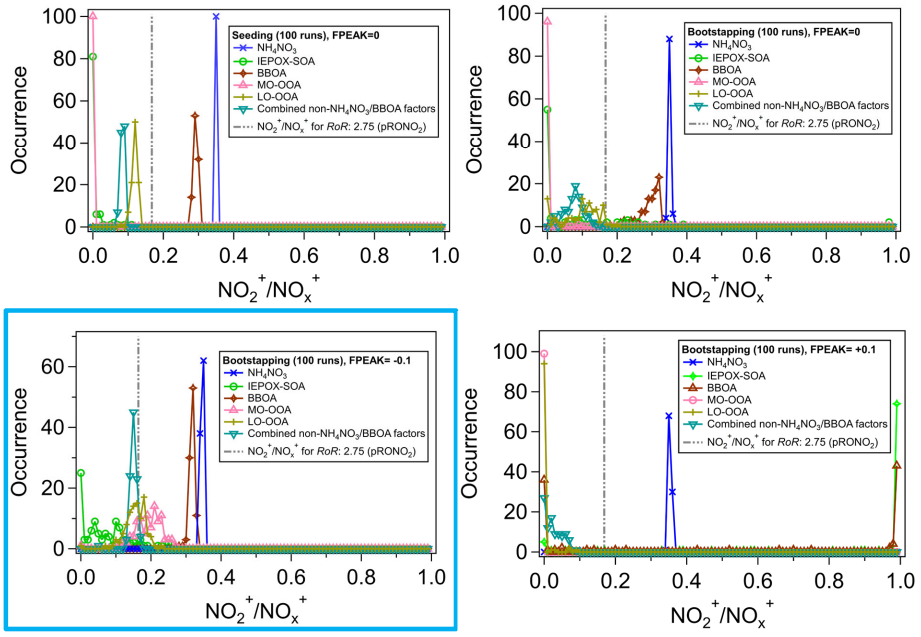

Figure S25. Histograms of NO_x^+ ratios for individual and combined PMF factors for SEAC[4]RS RF18 for 5-factor solutions with: (top left) seeding, FPEAK = 0; (top right) bootstrapping, FPEAK = 0; (bottom left) bootstrapping, FPEAK = -0.1; (bottom right) bootstrapping, FPEAK = +0.1 (see Fig. S14, S17 captions for more details on NO_x^+ ratio scale). The vertical line indicates the R_{pRONO2} using a *RoR* referenced to the NH_4NO_3 factor ratio. The FPEAK = -0.1 solution (highlighted with blue border) was used in all analyses and comparisons (see Sect. S4.2).

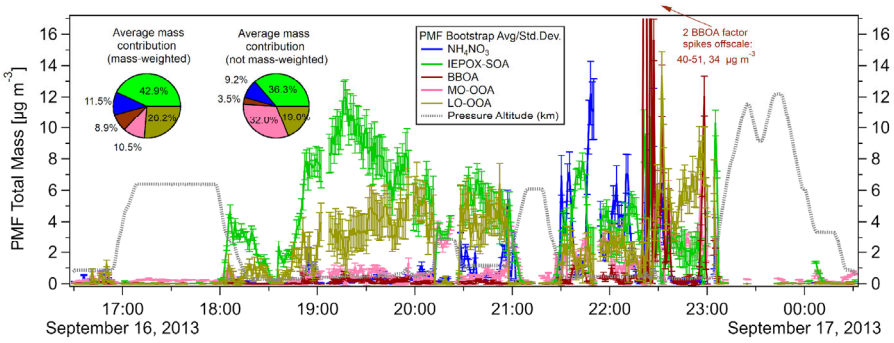

Figure S26. Time series of PMF factors (total signal, OA + nitrate) for SEAC[4]RS RF18 (FPEAK = -0.1). Averages and standard deviations for each point in the time series as well as the all-flight averages (shown as pies) were computed from 100 bootstrapping runs.

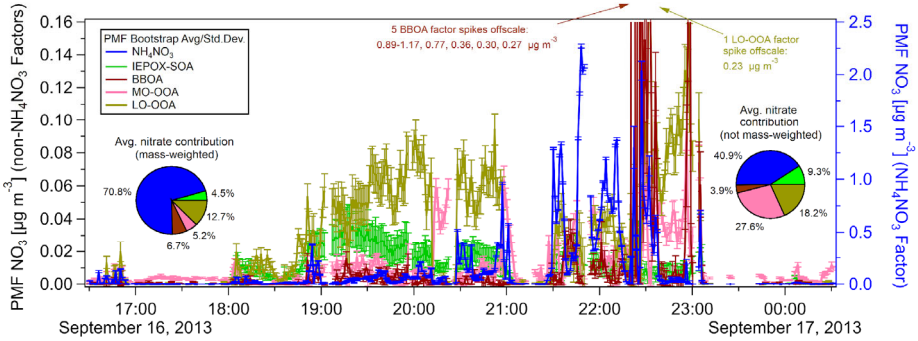

Figure S27. Time series of nitrate component of PMF factor for SEAC[4]RS RF18 (FPEAK = -0.1). Averages and standard deviations for each point in the time series as well as the all-flight averages (shown as pies) were computed from 100 bootstrapping runs. For aircraft sampling altitude see Fig. S26.

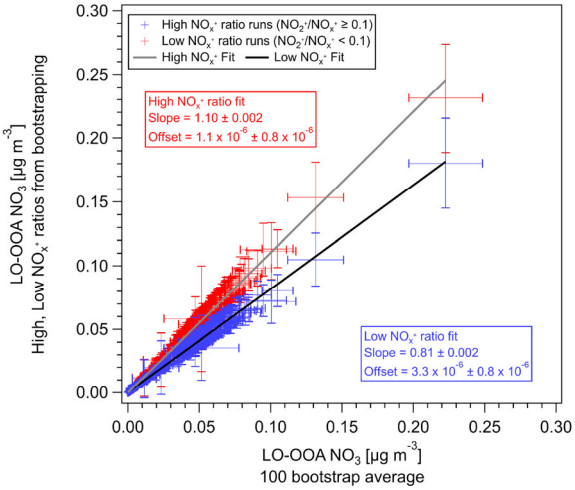

Figure S28. Nitrate concentrations apportioned to the PMF LO-OOA factor for different ranges of NO_x^+ ratios (in the factor spectra) vs the average of all runs for 100 bootstrapping runs (SEAC[4]RS RF18). The averages and standard deviations for the different subsets are shown for each time point.

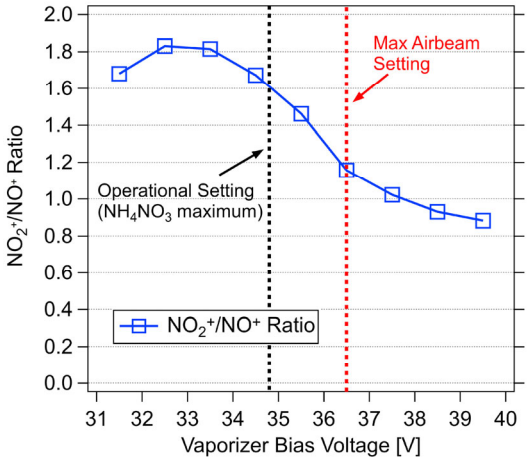

Figure S29. NO_x^+ ratio vs vaporizer bias voltage while sampling pure NH_4NO_3 particles. In this example the particle signal and airbeam signal (N_2^+) are not coincident; however, this is not always the case. In other cases, we have observed NO_x^+ ratio minima near the particle signal maxima and increasing with higher and lower vaporizer bias. Similar trends and magnitude of the NO_x^+ ratio (i.e., *m/z* 30 / *m/z* 46) changes vs vaporizer bias has been observed for the ACSMs (Jayne et al., 2015; slide 21).

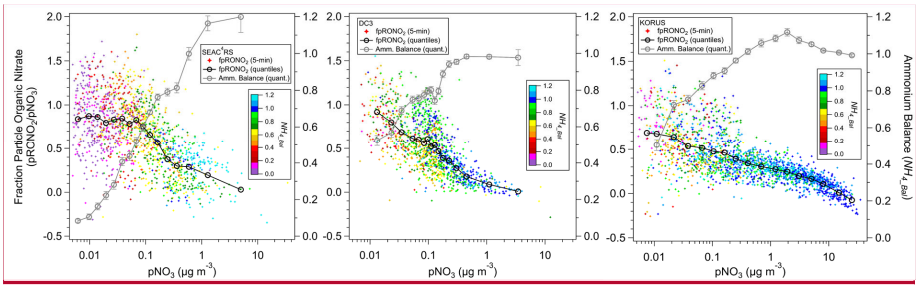

Figure S30. f_{pRONO2} vs. pNO_3 for aircraft campaigns (5-min, quantile averages). 5-min f_{pRONO2} is colored by ammonium balance (NH_{4_Bal}, molar ion charge ratio of NH_4^+ to NO_3^- + SO_4^{2-}) and quantile averages and standard errors of NH_{4_Bal} are also shown. At lower pNO_3, NH_{4_Bal} was much lower for SEAC[4]RS compared to the other campaigns, while DC3 was slightly lower than for KORUS.

Commented [15]: New versions replacing AMTD preprint versions, now showing standard errors for the ammonium balance quantiles and minor update to fPRONO2 binning for KORUS-AQ.

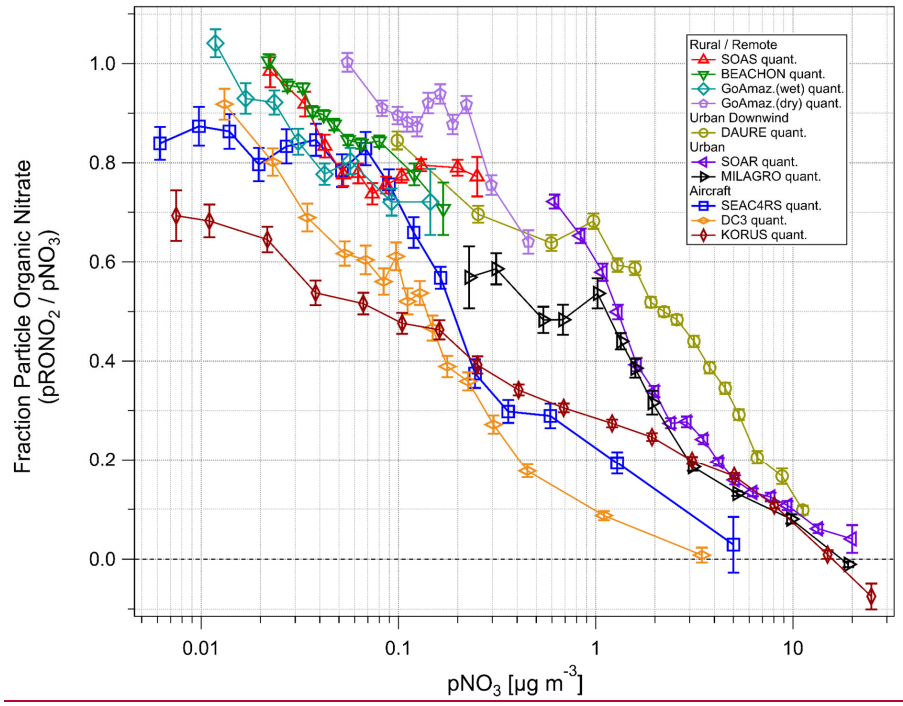

Figure S31. Same as Fig. 5 except that non-binned data are not shown, standard errors are shown as traditional error bars, gridlines are added, and it is slightly zoomed.

Supplementary References

Aiken, A. C., Decarlo, P. F., Kroll, J. H., Worsnop, D. R., Huffman, J. A., Docherty, K. S., Ulbrich, I. M., Mohr, C., Kimmel, J. R., Sueper, D., Sun, Y., Zhang, Q., Trimborn, A., Northway, M., Ziemann, P. J., Canagaratna, M. R., Onasch, T. B., Alfarra, M. R., Prevot, A. S. H., Dommen, J., Duplissy, J., Metzger, A., Baltensperger, U. and Jimenez, J. L.: O/C and OM/OC Ratios of Primary, Secondary, and Ambient Organic Aerosols with High-Resolution Time-of-Flight Aerosol Mass Spectrometry, Environ. Sci. Technol., 42(12), 4478–4485, 2008.

Aiken, A. C., Salcedo, D., Cubison, M. J., Huffman, J. A., DeCarlo, P. F., Ulbrich, I. M., Docherty, K. S., Sueper, D., Kimmel, J. R., Worsnop, D. R., Trimborn, A., Northway, M., Stone, E. A., Schauer, J. J., Volkamer, R. M., Fortner, E., de Foy, B., Wang, J., Laskin, A., Shutthanandan, V., Zheng, J., Zhang, R., Gaffney, J., Marley, N. A., Paredes-Miranda, G., Arnott, W. P., Molina, L. T., Sosa, G. and Jimenez, J. L.: Mexico City aerosol analysis during MILAGRO using high resolution aerosol mass spectrometry at the urban supersite (T0) – Part 1: Fine particle composition and organic source apportionment, Atmos. Chem. Phys., 9(17), 6633–6653, 2009.

Aiken, A. C., De Foy, B., Wiedinmyer, C., Decarlo, P. F., Ulbrich, I. M., Wehrli, M. N., Szidat, S., Prevot, A. S. H., Noda, J., Wacker, L., Volkamer, R., Fortner, E., Wang, J., Laskin, A., Shutthanandan, V., Zheng, J., Zhang, R., Paredes-Miranda, G., Arnott, W. P., Molina, L. T., Sosa, G., Querol, X., Jimenez, J. L., Prévôt, a. S. H., Noda, J., Wacker, L., Volkamer, R., Fortner, E., Wang, J., Laskin, A., Shutthanandan, V., Zheng, J., Zhang, R., Paredes-Miranda, G., Arnott, W. P., Molina, L. T., Sosa, G., Querol, X. and Jimenez, J. L.: Mexico city aerosol analysis during MILAGRO using high resolution aerosol mass spectrometry at the urban supersite (T0)-Part 2: Analysis of the biomass burning contribution and the non-fossil carbon fraction, Atmos. Chem. Phys., 10(12), 5315–5341, 2010.

Alfarra, M. R.: Insights into atmospheric organic aerosols using an aerosol mass spectrometer, PhD Thesis, University of Manchester Institute of Science and Technology., 2004.

Alfarra, M. R., Paulsen, D., Gysel, M., Garforth, A. a., Dommen, J., Prévôt, a. S. H., Worsnop, D. R., Baltensperger, U. and Coe, H.: A mass spectrometric study of secondary organic aerosols formed from the photooxidation of anthropogenic and biogenic precursors in a reaction chamber, Atmos. Chem. Phys., 6, 5279–5293, 2006.

Ayres, B. R., Allen, H. M., Draper, D. C., Brown, S. S., Wild, R. J., Jimenez, J. L., Day, D. A., Campuzano-Jost, P., Hu, W., de Gouw, J., Koss, A., Cohen, R. C., Duffey, K. C., Romer, P., Baumann, K., Edgerton, E., Takahama, S., Thornton, J. A., Lee, B. H. H., Lopez-Hilfiker, F. D., Mohr, C., Wennberg, P. O., Nguyen, T. B., Teng, A., Goldstein, A. H., Olson, K. and Fry, J. L.: Organic nitrate aerosol formation via NO_3 + biogenic volatile organic compounds in the southeastern United States, Atmos. Chem. Phys., 15(23), 13377–13392, 2015.

Bahreini, R., Ervens, B., Middlebrook, A. M., Warneke, C., De Gouw, J. A., DeCarlo, P. F., Jimenez, J. L., Brock, C. A., Neuman, J. A., Ryerson, T. B., Stark, H., Atlas, E., Brioude, J., Fried, A., Holloway, J. S., Peischl, J., Richter, D., Walega, J., Weibring, P., Wollny, a. G., Fehsenfeid, F. C. and Fehsenfeld, F. C.: Organic aerosol formation in urban and industrial plumes near Houston and Dallas, Texas, J. Geophys. Res., 114(16), D00F16–D00F16, 2009.

Barth, M. C., Cantrell, C. A., Brune, W. H., Rutledge, S. A., Crawford, J. H., Huntrieser, H., Carey, L. D., MacGorman, D., Weisman, M., Pickering, K. E., Bruning, E., Anderson, B., Apel, E., Biggerstaff, M., Campos, T., Campuzano-Jost, P., Cohen, R., Crounse, J., Day, D. A., Diskin, G., Flocke, F., Fried, A., Garland, C., Heikes, B., Honomichl, S., Hornbrook, R., Huey, L. G., Jimenez, J. L., Lang, T., Lichtenstern, M., Mikoviny, T., Nault, B., O'Sullivan, D., Pan, L. L., Peischl, J., Pollack, I., Richter, D.,

Riemer, D., Ryerson, T., Schlager, H., Clair, J. S., Walega, J., Weibring, P., Weinheimer, A., Wennberg, P., Wisthaler, A., Wooldridge, P. J. and Ziegler, C.: The deep convective clouds and chemistry (DC3) field campaign, Bull. Am. Meteorol. Soc., 96(August), 1281–1309, 2015.

Boyd, C. M., Sanchez, J., Xu, L., Eugene, a. J., Nah, T., Tuet, W. Y., Guzman, M. I. and Ng, N. L.: Secondary organic aerosol formation from the β-pinene+NO_3 system: effect of humidity and peroxy radical fate, Atmos. Chem. Phys., 15(13), 7497–7522, 2015.

Bruns, E. A., Perraud, V., Zelenyuk, A., Ezell, M. J., Johnson, S. N., Yu, Y., Imre, D., Finlayson-Pitts, B. J., Alexander, M. L., Bruns, A. E., Perraud, V., Zelenyuk, A., Ezell, M. J., Johnson, S. N., Yu, Y., Imre, D., Finlayson-Pitts, B. J. and Alexander, M. L.: Comparison of FTIR and particle mass spectrometry for the measurement of particulate organic nitrates, Environ. Sci. Technol., 44(3), 1056–1061, 2010.

Canagaratna, M. R., Jimenez, J. L., Kroll, J. H., Chen, Q., Kessler, S. H., Massoli, P., Hildebrandt Ruiz, L., Fortner, E., Williams, L. R., Wilson, K. R., Surratt, J. D., Donahue, N. M., Jayne, J. T., Worsnop, D. R., Ruiz, L. H., Hildebrandt Ruiz, L., Fortner, E., Williams, L. R., Wilson, K. R., Surratt, J. D., Donahue, N. M., Jayne, J. T., Worsnop, D. R., Attribution, C. C., Canagaratna, M. R., Canagaratna, M. R., Jimenez, J. L., Kroll, J. H., Chen, Q., Kessler, S. H., Massoli, P., Hildebrandt Ruiz, L., Fortner, E., Williams, L. R., Wilson, K. R., Surratt, J. D., Donahue, N. M., Jayne, J. T. and Worsnop, D. R.: Elemental ratio measurements of organic compounds using aerosol mass spectrometry: characterization, improved calibration, and implications, Atmos. Chem. Phys., 15(1), 253–272, 2015.

Canonaco, F., Crippa, M., Slowik, J. G., Baltensperger, U. and Prévôt, A. S. H.: Atmos. Meas. Tech.SoFi, an IGOR-based interface for the efficient use of the generalized multilinear engine (ME-2) for the source apportionment: ME-2 application to aerosol mass spectrometer data, Atmos. Meas. Tech., 6(12), 3649–3661, 2013.

Carlton, A. G., de Gouw, J., Jimenez, J. L., Ambrose, J. L., Attwood, A. R., Brown, S., Baker, K. R., Brock, C., Cohen, R. C., Edgerton, S., Farkas, C. M., Farmer, D., Goldstein, A. H., Gratz, L., Guenther, A., Hunt, S., Jaeglé, L., Jaffe, D. A., Mak, J., McClure, C., Nenes, A., Nguyen, T. K., Pierce, J. R., de Sa, S., Selin, N. E., Shah, V., Shaw, S., Shepson, P. B., Song, S., Stutz, J., Surratt, J. D., Turpin, B. J., Warneke, C., Washenfelder, R. A., Wennberg, P. O. and Zhou, X.: Synthesis of the Southeast Atmosphere Studies: Investigating Fundamental Atmospheric Chemistry Questions, Bull. Am. Meteorol. Soc., 99(3), 547–567, 2018.

Chen, Y., Takeuchi, M., Nah, T., Xu, L., Canagaratna, M. R., Stark, H., Baumann, K., Canonaco, F., Prévôt, A. S. H., Gregory Huey, L., Weber, R. J. and Ng, N. L.: Chemical characterization of secondary organic aerosol at a rural site in the southeastern US: insights from simultaneous high-resolution time-of-flight aerosol mass spectrometer (HR-ToF-AMS) and FIGAERO chemical ionization mass spectrometer (CIMS) measurements, Atmospheric Chemistry and Physics, 20(14), 8421–8440, doi:10.5194/acp-20-8421-2020, 2020.

Cubison, M. J. and Jimenez, J. L.: Statistical precision of the intensities retrieved from constrained fitting of overlapping peaks in high-resolution mass spectra, Atmos. Meas. Tech., 8(6), 2333–2345, 2015.

DeCarlo, P. F., Kimmel, J. R., Trimborn, A., Northway, M. J., Jayne, J. T., Aiken, A. C., Gonin, M., Fuhrer, K., Horvath, T., Docherty, K. S., Worsnop, D. R. and Jimenez, J. L.: Field-Deployable, High-Resolution, Time-of-Flight Aerosol Mass Spectrometer, Anal. Chem., 78(24), 8281–8289, 2006.

Docherty, K. S., Aiken, A. C., Huffman, J. A., Ulbrich, I. M., DeCarlo, P. F., Sueper, D., Worsnop, D. R., Snyder, D. C., Peltier, R. E., Weber, R. J., Grover, B. D., Eatough, D. J., Williams, B. J., Goldstein, A. H., Ziemann, P. J. and Jimenez, J. L.: The 2005 Study of Organic Aerosols at Riverside (SOAR-1):

instrumental intercomparisons and fine particle composition, Atmos. Chem. Phys., 11(23), 12387–12420, 2011.

Drewnick, F., Diesch, J.-M., Faber, P. and Borrmann, S.: Aerosol mass spectrometry: particle–vaporizer interactions and their consequences for the measurements, Atmos. Meas. Tech., 8(9), 3811–3830, 2015.

Eris, G., Takeuchi, M., Wood, E. C., Tanner, D. J., Huey, L. G. and Ng, N. L.: Characterization of Thermal Dissociation Cavity Attenuated Phase Shift Spectroscopy (TD-CAPS) for Total Gas-Phase and Particle-Phase Alkyl Nitrates and Peroxy Nitrates Measurements, p. Conference abstract 11IM.6–Conference abstract 11IM.6., 2018.

Farmer, D. K., Matsunaga, A., Docherty, K. S., Surratt, J. D., Seinfeld, J. H., Ziemann, P. J. and Jimenez, J. L.: Response of an aerosol mass spectrometer to organonitrates and organosulfates and implications for atmospheric chemistry, Proceedings of the National Academy of Sciences, 107(15), 6670–6675, 2010.

Fisher, J. A., Jacob, D. J., Travis, K. R., Kim, P. S., Marais, E. A., Chan Miller, C., Yu, K., Zhu, L., Yantosca, R. M., Sulprizio, M. P., Mao, J., Wennberg, P. O., Crounse, J. D., Teng, A. P., Nguyen, T. B., St. Clair, J. M., Cohen, R. C., Romer, P., Nault, B. A., Wooldridge, P. J., Jimenez, J. L., Campuzano-Jost, P., Day, D. A., Hu, W., Shepson, P. B., Xiong, F., Blake, D. R., Goldstein, A. H., Misztal, P. K., Hanisco, T. F., Wolfe, G. M., Ryerson, T. B., Wisthaler, A. and Mikoviny, T.: Organic nitrate chemistry and its implications for nitrogen budgets in an isoprene- and monoterpene-rich atmosphere: constraints from aircraft (SEAC^{4}RS) and ground-based (SOAS) observations in the Southeast US, Atmos. Chem. Phys., 16(9), 5969–5991, 2016.

Fry, J. L., Kiendler-Scharr, A., Rollins, A. W., Wooldridge, P. J., Brown, S. S., Fuchs, H., Dubé, W., Mensah, A., dal Maso, M., Tillmann, R., Dorn, H.-P., Brauers, T. and Cohen, R. C.: Organic nitrate and secondary organic aerosol yield from NO_3 oxidation of β-pinene evaluated using a gas-phase kinetics/aerosol partitioning model, Atmos. Chem. Phys., 9(4), 1431–1449, 2009.

Fry, J. L., Kiendler-Scharr, A., Rollins, A. W., Brauers, T., Brown, S. S., Dorn, H.-P., Dubé, W. P., Fuchs, H., Mensah, A., Rohrer, F., Tillmann, R., Wahner, A., Wooldridge, P. J., Cohen, R. C. and Dube, W.: SOA from limonene: role of NO_3 in its generation and degradation, Atmos. Chem. Phys., 11(8), 3879–3894, 2011.

Fry, J. L., Draper, D. C., Zarzana, K. J., Campuzano-Jost, P., Day, D. A., Jimenez, J. L., Brown, S. S., Cohen, R. C., Kaser, L., Hansel, A., Cappellin, L., Karl, T., Hodzic Roux, A., Turnipseed, A., Cantrell, C., Lefer, B. L. and Grossberg, N.: Observations of gas- and aerosol-phase organic nitrates at BEACHON-RoMBAS 2011, Atmos. Chem. Phys., 13(17), 8585–8605, 2013.

Hao, L. Q., Kortelainen, A., Romakkaniemi, S., Portin, H., Jaatinen, A., Leskinen, A., Komppula, M., Miettinen, P., Sueper, D., Pajunoja, A., Smith, J. N., Lehtinen, K. E. J., Worsnop, D. R., Laaksonen, A. and Virtanen, A.: Atmospheric submicron aerosol composition and particulate organic nitrate formation in a boreal forestland–urban mixed region, Atmos. Chem. Phys., 14(24), 13483–13495, 2014.

Huang, W., Saathoff, H., Shen, X., Ramisetty, R., Leisner, T. and Mohr, C.: Chemical Characterization of Highly Functionalized Organonitrates Contributing to Night-time Organic Aerosol Mass Loadings and Particle Growth, Environ. Sci. Technol., 53(3), acs.est.8b05826–acs.est.8b05826, 2019.

Hu, W., Palm, B. B., Day, D. A., Campuzano-Jost, P., Krechmer, J. E., Peng, Z., de Sá, S. S., Martin, S. T., Alexander, M. L. L., Baumann, K., Hacker, L., Kiendler-Scharr, A., Koss, A. R., de Gouw, J. A., Goldstein, A. H., Seco, R., Sjostedt, S. J., Park, J.-H., Guenther, A. B., Kim, S., Canonaco, F., Prévôt, A. S. H., Brune, W. H. and Jimenez, J. L.: Volatility and lifetime against OH heterogeneous reaction of

ambient isoprene-epoxydiols-derived secondary organic aerosol (IEPOX-SOA), Atmos. Chem. Phys., 16(18), 11563–11580, 2016.

Hu, W., Campuzano-Jost, P., Day, D. A., Croteau, P., Canagaratna, M. R., Jayne, J. T., Worsnop, D. R. and Jimenez, J. L.: Evaluation of the new capture vapourizer for aerosol mass spectrometers (AMS) through laboratory studies of inorganic species, Atmos. Meas. Tech., 10(6), 2897–2921, 2017.

Jayne, J. T., Croteau, P. L., Lambe, A. T., Xu, W., Onasch, T. B., Wolff, L. and Canagaratna, M. R.: Investigation of f44 variability in AMS and ACSM instruments, in 16th Aerosol Mass Spectrometer Users' Meeting, Milan, Italy. [online] Available from: http://cires1.colorado.edu/jimenez-group/UsrMtgs/UsersMtg16/Jayne_f44Intro.pdf (Accessed 11 August 2021), 2015.

Jimenez, J. L., Canagaratna, M. R., Drewnick, F., Allan, J. D., Alfarra, M. R., Middlebrook, A. M., Slowik, J. G., Zhang, Q., Coe, H., Jayne, J. T. and Worsnop, D. R.: Comment on "The effects of molecular weight and thermal decomposition on the sensitivity of a thermal desorption aerosol mass spectrometer," Aerosol Sci. Technol., 50(9), i–xv, 2016.

Joo, T., Rivera-Rios, J. C., Takeuchi, M., Alvarado, M. J. and Ng, N. L.: Secondary Organic Aerosol Formation from Reaction of 3-Methylfuran with Nitrate Radicals, ACS Earth and Space Chemistry, 3(6), acsearthspacechem.9b00068–acsearthspacechem.9b00068, 2019.

Kang, H., Day, D. A., Krechmer, J. E., Ayres, B. R., Keehan, N. I., Thompson, S., Hu, W., Campuzano-Jost, P., Schroder, J. C., Stark, H., Ranney, A., Ziemann, P. J., Zarzana, K. J., Wild, R. J., Dube, W. P., Brown, S. S., Fry, J. L. and Jimenez, J. L.: Secondary organic aerosol mass yields from the dark NO_3 oxidation of α-pinene and Δ-carene: effect of RO_2 radical fate, in American Geophysical Union Fall Meeting, San Francisco. [online] Available from: https://agu.confex.com/agu/fm16/meetingapp.cgi/Paper/135842 (Accessed 11 August, 2021), 2016.

Keehan, N. I., Brownwood, B., Marsavin, A., Day, D. A. and Fry, J. L.: A thermal-dissociation–cavity ring-down spectrometer (TD-CRDS) for the detection of organic nitrates in gas and particle phases, Atmos. Meas. Tech., 13(11), 6255–6269, 2020.

Kenagy, H. S., Romer, P. S., Wooldridge, P. J., Nault, B. A., Campuzano-Jost, P., Day, D. A., Jimenez, J. L., Zare, A., Pye, H. O. T., Yu, J., Song, C. H., Blake, D. R., Woo, J.-H., Kim, Y. and Cohen, R. C.: Contribution of organic nitrates to organic aerosol over South Korea during KORUS-AQ, In Prep., 2021.

Kiendler-Scharr, A., Mensah, A. A., Friese, E., Topping, D., Nemitz, E., Prevot, A. S. H., Äijälä, M., Allan, J., Canonaco, F., Canagaratna, M., Carbone, S., Crippa, M., Dall Osto, M., Day, D. A., DeCarlo, P., Di Marco, C. F., Elbern, H., Eriksson, A., Freney, E., Hao, L., Herrmann, H., Hildebrandt, L., Hillamo, R., Jimenez, J. L., Laaksonen, A., McFiggans, G., Mohr, C., O'Dowd, C., Otjes, R., Ovadnevaite, J., Pandis, S. N., Poulain, L., Schlag, P., Sellegri, K., Swietlicki, E., Tiitta, P., Vermeulen, A., Wahner, A., Worsnop, D. and Wu, H.-C.: Organic nitrates from night-time chemistry are ubiquitous in the European submicron aerosol, Geophys. Res. Lett., 43(14), 7735–7744, 2016.

Kim, H., Zhang, Q. and Heo, J.: Influence of intense secondary aerosol formation and long-range transport on aerosol chemistry and properties in the Seoul Metropolitan Area during spring time: Results from KORUS-AQ, Atmos. Chem. Phys., 18(10), 7149–7168, 2018.

Kimmel, J. R., Farmer, D. K., Cubison, M. J., Sueper, D., Tanner, C., Nemitz, E., Worsnop, D. R., Gonin, M. and Jimenez, J. L.: Real-time aerosol mass spectrometry with millisecond resolution, Int. J. Mass Spectrom., 303(1), 15–26, 2011.

Kortelainen, A., Hao, L., Tiitta, P., Jaatinen, A., Miettinen, P., Kulmala, M., Smith, J. N., Laaksonen, A., Worsnop, D. R. and Virtanen, A.: Sources of particulate organic nitrates in the boreal forest in Finland, Boreal Environ. Res., 22, 13–26, 2017.

Kostenidou, E., Florou, K., Kaltsonoudis, C., Tsiflikiotou, M., Vratolis, S., Eleftheriadis, K. and Pandis, S. N.: Sources and chemical characterization of organic aerosol during the summer in the eastern Mediterranean, Atmos. Chem. Phys., 15(19), 11355–11371, 2015.

Krechmer, J. E., Day, D. A., Ziemann, P. J. and Jimenez, J. L.: Direct Measurements of Gas/Particle Partitioning and Mass Accommodation Coefficients in Environmental Chambers, Environ. Sci. Technol., 51(20), 11867–11875, 2017.

Lee, B. H., Mohr, C., Lopez-Hilfiker, F. D., Lutz, A., Hallquist, M., Lee, L., Romer, P., Cohen, R. C., Iyer, S., Kurtén, T., Hu, W., Day, D. A., Campuzano-Jost, P., Jimenez, J. L., Xu, L., Ng, N. L., Guo, H., Weber, R. J., Wild, R. J., Brown, S. S., Koss, A., de Gouw, J., Olson, K., Goldstein, A. H., Seco, R., Kim, S., McAvey, K., Shepson, P. B., Starn, T., Baumann, K., Edgerton, E. S., Liu, J., Shilling, J. E., Miller, D. O., Brune, W., Schobesberger, S., D'Ambro, E. L. and Thornton, J. A.: Highly functionalized organic nitrates in the southeast U.S.: Contribution to secondary organic aerosol and reactive nitrogen budgets, Proc. Natl. Acad. Sci., 113(6), 1516–1521, 2016.

Lin, C., Huang, R.-J., Duan, J., Zhong, H. and Xu, W.: Primary and Secondary Organic Nitrate in Northwest China: A Case Study, Environmental Science & Technology Letters, doi:10.1021/acs.estlett.1c00692, 2021.

Liu, S., Shilling, J. E., Song, C., Hiranuma, N., Zaveri, R. A. and Russell, L. M.: Hydrolysis of Organonitrate Functional Groups in Aerosol Particles, Aerosol Sci. Technol., 46(12), 1359–1369, 2012.

Liu, X., Day, D. A., Krechmer, J. E., Brown, W., Peng, Z., Ziemann, P. J. and Jimenez, J. L.: Direct measurements of semi-volatile organic compound dynamics show near-unity mass accommodation coefficients for diverse aerosols, Commun. Chem., 2(98), 1–9, 2019.

Martin, S. T., Artaxo, P., Machado, L. A. T., Manzi, A. O., Souza, R. A. F., Schumacher, C., Wang, J., Andreae, M. O., Barbosa, H. M. J., Fan, J., Fisch, G., Goldstein, A. H., Guenther, A., Jimenez, J. L., Pöschl, U., Silva Dias, M. A., Smith, J. N. and Wendisch, M.: Introduction: Observations and Modeling of the Green Ocean Amazon (GoAmazon2014/5), Atmos. Chem. Phys., 16(8), 4785–4797, 2016.

Martin, S. T., Artaxo, P., Machado, L., Manzi, A. O., Souza, R. A. F., Schumacher, C., Wang, J., Biscaro, T., Brito, J., Calheiros, A., Jardine, K., Medeiros, A., Portela, B., de Sá, S. S., Adachi, K., Aiken, A. C., Albrecht, R., Alexander, L., Andreae, M. O., Barbosa, H. M. J., Buseck, P., Chand, D., Comstock, J. M., Day, D. A., Dubey, M., Fan, J., Fast, J., Fisch, G., Fortner, E., Giangrande, S., Gilles, M., Goldstein, A. H., Guenther, A., Hubbe, J., Jensen, M., Jimenez, J. L., Keutsch, F. N., Kim, S., Kuang, C., Laskin, A., McKinney, K., Mei, F., Miller, M., Nascimento, R., Pauliquevis, T., Pekour, M., Peres, J., Petäjä, T., Pöhlker, C., Pöschl, U., Rizzo, L., Schmid, B., Shilling, J. E., Silva Dias, M. A., Smith, J. N., Tomlinson, J. M., Tóta, J. and Wendisch, M.: The green ocean amazon experiment (GOAMAZON2014/5) observes pollution affecting gases, aerosols, clouds, and rainfall over the rain forest, Bull. Am. Meteorol. Soc., 98(5), 981–997, 2017.

Middlebrook, A. M., Bahreini, R., Jimenez, J. L. and Canagaratna, M. R.: Evaluation of Composition-Dependent Collection Efficiencies for the Aerodyne Aerosol Mass Spectrometer using Field Data, Aerosol Sci. Technol., 46(3), 258–271, 2012.

Minguillon´, M. C., Perron, N., Querol, X., Szidat, S., Fahrni, S. M., Alastuey, A., Jimenez, J. L., Mohr, C., Ortega, A. M., Day, D. A., Lanz, V. A., Wacker, L., Reche, C., Cusack, M., Amato, F., Kiss, G., Hoffer, A., Decesari, S., Moretti, F., Hillamo, R., Teinila, K., Seco, R., Penuelas, J., Metzger, A., Schallhart, S., Muller, M., Hansel, A., Burkhart, J. F., Baltensperger, U. and Prevot, A. S. H.: Fossil versus contemporary sources of fine elemental and organic carbonaceous particulate matter during the DAURE campaign in Northeast Spain, Atmos. Chem. Phys., 11(23), 12067–12084, 2011.

Molina, L. T., Madronich, S., Gaffney, J. S., Apel, E., de Foy, B., Fast, J., Ferrare, R., Herndon, S., Jimenez, J. L., Lamb, B., Osornio-Vargas, A. R., Russell, P., Schauer, J. J., Stevens, P. S., Volkamer, R. and Zavala, M.: An overview of the MILAGRO 2006 Campaign: Mexico City emissions and their transport and transformation, Atmos. Chem. Phys., 10(18), 8697–8760, 2010.

Nault, B. A., Garland, C., Wooldridge, P. J., Brune, W. H., Campuzano-Jost, P., Crounse, J. D., Day, D. A., Dibb, J., Hall, S. R., Huey, L. G., Jimenez, J. L., Liu, X., Mao, J., Mikoviny, T., Peischl, J., Pollack, I. B., Ren, X., Ryerson, T. B., Scheuer, E., Ullmann, K., Wennberg, P. O., Wisthaler, A., Zhang, L. and Cohen, R. C.: Observational Constraints on the Oxidation of NO_x in the Upper Troposphere, J. Phys. Chem. A, 120(9), doi:10.1021/acs.jpca.5b07824, 2016.

Nault, B. A., Campuzano-Jost, P., Day, D. A., Schroder, J. C., Anderson, B., Beyersdorf, A. J., Blake, D. R., Brune, W. H., Choi, Y., Corr, C. A., de Gouw, J. A., Dibb, J., DiGangi, J. P., Diskin, G. S., Fried, A., Huey, L. G., Kim, M. J., Knote, C. J., Lamb, K. D., Lee, T., Park, T., Pusede, S. E., Scheuer, E., Thornhill, K. L., Woo, J.-H. and Jimenez, J. L.: Secondary organic aerosol production from local emissions dominates the organic aerosol budget over Seoul, South Korea, during KORUS-AQ, Atmos. Chem. Phys., 18(24), 17769–17800, 2018.

Ortega, J., Turnipseed, A., Guenther, A. B., Karl, T. G., Day, D. A., Gochis, D., Huffman, J. A., Prenni, A. J., Levin, E. J. T., Kreidenweis, S. M., DeMott, P. J., Tobo, Y., Patton, E. G., Hodzic, A., Cui, Y. Y., Harley, P. C., Hornbrook, R. S., Apel, E. C., Monson, R. K., Eller, A. S. D., Greenberg, J. P., Barth, M. C., Campuzano-Jost, P., Palm, B. B., Jimenez, J. L., Aiken, A. C., Dubey, M. K., Geron, C., Offenberg, J., Ryan, M. G., Fornwalt, P. J., Pryor, S. C., Keutsch, F. N., Digangi, J. P., Chan, A. W. H., Goldstein, A. H., Wolfe, G. M., Kim, S., Kaser, L., Schnitzhofer, R., Hansel, A., Cantrell, C. A., Mauldin, R. L. and Smith, J. N.: Overview of the Manitou experimental forest observatory: Site description and selected science results from 2008 to 2013, Atmos. Chem. Phys., 14(12), 6345–6367, 2014.

Paatero, P.: The Multilinear Engine: A Table-Driven, Least Squares Program for Solving Multilinear Problems, including the n-Way Parallel Factor Analysis Model, J. Comput. Graph. Stat., 8(4), 854–854, 1999.

Pagonis, D., Campuzano-Jost, P., Guo, H., Day, D. A., Schueneman, M. K., Brown, W. L., Nault, B. A., Stark, H., Siemens, K., Laskin, A., Piel, F., Tomsche, L., Wisthaler, A., Coggon, M. M., Gkatzelis, G. I., Halliday, H. S., Krechmer, J. E., Moore, R. H., Thomson, D. S., Warneke, C., Wiggins, E. B. and Jimenez, J. L.: Airborne extractive electrospray mass spectrometry measurements of the chemical composition of organic aerosol, Atmos. Chem. Phys., 14(2), 1545–1559, 2021.

Palm, B. B., Campuzano-Jost, P., Day, D. A., Ortega, A. M., Fry, J. L., Brown, S. S., Zarzana, K. J., Dube, W., Wagner, N. L., Draper, D. C., Kaser, L., Jud, W., Karl, T., Hansel, A., Gutiérrez-Montes, C. and Jimenez, J. L.: Secondary organic aerosol formation from in situ OH, O_3, and NO_3 oxidation of ambient forest air in an oxidation flow reactor, Atmos. Chem. Phys., 17(8), 5331–5354, 2017.

Palm, B. B., de Sá, S. S., Day, D. A., Campuzano-Jost, P., Hu, W., Seco, R., Sjostedt, S. J., Park, J.-H., Guenther, A. B., Kim, S., Brito, J., Wurm, F., Artaxo, P., Thalman, R., Wang, J., Yee, L. D., Wernis, R., Isaacman-VanWertz, G., Goldstein, A. H., Liu, Y., Springston, S. R., Souza, R., Newburn, M. K.,

Alexander, M. L., Martin, S. T. and Jimenez, J. L.: Secondary organic aerosol formation from ambient air in an oxidation flow reactor in central Amazonia, Atmos. Chem. Phys., 18(1), 467–493, 2018.

Pandolfi, M., Querol, X., Alastuey, A., Jimenez, J. L., Jorba, O., Day, D. A., Ortega, A., Cubison, M. J., Comerón, A., Sicard, M., Mohr, C., Prévôt, A. S. H., Minguillón, M. C., Pey, J., Baldasano, J. M., Burkhart, J. F., Seco, R., Peñuelas, J., Van Drooge, B. L., Artiñano, B., Di Marco, C., Nemitz, E., Schallhart, S., Metzger, A., Hansel, A., Llorente, J., Ng, S., Jayne, J. and Szidat, S.: Effects of sources and meteorology on particulate matter in the Western Mediterranean Basin: An overview of the DAURE campaign, J. Geophys. Res. D: Atmos., 119(8), 4978–5010, 2014.

Paul, D., Furgeson, A. and Osthoff, H. D.: Measurements of total peroxy and alkyl nitrate abundances in laboratory-generated gas samples by thermal dissociation cavity ring-down spectroscopy, Rev. Sci. Instrum., 80(11), 114101–114101, 2009.

Reyes-Villegas, E., Priestley, M., Ting, Y.-C., Haslett, S., Bannan, T., Le Breton, M., Williams, P. I., Bacak, A., Flynn, M. J., Coe, H., Percival, C., Allan, J. D., Breton, M. L., Attribution, Creative Commons, Reyes-Villegas, E., Reyes-Villegas, E. and By, C. C.: Simultaneous aerosol mass spectrometry and chemical ionisation mass spectrometry measurements during a biomass burning event in the UK : insights into nitrate chemistry, Atmos. Chem. Phys., 18(6), 4093–4111, 2018.

Rollins, A. W., Kiendler-Scharr, A., Fry, J. L., Brauers, T., Brown, S. S., Dorn, H.-P., Dubé, W. P., Fuchs, H., Mensah, A., Mentel, T. F., Rohrer, F., Tilmann, R., Wegener, R., Wooldridge, P. J. and Cohen, R. C.: Isoprene oxidation by nitrate radical: alkyl nitrate and secondary organic aerosol yields, Atmos. Chem. Phys., 9, 6685–6703, 2009.

Rollins, A. W., Fry, J. L., Hunter, J. F., Kroll, J. H., Worsnop, D. R., Singaram, S. W. and Cohen, R. C.: Elemental analysis of aerosol organic nitrates with electron ionization high-resolution mass spectrometry, Atmos. Meas. Tech., 3(1), 301–310, 2010a.

Rollins, A. W., Smith, J. D., Wilson, K. R. and Cohen, R. C.: Real time in situ detection of organic nitrates in atmospheric aerosols, Environ. Sci. Technol., 44(14), 5540–5545, 2010b.

Rollins, A. W., Pusede, S., Wooldridge, P., Min, K.-E., Gentner, D. R., Goldstein, A. H., Liu, S., Day, D. A., Russell, L. M., Rubitschun, C. L., Surratt, J. D. and Cohen, R. C.: Gas/particle partitioning of total alkyl nitrates observed with TD-LIF in Bakersfield, J. Geophys. Res. D: Atmos., 118(12), 6651–6662, 2013.

de Sá, S. S., Palm, B. B., Campuzano-Jost, P., Day, D. A., Hu, W., Isaacman-VanWertz, G., Yee, L. D., Brito, J., Carbone, S., Ribeiro, I. O., Cirino, G. G., Liu, Y. J., Thalman, R., Sedlacek, A., Funk, A., Schumacher, C., Shilling, J. E., Schneider, J., Artaxo, P., Goldstein, A. H., Souza, R. A. F., Wang, J., McKinney, K. A., Barbosa, H., Alexander, M. L., Jimenez, J. L. and Martin, S. T.: Urban influence on the concentration and composition of submicron particulate matter in central Amazonia, Atmos. Chem. Phys., 18(16), 12185–12206, 2018.

de Sá, S. S., Rizzo, L. V., Palm, B. B., Campuzano-Jost, P., Day, D. A., Yee, L. D., Wernis, R., Isaacman-VanWertz, G., Brito, J., Carbone, S., Liu, Y. J., Sedlacek, A., Springston, S., Goldstein, A. H., Barbosa, H. M. J., Alexander, M. L., Artaxo, P., Jimenez, J. L. and Martin, S. T.: Contributions of biomass-burning, urban, and biogenic emissions to the concentrations and light-absorbing properties of particulate matter in central Amazonia during the dry season, Atmos. Chem. Phys., 19, 7973–8001, 2019.

Sato, K., Takami, A., Isozaki, T., Hikida, T., Shimono, A. and Imamura, T.: Mass spectrometric study of secondary organic aerosol formed from the photo-oxidation of aromatic hydrocarbons, Atmos. Environ., 44(8), 1080–1087, 2010.

Sato, K., Takami, A., Kato, Y., Seta, T., Fujitani, Y., Hikida, T., Shimono, A. and Imamura, T.: AMS and LC/MS analyses of SOA from the photooxidation of benzene and 1,3,5-trimethylbenzene in the presence of NO_x: effects of chemical structure on SOA aging, Atmos. Chem. Phys., 12(10), 4667–4682, 2012.

Schroder, J. C., Campuzano-Jost, P., Day, D. A., Shah, V., Larson, K., Sommers, J. M., Sullivan, A. P., Campos, T., Reeves, J. M., Hills, A., Hornbrook, R. S., Blake, N. J., Scheuer, E., Guo, H., Fibiger, D. L., McDuffie, E. E., Hayes, P. L., Weber, R. J., Dibb, J. E., Apel, E. C., Jaeglé, L., Brown, S. S., Thornton, J. A. and Jimenez, J. L.: Sources and Secondary Production of Organic Aerosols in the Northeastern United States during WINTER, J. Geophys. Res. D: Atmos., 123(14), 7771–7796, 2018.

Schwantes, R. H., Charan, S. M., Bates, K. H., Huang, Y., Nguyen, T. B., Mai, H., Kong, W., Flagan, R. C. and Seinfeld, J. H.: Low-volatility compounds contribute significantly to isoprene secondary organic aerosol (SOA) under high-NO_x conditions, Atmos. Chem. Phys., 19(11), 7255–7278, 2019.

Shingler, T., Crosbie, E., Ortega, A., Shiraiwa, M., Zuend, A., Beyersdorf, A., Ziemba, L., Anderson, B., Thornhill, L., Perring, A. E., Schwarz, J. P., Campazano-Jost, P., Day, D. A., Jimenez, J. L., Hair, J. W., Mikoviny, T., Wisthaler, A. and Sorooshian, A.: Airborne Characterization of Sub-saturated Aerosol Hygroscopicity and Dry Refractive Index from the Surface to 6.5 km during the SEAC4RS Campaign, J. Geophys. Res. D: Atmos., 121(8), 4188–4210, 2016.

Sueper, D.: ToF-AMS Data Analysis Software Webpage, [online] Available from: http://cires1.colorado.edu/jimenez-group/wiki/index.php/ToF-AMS_Analysis_Software (Accessed 11 August 2021), 2021.

Sun, Y. L., Zhang, Q., Schwab, J. J., Yang, T., Ng, N. L. and Demerjian, K. L.: Factor analysis of combined organic and inorganic aerosol mass spectra from high resolution aerosol mass spectrometer measurements, Atmos. Chem. Phys., 12(18), 8537–8551, 2012.

Takeuchi, M. and Ng, N. L.: Chemical composition and hydrolysis of organic nitrate aerosol formed from hydroxyl and nitrate radical oxidation of α-pinene and β-pinene, Atmos. Chem. Phys., 19(19), 12749–12766, 2019.

Thieser, J., Schuster, G., Schuladen, J., Phillips, G. J., Reiffs, A., Parchatka, U., Pöhler, D., Lelieveld, J. and Crowley, J. N.: A two-channel thermal dissociation cavity ring-down spectrometer for the detection of ambient NO_2, RO_2NO_2 and $RONO_2$, Atmos. Meas. Tech., 9(2), 553–576, 2016.

Tiitta, P., Leskinen, A., Hao, L., Yli-Pirilä, P., Kortelainen, M., Grigonyte, J., Tissari, J., Lamberg, H., Hartikainen, A., Kuuspalo, K., Kortelainen, A.-M. M., Virtanen, A., Lehtinen, K. E. J., Komppula, M., Pieber, S., Prévôt, A. S. H., Onasch, T. B., Worsnop, D. R., Czech, H., Zimmermann, R., Jokiniemi, J. and Sippula, O.: Transformation of logwood combustion emissions in a smog chamber: formation of secondary organic aerosol and changes in the primary organic aerosol upon daytime and nighttime aging, Atmos. Chem. Phys., 16(20), 13251–13269, 2016.

Toon, O. B., Maring, H., Dibb, J., Ferrare, R., Jacob, D. J., Jensen, E. J., Luo, Z. J., Mace, G. G., Pan, L. L., Pfister, L., Rosenlof, K. H., Redemann, J., Reid, J. S., Singh, H. B., Thompson, A. M., Yokelson, R., Minnis, P., Chen, G., Jucks, K. W. and Pszenny, A.: Planning, implementation, and scientific goals of the Studies of Emissions and Atmospheric Composition, Clouds and Climate Coupling by Regional Surveys (SEAC 4 RS) field mission, J. Geophys. Res. D: Atmos., 121(9), 4967–5009, 2016.

Ulbrich, I. M., Canagaratna, M. R., Zhang, Q., Worsnop, D. R. and Jimenez, J. L.: Interpretation of organic components from Positive Matrix Factorization of aerosol mass spectrometric data, Atmos. Chem. Phys., 9(9), 2891–2918, 2009.

Xu, L., Suresh, S., Guo, H., Weber, R. J. and Ng, N. L.: Aerosol characterization over the southeastern United States using high-resolution aerosol mass spectrometry: spatial and seasonal variation of aerosol composition and sources with a focus on organic nitrates, Atmos. Chem. Phys., 15(13), 7307–7336, 2015a.

Xu, L., Guo, H., Boyd, C. M., Klein, M., Bougiatioti, A., Cerully, K. M., Hite, J. R., Isaacman-VanWertz, G., Kreisberg, N. M., Knote, C., Olson, K., Koss, A., Goldstein, A. H., Hering, S. V., de Gouw, J., Baumann, K., Lee, S.-H., Nenes, A., Weber, R. J. and Ng, N. L.: Effects of anthropogenic emissions on aerosol formation from isoprene and monoterpenes in the southeastern United States, Proceedings of the National Academy of Sciences, 112(1), 37–42, 2015b.

Xu, W., Lambe, A., Silva, P., Hu, W., Onasch, T., Williams, L., Croteau, P., Zhang, X., Renbaum-Wolff, L., Fortner, E., Jimenez, J. L., Jayne, J., Worsnop, D. and Canagaratna, M.: Laboratory evaluation of species-dependent relative ionization efficiencies in the Aerodyne Aerosol Mass Spectrometer, Aerosol Sci. Technol., 52(6), 626–641, 2018.

Xu, W., Takeuchi, M., Chen, C., Qiu, Y., Xie, C., Xu, W., Ma, N., Worsnop, D. R., Ng, N. L. and Sun, Y.: Estimation of particulate organic nitrates from thermodenuder–aerosol mass spectrometer measurements in the North China Plain, Atmospheric Measurement Techniques, 14(5), 3693–3705, doi:10.5194/amt-14-3693-2021, 2021.

Yu, K., Zhu, Q., Du, K. and Huang, X.-F.: Characterization of nighttime formation of particulate organic nitrates based on high-resolution aerosol mass spectrometry in an urban atmosphere in China, Atmos. Chem. Phys., 19(7), 5235–5249, 2019.

Zare, A., Fahey, K. M., Sarwar, G., Cohen, R. C. and Pye, H. O. T.: Vapor-Pressure Pathways Initiate but Hydrolysis Products Dominate the Aerosol Estimated from Organic Nitrates, ACS Earth and Space Chemistry, 3(8), 1426–1437, 2019.

Zhang, J. K., Cheng, M. T., Ji, D. S., Liu, Z. R., Hu, B., Sun, Y. and Wang, Y. S.: Characterization of submicron particles during biomass burning and coal combustion periods in Beijing, China, Sci. Total Environ., 562, 812–821, 2016.

Zhu, Q., Cao, L.-M., Tang, M.-X., Huang, X.-F., Saikawa, E. and He, L.-Y.: Characterization of Organic Aerosol at a Rural Site in the North China Plain Region: Sources, Volatility and Organonitrates, Adv. Atmos. Sci., 38(7), 1115–1127, 2021.